Ph.D. Thesis

Theory of Phase Transition and Quantum Transport in Interacting One Dimensional Electron Systems

相互作用する１次元電子系の相転移と量子輸送に関する理論

March, 2007

Graduate School of Science and Engineering
Waseda University
Major in Pure and Applied Physics

Kenji Kamide

Acknowledgment

My sincere gratitude is first of all due to my supervisor Professor Susumu Kurihara for his guidance, encouragements, and support throughout the course of the work. He always makes me comfortable to have discussions, and teaches me the important spirit of "renormalization group" to extract the most important physics from the complicated matters. I would like to thank Professor Yoji Aizawa, Professor Ichiro Terasaki, and Professor Yoshihiro Yamazaki for their critical readings of the manuscript and their useful comments.

I am grateful to Professor Munehiro Nishida for his encouragements, advice and stimulating discussions through the collaborations. I am also grateful to Dr. Takashi Kimura for his sincere encouragements and fruitful discussions through the collaborations. I am grateful to Professor Noriyuki Hatakenaka for his advice, helpful comments and discussions. I am grateful to Dr. Akira Furusaki and Professor Toshiya Hikihara for their helpful comments and discussions on the tunneling in Tomonaga-Luttinger liquid. I also thank Mr. Nobuhiko Yokoshi and Dr. Hirofumi Yanagisawa for their encouragements and stimulating discussions as colleagues and at the same time as friends. Especially, I would like to thank Mr. Yuji Tsukada for his encouragements, stimulating discussions and sharing the interests through the collaborations.

I would also like to thank all members of Professor Kurihara's laboratory for stimulating discussions and encouragements. Especially, I would like to thank Dr. August J. Moralez Jr., Dr. Hiroyuki Yoshimoto, Dr. Shunji Tsuchiya, Mr. Bernhard Hikaru Valtan, Mr. Yujiro Yanai, Mr. Yuhei Saito, Mr. Hidehisa Iwasaki, Mr. Kazuhiro Kanai, Mr. Shunji Takei, Mr. Ippei Danshita, Mr. Itaru Yanagi, Mr. Masato Yamaguchi, Mr. Kyota Egawa, Mr. Yusuke Yamaguchi, Mr. Yoshinori Watanabe, Mr. Kazuhisa Suzuki, Mr. Hiroyuki Shibata, Mr. Norikazu Naruse, Mr. Kiyohito Iigaya, Mr. Daisuke Yamamoto, and Mr. Yuki Terakawa.

I acknowledge the financial support from Japan Society for the Promotion of Science.

Finally, I would like thank my family for their patience and lifelong encouragements. Special thanks also goes to Grandfather for making corrections in English for this thesis.

Contents

Chapter 1

Introduction

1.1 Mesoscopic Transport in One-Dimensional Systems

"Electrons behave as waves" is understood as common knowledge for people who have learned quantum physics. However, we can not see this fact so often in our real life, since infinite numbers of sources which could violate quantum coherence of electron waves exist in a macroscopic system coupled with environments. Taking transmission electron microscope (TEM) as a rare example, an electron beam transmitted through a crystal medium gives electron diffraction patterns on a fluorescent plate. In this case, electrons traveling in a high vacuum inside TEM, are isolated from any decoherence factors. Without such special conditions, the wave nature of electrons disappears in macroscopic scales.

For a similar reason, conduction electrons in metals seldom show their wave nature in their transport properties of macroscopic systems. In macroscopic objects, the electron conduction of diffusive metals is explained by Drude's formula for conductance σ [1, 2],

$$\sigma = \frac{n_{\mathrm{e}} e^2 \tau}{m}, \tag{1.1}$$

where e, n_{e} and τ represent, respectively, electric charge, number density and mean free time of conduction electrons. This formula is understood as a classical equation of motion derived from the balancing relation between momentum loss per unit time and electrostatic force by external electric field E, i.e. $\Delta p/\tau = mv/\tau = eE$. Conductance is defined as the ratio of current density $j = evn_{\mathrm{e}}$ to the electric field E, yielding Eq. (1.1). In this classical explanation, we do not need to assume the wave nature of electrons. Instead, the

average time τ between the scattering events, which occur for some reason, takes place as the one and only factor governing electron transport. As the system size gets smaller and the temperature goes down, the frequency of scattering events that an electron faces during a travel from one reserver to another, becomes rare, and eventually, the average scattering time τ will lose its sense. In such small systems called *mesoscopic systems*, electrons are free from inelastic scatterings, and only affected by elastic scatterings due to boundaries of the sample, interparticle interactions or some scattering sources. The type of the electron transport changes from diffusive transport to the other one that shows the wave nature of electrons. This type of conduction free from inelastic scatterings and with memories of the phase dynamics, is called *ballistic transport*, and is one important concept in mesoscopic transport. Many transport experiments of ballistic samples are explained by assuming free electrons with effective mass m^*.

The characteristic length scale which separates macroscopic systems from mesoscopic systems, is the phase coherence length $l_\phi \sim 1$ μm. Reflecting this fact, mesoscopic transport has come to be studied intensively from 1980's in parallel to the progress of micro-fabrication techniques such as, e.g. molecular beam epitaxy (MBE), electron beam lithography and scanning tunneling microscopy (STM) [3, 4]. In mesoscopic systems, electronic wave pockets spread over the system and the electronic transport is described by its coherent phase dynamics. Thus, their transport properties depend on details of electronic wave function. Nowadays, mesoscopic devices with the size $L < l_\phi \sim 1$ μm can be realized through the techniques mentioned above. Wave nature was observed in transport properties, firstly, as Aharonov-Bohm (AB) oscillation of conductance as function of magnetic flux through microscopic AB ring of 0.78 μm in diameter [5]. Universal conductance fluctuation (UCF) of the order of $\delta G \sim 2e^2/h$ induced by a small change in external parameters, was detected in a quantum wire, showing a fingerprint of diffraction of electron waves in mesoscopic systems [6]. In these mesoscopic systems, two terminal conductance is given by Landauer-Buttiker formula [7, 8] instead of Eq. (1.1),

$$G = \frac{2e^2}{h} \sum_{i,j} T_{i,j}, \tag{1.2}$$

where $T_{i,j}$ indicates the probability that the electron in an initial state i injected from the left reserver, can reach the right reserver in a final state j. Landauer-Buttiker formula connects conductance with the wave nature of electrons through $T_{i,j}$: electrons are assumed to go through independent paths = channels ($i \to j$) with the transmission probability $T_{i,j}$, and the summation of transmission probability of each channel gives the conductance. In the ballistic regime at low temperature around sub-Kelvin, quantum size effect is expected, and actually observed in quantum point contacts (QPCs) [9], and clean

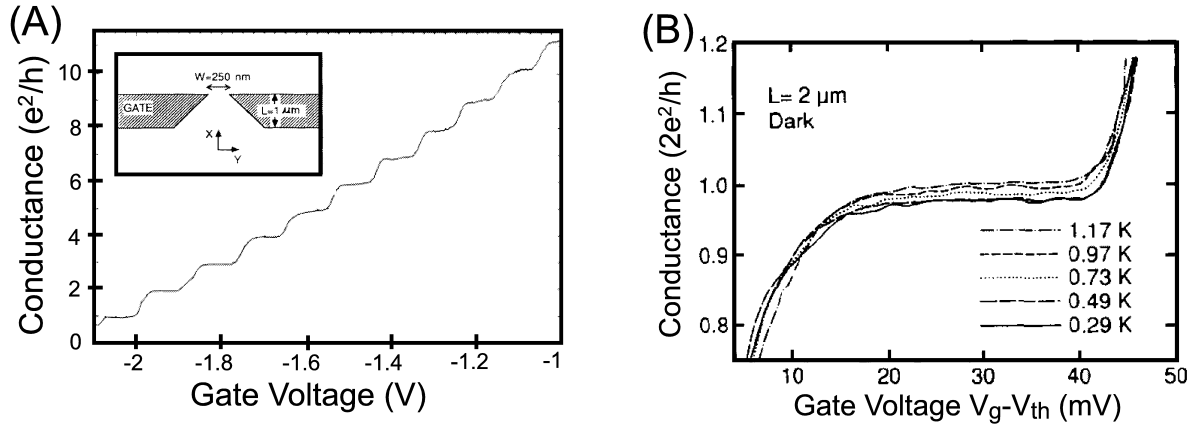

Figure 1.1: (A) Conductance of QPC is plotted as a function of applied gate voltage. Plateaus are seen at multiples of $2e^2/h$. (Inset) Layout of QPC. Figures are taken from Ref. [9]. (B) Conductance of a quantum wire of 2 μm is plotted near the first plateau $G \sim 2e^2/h$ for several temperatures. The figure is taken from Ref. [10].

quantum wires longer than 1 μm [10, 11], which are defined in a two-dimensional electron system at GaAs-AlGaAs heterostructure. Their results are shown in Fig. 1.1 (A) and Fig. 1.1 (B).

In these experiments, all conduction channels are highly transparent $T_{i,j} = \delta_{i,j}$ and the conductance is given by $G = 2e^2/h \times N_{\rm ch}$, in which $N_{\rm ch}$ counts the numbers of conduction channels. By changing a confining potential or the electron density by the gate voltage, it is possible to reduce the numbers of conduction channels. In the figures, conductance steps in the unit of $2e^2/h$ are seen and an ultimate limit $N_{\rm ch} = 1$ is reached. In case of $N_{\rm ch} = 1$, all electrons are considered to move along a path, thus the quantum wire can be regarded as *"One-Dimensional Electron System"*.

Not only such artificial quantum wires in semiconductors, carbon nanotubes (CNs) are also known as one-dimensional electron systems [12], which are naturally produced and show the quantum coherent transport. An individual CN has a mechanically robust structure so that a graphene sheet is rolled up into a cylinder with the diameter $2R \sim$ 1 nm. Depending on the periodic boundary condition in the circumferential direction, which is defined by a chiral vector $\mathbf{T} = n_1\mathbf{a} + n_2\mathbf{b}$ with unit vectors of a graphene $\mathbf{a}$, $\mathbf{b}$ and $n_1, n_2 \in \mathbb{Z}$, a CN can be either a metal or a semiconductor [13]. Metallic CNs have rich conduction electrons since one carbon atom supplies one conduction electron ($\pi-$electron). This means a metallic CN is a good metal with the large electron band

width ~ 2.5 eV and the large Fermi velocity $v_{\rm F} = 8.1\times10^5$ m/s. Owing to the fact that the band width for CNs are much larger than the Fermi energy of semiconductor ~ 10 meV, thermal coherence length of electrons $l_{\rm T} = hv_{\rm F}/(k_{\rm B}T)$ can be much larger in CNs than in semiconductors: it becomes more than 0.1 μm even at the room temperature ! In order to observe the quantum coherent transport in CNs, we don't need such a low temperature as in the semiconductor based devices [14, 15, 16, 17]. It is reported that, reflecting this advantage, an individual metallic single-wall CN works as a single electron transistor even at the room temperature, but with a small peak current due to the presence of Schottky barriers at the contacts [14]. By choosing the material used in contacts, now it became possible to reduce the Schottky barriers, and a ballistic regime can be achieved in many devices based on CNs. At the room temperature, by using 4 μm long CNs contacted by liquid metals, the ballistic limit $G = 2e^2/h$ was achieved [15]. A single-wall CN between titanium contacts revealed the nature of ballistic electron waveguide, and Fabry-Perot oscillations were observed near the full transparency $G = 4e^2/h \times T \sim 4e^2/h \times 1$ [16]. A mesoscopic device based on CNs was reported to work as a room-temperature field effect transistor with the ballistic on-current [17]. In this thesis, we focus on the physics of one-dimensional electron systems above mentioned, such as CNs and a quantum wire in semiconductors. Our interests are not only in the quantum coherent transport seen in mesoscopic systems, but also in the interaction effects. We will see the interesting feature coming from the interaction effects in one-dimensional systems.

1.2 Interaction Effects in One Dimension

As mentioned in the previous section, many physics of ballistic transport in mesoscopic systems, can be explained by a semiclassical kinematics of free electrons with some modification in the effective mass m^*. In that case, interaction effects enter only through the effective mass, and there is no difference in the physics qualitatively from noninteracting systems. But this is not always the case for large ballistic systems such that $1/k_{\rm F} \ll L < L_\phi$, where the long-wavelength and low-energy excitations dominate in the transport property. In such long-wavelength and low-energy physics, interactions between electrons become crucial. Nowadays, the quantum coherent transport can be achieved in long spatial scales up to several micron meters using carbon nanotubes. Thus, we can never talk about the mesoscopic transport without interaction effects. In addition, the electron interaction potential is long-ranged in a CN since it is a natural one-dimensional material where the screenings of the interaction potential do not work well. As for long wavelength excitations in CNs, the Coulomb potential must be regarded as a strong repulsion. In this section, we will highlight the significance of electron interactions to the bulk

quantities, although the discussions here are seen in many excellent reviews or textbooks on this issue [18, 19, 20, 21, 22]. We will see, especially in purely one-dimensional systems with infinite length, the bulk quantity such as the heat capacity, the magnetic susceptibility, and the electronic conductivity changes qualitatively in the presence of interactions, no matter how small it is.

Firstly, let's see the interaction effects in the phenomenological theory of weakly interacting Fermi liquid by Landau [23, 24]. It is assumed that, at sufficiently low temperatures, thermodynamic quantities are well described by excitations of quasi-particles near the Fermi surface, which are in one-to-one correspondence to those of the noninteracting system, with some modification in the effective mass m^*. The heat capacity of Fermi liquid, coming from the contribution of quasi-particles, is expected to be expanded in the series of even-powers of temperature,

$$C(T)/T \sim \frac{1}{T}\int_{-\infty}^{\infty} \epsilon D(\epsilon)\frac{\partial f}{\partial T}d\epsilon = \sum_{n=0}^{\infty} A_n T^{2n}, \tag{1.3}$$

where $f = 1/(1+e^{\epsilon/k_{\rm B}T})$ and $D(\epsilon)$ are, respectively, Fermi distribution function and the density of states at energy ϵ measured from the Fermi level $\epsilon_{\rm F}$. The leading term $A_0 = \pi^2 k_{\rm B}^2 D(0)/3$ is the coefficient of well-known T-linear heat capacity, and the even powers of T arise from particle-hole symmetry of the Fermi function $\partial f(\epsilon)/\partial T = \partial\left(1-f(-\epsilon)\right)/\partial T$. Interactions between the quasi-particles are assumed to change the coefficients A_n through the modification of effective mass m^*.

Soon after the phenomenological study, the microscopic theory of weakly interacting Fermi liquid [25] was developed, which incorporated the interaction effects by Green function method. The microscopic theory gives the T-linear heat capacity with the same coefficient A_0. But it also gives the other corrections to the heat capacity [26, 27], which can not be regarded as the correction to the coefficients A_n of regular terms in Eq. (1.3). They appear already in the second order of interactions,

$$\delta C/T = \begin{cases} \propto T^2 \ln T & \text{in 3D,} \\ \propto T & \text{in 2D,} \\ \propto \ln T & \text{in 1D.} \end{cases} \tag{1.4}$$

As the dimensionality is reduced, these corrections get stronger, and especially in one-dimensional systems, the second order correction dominates the leading term for $T \to 0$. This means that in one dimension, interparticle interactions can trigger the breakdown of the Fermi liquid ground states, which are based on the assumption that the thermodynamic quantity is determined by single-particle excitations at least at zero temperature.

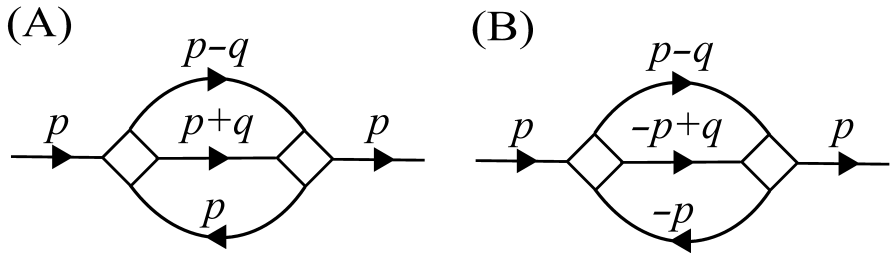

Figure 1.2: (A),(B) Second-order diagrams for the self-energy relevant to the corrections in the heat capacity in Eq. (1.4). p is the quasi-particle momentum near the Fermi surface $|p| \sim p_{\rm F}$, and $|q| \ll p_{\rm F}$.

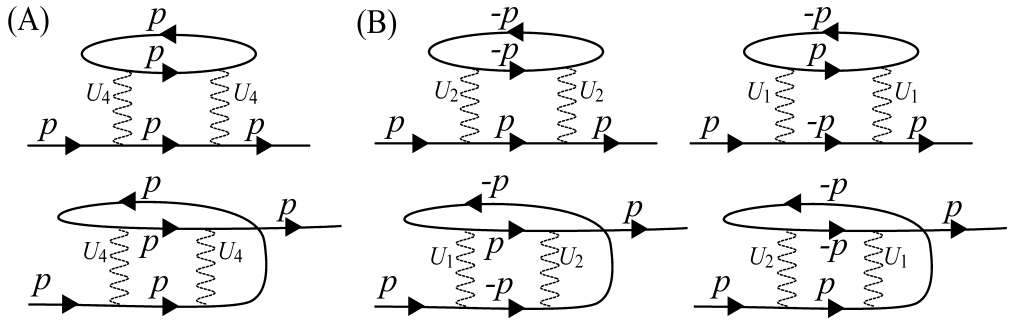

Figure 1.3: (A),(B) The same diagrams as Fig. 1.2 expanded at the vertices which are classified as three scattering processes U_1, U_2 and U_4. The indices $1, 2, 4$ are following the convention of $g-$ology [18]. See the text for explanations.

The corrections to Fermi liquid theory in the heat capacity were also observed in liquid ^{3}He in three dimension [28], and in two dimension [29].

Next we will see more precisely how the difference due to the dimensionality comes from. Those corrections stem from the nonanalytic corrections to the self-energy of the quasi-particles with small energy $\epsilon \ll \epsilon_{\rm F}$, adding to the regular corrections $\delta({\rm Re}\Sigma) \propto \epsilon$,

$$
{\rm Re}\left[\Sigma^{\rm R}(\epsilon = \frac{p^2}{2m} - \epsilon_{\rm F}, p)\right] = \begin{cases} \propto \epsilon^3 \ln \epsilon & \text{in 3D,} \\ \propto \epsilon|\epsilon| & \text{in 2D,} \\ \propto \epsilon \ln \epsilon & \text{in 1D.} \end{cases} \tag{1.5}
$$

The second-order self-energy corrections relevant to the nonanalytic corrections, are expressed by the diagrams in Fig. 1.2 (A) or Fig. 1.2 (B), and the set of diagrams in Fig. 1.3

(A) and Fig. 1.3 (B) are the same diagrams expanded at the vertices. Especially in one and two dimensions, it is shown that the diagrams, which contain scattering processes between particles with zero total momentum like Fig. 1.2 (B) or Fig. 1.3 (B), are relevant to the leading corrections in Eq. (1.4) [30]. The important scattering processes for the nonanalytic corrections are the ones which induce a small momentum transfer $|q| \sim 0$ and a large momentum transfer $|q| \sim 2p_{\rm F}$. They are labeled by U_1, U_2, and U_4 in Fig. 1.3. Those scattering processes occur between two particles on the same side or the other side of the Fermi surface: U_1 is a scattering process between particles on the other sides exchanging a large momentum $|q| \sim 2p_{\rm F}$: U_2 and U_4 exchange a small momentum $q \sim 0$ between particles on the other sides and the same sides, respectively. These processes are known as g_1, g_2 and g_4 in g-ology of one-dimensional systems [18], and also play important roles in the higher dimensions. There are similarities between one and higher dimensions in the sense that nonanalytic corrections to the quasi-particle self-energy and hence the corrections to the Fermi liquid stem from the similar types of scattering processes.

The non-analytical features come from the restriction of the scattering processes assigned by Pauli principle. Consider a scattering process in two or three dimensions that particle 1 with a momentum $|p_1| > p_{\rm F}$ and an energy $\epsilon_1 = p_1^2/(2m) - \epsilon_{\rm F}$ interacts with particle 2 of p_2 and ϵ_2 exchanging a small energy ϵ and a momentum q between them, which is shown in Fig. 1.4 (A). At low temperature, it is most likely to occur when particle 1 and particle 2 are, respectively, in the slight outside and in the slight inside of the Fermi surface. This is because the probability P_{p-p} for two excited-particles to be scattered off is much less than the probability P_{p-h} for a particle and a hole to be scattered off: $P_{p-h} \gg P_{p-p}$ as $T \to 0$, since $P_{p-p} \sim f^2 \propto T^2$ and $P_{p-h} \sim f(1-f) \propto T$. Thus, a scattering event at low temperature is viewed as such that a single-particle lose its energy by exciting a particle-hole pair from the Fermi sea, which is essentially the same as *Landau damping*. Such scattering events take place only when particle 1 can lose its energy by exciting particle 2 to the outside of the Fermi surface: (i) $0 < \epsilon < \epsilon_1 = (p_1^2/2m) - \epsilon_{\rm F}$ and (ii) $-\epsilon < \epsilon_2 = (p_2^2/2m) - \epsilon_{\rm F} < 0$. For the conservation of total energy and momentum, it is given,

$$\begin{aligned} -\epsilon &= \frac{(p_1 - q)^2 - p_1^2}{2m} = -\frac{|p_1||q|}{m}\cos\theta_1 + \frac{q^2}{2m}, \\ \epsilon &= \frac{(p_2 + q)^2 - p_2^2}{2m} = \frac{|p_2||q|}{m}\cos\theta_2 + \frac{q^2}{2m}, \end{aligned} \tag{1.6}$$

where θ_i is the angle between the momentum q and p_i for $i = 1, 2$. Since $|\cos\theta_1|, |\cos\theta_2| \leq$

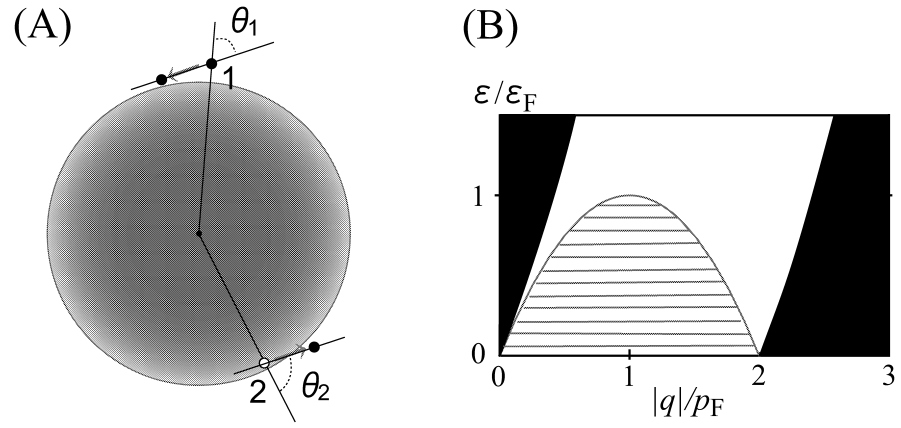

Figure 1.4: (A) Scattering processes between particle 1 and particle 2. $\theta_{1(2)}$ is the angle between the momentum of particle 1 (2) and the momentum transfer ($p_{1(2)}$ and q in the text) (B) Continuum of the particle-hole excitations. Forbidden regions in all dimensions and in one dimension are, respectively, shown by black areas and gray shaded area.

1, the condition for the solution of Eq. (1.6) to exist is (iii):

$$|\epsilon + \frac{q^2}{2m}| < \frac{|p_1||q|}{m} \sim v_{\rm F}|q|,$$
$$|\epsilon - \frac{q^2}{2m}| < \frac{|p_2||q|}{m} \sim v_{\rm F}|q|. \tag{1.7}$$

These three conditions (i)−(iii) limit the area in (q,ϵ) space for particle-hole excitations to exist to $\max[0, q^2/(2m) - v_{\rm F}|q|] < \epsilon < q^2/(2m) + v_{\rm F}|q|$, which is shown in white and gray shaded areas in Fig. 1.4 (B). One can apply the similar discussion to one dimension, but with some differences. In one dimension, the condition (iii) becomes more severe, since there is no other choice of cosine terms than $|\cos\theta_1| = |\cos\theta_2| = 1$. Moreover, in two or three dimensions, one can find at any time a region which satisfies the condition (ii) in the momentum space for any $q, \epsilon > 0$, and hence (ii) does not put any restriction. On the other hand, in one dimension, (ii) does put additional conditions restricting the particle-hole continuum to $|q^2/(2m) - v_{\rm F}|q|| < \epsilon < q^2/(2m) + v_{\rm F}|q|$. Adding to the black area in Fig. 1.4 (B), the gray shaded area also becomes forbidden in one dimension. The major difference between one and higher dimensions comes from whether the Fermi surface is compact or not. However, in this way, the range of q-integration for the correction to the self-energy in Fig. 1.2 depends on ϵ, regardless of the dimensionality, yielding the nonanalytic corrections.

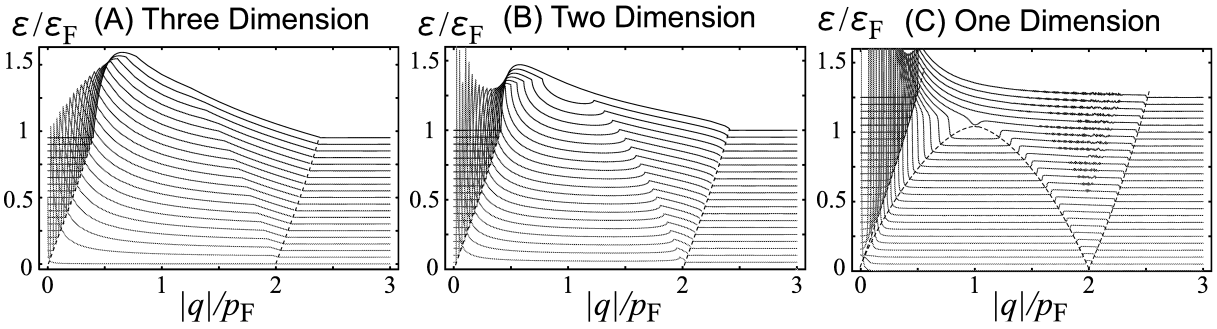

Figure 1.5: Dynamical structure function $S(q,\epsilon)$ of noninteracting fermions at zero temperature are shown in a (q,ϵ) plane for (A) three dimension, (B) two dimension, and (C) one dimension.

What about the strength of nonanalytic corrections? As seen in Fig. 1.4 (B), different from higher dimensions, the possible scattering processes are U_1, U_2, U_4 for small energy transfer since the unforbidden area lies just on a line $\epsilon = v_{\rm F}q$ or around $q \sim 2p_{\rm F}$ for small ϵ in one dimension. Thus, all possible scattering processes are relevant to the nonanalytic corrections in one dimension. In higher dimensions, other scattering processes $\epsilon/v_{\rm F} \ll q, 2p_{\rm F}-q$ also take place, which give regular contributions. In order to understand the quantitative difference due to the dimensionality more clearly, it is helpful to see the difference in the dynamical structure function $S(q,\epsilon)$ shown in Fig. 1.5, which directly shows the distribution of particle-hole excitations:

$$S(q,\epsilon) = \int (dk/2\pi)^D \; \delta\left(\epsilon - \epsilon_{k+q} + \epsilon_k\right) f_k(1-f_{k+q}), \tag{1.8}$$

where $D = 1, 2, 3$ is the dimensionality. In figures, one finds the non-analyticities in all dimensions at a line $\epsilon = -q^2/2m + v_{\rm F}q$ that is a boundary between the gray shaded and the white areas in Fig. 1.4 (B). At the line, $S(q,\epsilon)$ itself jumps in one dimension while the slope $\partial_q S(q,\epsilon)$ does in two or three dimensions. Thus, one can again reach the point where the nonanalytic features come from the same physics for all dimensions and the differences are in their magnitudes. In the limit $\epsilon \to 0$, $S(q,\epsilon)$ experiences a peak at $\epsilon = v_{\rm F}|q|$, which gives a constant peak line for three dimension, and the peak diverges in one and two dimensions. The strength of the singularity becomes stronger for lower dimensions as $S(q, \epsilon = v_{\rm F}|q|) \propto (\epsilon/\epsilon_{\rm F})^{(D-3)/2}$. This straightforwardly means that, in one and two dimensions, a single-particle excitation near the Fermi surface can strongly couples with a large number of particle-hole excitations, and can easily lose its energy decaying into a long-wavelength density fluctuation.

Due to the strong coupling between a single-particle and particle-hole continuum at small q, Fermi liquid theory essentially breaks down in one dimension at low temperature, as already seen in Eq. (1.4) where the corrections due to interactions dominate the leading term. The crossover temperature T^*, below which non-Fermi-liquid behavior dominates the physics, is roughly estimated as $T^* = \epsilon_{\rm F} e^{-g^2}$ where g is the dimensionless interaction parameter normalized by the Fermi energy. Thus if we assume the weak interactions, T^* is exponentially suppressed and the perturbation theory assuming the Fermi liquid ground state works well down to a quite low temperature. There are two types of approaches to treat the logarithmically divergent corrections in interacting one-dimensional electron systems, and we can choose them depending on what our problems of interest are. One is to investigate the physics for $T > T^*$ assuming the Fermi liquid ground states and take into account interactions as perturbation. In this approach, one can not trust the result down to zero temperature, but one can predict what kind of instabilities will first arise as lowering the temperature. This approach is known as g-ology [18] and widely applied to predict the ground state of low-dimensional electron systems where one-dimensional scattering processes such as U_1, U_2 and U_4 in Fig. 1.3 are relevant. Another approach is to construct the non-Fermi liquid ground state called "*Tomonaga-Luttinger liquid*" [31, 32], which allow us to study the normal state physics of one-dimensional fermions down to zero temperature [19, 20, 21]. It is known that including carbon nanotubes and quantum wires, a wide range of theoretical models for strongly interacting fermions in one dimension can be described as Tomonaga-Luttinger liquid. In this thesis, we will adopt both approaches to investigate the physics of one-dimensional electron systems.

1.3 Outline

In this thesis, we consider three topics related to the interaction effects in one-dimensional electron systems. One is on the superconducting transition in carbon nanotubes discussed in Chapter 2. Other two topics are on the scaling problems of the impurity potentials in a Tomonaga-Luttinger liquid, shown in Chapter 3 and Chapter 4.

In Chapter 2, we will present renormalization group (RG) study (g-ology) for the phase diagrams of $(5,0)$ CNs [33, 34], which was reported to be superconducting at 15K [35]. According to the electronic band structure [36, 37, 38, 39, 40, 41], a $(5,0)$ CN has doubly degenerate bands and a singly degenerate band crossing the Fermi energy with circumferential momenta. By considering a $(5,0)$ CN as a three-band quasi-one-dimensional electron system, we calculate the temperature dependent correlation functions for superconductivity and density waves, which will be expected to cause instabilities of normal Fermi liquid states at low temperature. In this system we must specify scattering channels

in terms of the momentum along the circumferential direction as well as the axis direction, since a $(5, 0)$ CN has two degenerate bands crossing the Fermi energy with circumferential momenta. Therefore, there will be scattering processes that change the circumferential momentum of electrons. We found singlet-superconducting phases with $5\hbar$ circumferential angular momentum caused by a relevant renormalization of the scattering processes like Umklapp processes, which change the total momentum in the circumferential direction.

In Chapter 3 and Chapter 4, transport properties of Tomonaga-Luttinger liquid are discussed in the presence of localized potentials such as impurities and junctions. Localized potentials in TL liquid is known to drive the system to be metallic or insulating at zero temperature depending on whether the electron-electron interactions are repulsive or attractive [42, 43, 44, 45]. This has been understood as the scaling of effective potential that the electrons feel. The transmission amplitude through the potential barrier scales as a power-law of temperature, and the sign of the scaling exponent depends on the interaction parameters.

In Chapter 3, we consider the transport properties of TL liquid under magnetic field [46, 47, 48, 49, 50, 51, 52]. The effects of impurity potentials are being considered, while the impurity potential is assumed to be very weak $V \ll \hbar v_{\mathrm{F}}$ or very strong $V \gg \hbar v_{\mathrm{F}}$. It is known that the scaling exponent of a single impurity potential depends on electron spins in the presence of a magnetic field, which gives a large polarized current at low temperature [47, 48]. We consider the spin-polarized current through double impurities in TL liquid in the presence of magnetic fields [50, 51]. An interesting feature caused by a magnetic field is the violation of "*spin-charge separation*". While electron-electron interaction preferably separates the excitation spectrum of the charge density wave and the spin density wave, which is known as spin-charge separation, spin Zeeman energy couples the spin and the charge degrees of freedom. With these competing effects, the transport properties are described by two branches of spin-charge mixed density waves. How the spin-charge mixing affects the spin and charge transport is being considered. Zero bias conductance is calculated as a function of gate voltage V_{g}, gate magnetic field B_{g}, temperature and a magnetic field applied to the system. Mixing effect is shown to cause rotation of the lattice pattern of the conductance peaks in $(V_{\mathrm{g}}, B_{\mathrm{g}})$ plane, which can be observed in experiments. At low temperatures, the contour shapes are classified into three types, reflecting the fact that effective barrier potential is renormalized towards "perfect reflection", "perfect transmission" and "spin-filtering" induced by a magnetic field, respectively.

In Chapter 4, the bosonization formula is developed to include a single impurity potential of arbitrary strength [53]. Many works on the impurity problem in TL liquid [42, 43, 44, 45], assume the potential is very weak or very strong, as is also done in Chapter 3. For a spinful TL liquid with spin independent interaction or a spinless TL

liquid, the critical value of the interaction parameters where the directions of the scaling flows change, which we call *a fixed point*, is the same for the strong potential limit and the weak potential limit. Thus the effective impurity potential is expected to flow in one direction between the weak and the strong potential. However, for a spinful TL with spin dependent interactions, renormalization equations give the different fixed points in the two limits, indicating that the phase boundary lies at a finite potential strength. In order to determine such phase boundary for arbitrary strength of electron-electron interaction and localized potential, we develop the open boundary bosonization method, which is valid only in the strong barrier limit, to the one valid for arbitrary potential barrier by introducing the electron phase shift as the boundary condition between right-moving and left-moving TL bosons. Using the bosonization formula, we derived a scaling equation for the zero bias conductance from the relation between transmission probability and local density of states. We found the phase boundary has a reentrance structure for spin dependent model, which suggests the existence of stable fixed points at some finite transmission probability neither 0 nor 1, at zero temperature.

In the last chapter, we summarize the results obtained here, and make some remarks on the future problems.

Throughout the thesis, we set $\hbar = k_{\mathrm{B}} = 1$ unless specified otherwise.

Chapter 2

Superconductivity in Carbon Nanotubes

2.1 Introduction

The discovery of carbon nanotubes (CN) in 1991 [12] has attracted much attention because of its potential for new physics as well as applications in electronic devices [13]. A single-wall CN (SWCN) is made of a graphite layer rolled up into a cylinder with a small diameter. As is known, SWCNs can be regarded as one-dimensional electron systems due to quantization of the circumferential momentum, as confirmed by experiments [54].

Recently, Tang *et al.* [35] reported evidence for superconductivity in a SWCN system below 15K. This system consists of $(5, 0)$ CN with the diameter 4Å, separated from each other by zeolite walls. So this experiment implies that well-developed superconducting correlation (SCC) can exist in each individual nanotube. The microscopic origin of the SCC in a SWCN is an interesting question to ask, since divergent one-dimensional SCC will eventually cause three-dimensional superconductivity with electron tunneling through zeolite walls.

On the other hand, bosonization [55, 56] and renormalization group [57, 58] methods have been applied to the (n, n) CN to explain the superconductivity in the ropes of (n, n) CNs [59]. They have shown that a singlet superconducting phase is more favored if short-range attractive interactions exist between electrons. Moreover, some theories [60, 61, 62] have suggested the presence of short-range attractive interactions in (n, n) CN. However, results of bosonization and renormalization group [55, 56, 57, 58] cannot be directly applied to $(5, 0)$ CN case, because the band structure of $(5, 0)$ CN is very different from that of (n, n) CN.

Within the local-density approximation, (5,0) CN has three bands crossing the Fermi energy [37, 38, 39, 40, 41]; one non-degenerate band and two two-fold-degenerate bands with opposite circumferential momenta, as shown in Fig. 2.1 (A) and Fig. 2.1 (B). Such a band structure cannot be obtained within the tight-binding approximation because σ-π hybridization effects change it significantly in a SWCN with the diameter 4Å [36]. This band structure will provide opportunities to develop SCC with total circumferential momentum. We should also take into account the interaction between electrons with momentum transfer in the circumferential direction as well as in the axis direction.

In this chapter, we perform one-loop RG calculation and derive the scaling equations for the three-band system, including the interactions with angular momentum transfer [33, 34]. We find phase diagrams in terms of several coupling constants by solving these equations numerically. Critical exponents which govern the temperature dependence of correlation functions near T_c are also calculated.

2.2 Three-Band Model and Three Groups

We consider a system consisting of three linear bands near the Fermi level [Fig. 2.1 (C)]. Band 0 has no angular momentum ($\mathrm{L}_0 = 0$), band 1 and 2 have a finite angular momentum and are two-fold degenerate ($\mathrm{L}_{1,2} = \pm\hbar n_{1,2}$). In general, the relevant two-particle correlation is formed between branches with the different signs in Fermi velocity in one-dimensional electron systems. As we have three bands, six channels of two-particle correlations are produced. We take into account forward and backward scatterings in this three-band system and perform g-ology [18], and determine the most divergent two-particle correlation among all possible ones by solving scaling equations. We start from a Hamiltonian for non-interacting electrons:

$$\begin{aligned} H_0 = & \sum_{\tau,\sigma,k} \tau v_{F,0}(k - \tau k_{F,0})\ \psi^\dagger_{0,\tau,\sigma}(k)\psi_{0,\tau,\sigma}(k) \\ & - \sum_{\substack{\gamma=1,2 \\ \tau,l,\sigma,k}} \tau v_{F,\gamma}(k - \tau k_{F,\gamma})\ \psi^\dagger_{\gamma,\tau,l,\sigma}(k)\psi_{\gamma,\tau,l,\sigma}(k), \end{aligned} \tag{2.1}$$

where $v_{F,\gamma}$ and $k_{F,\gamma}$ represent Fermi velocity and Fermi momentum for band γ. Spin, signs in Fermi momentum and in angular momentum L_γ are denoted by σ, τ and $l = \pm$ respectively. We carry out a perturbation calculation with the interaction between

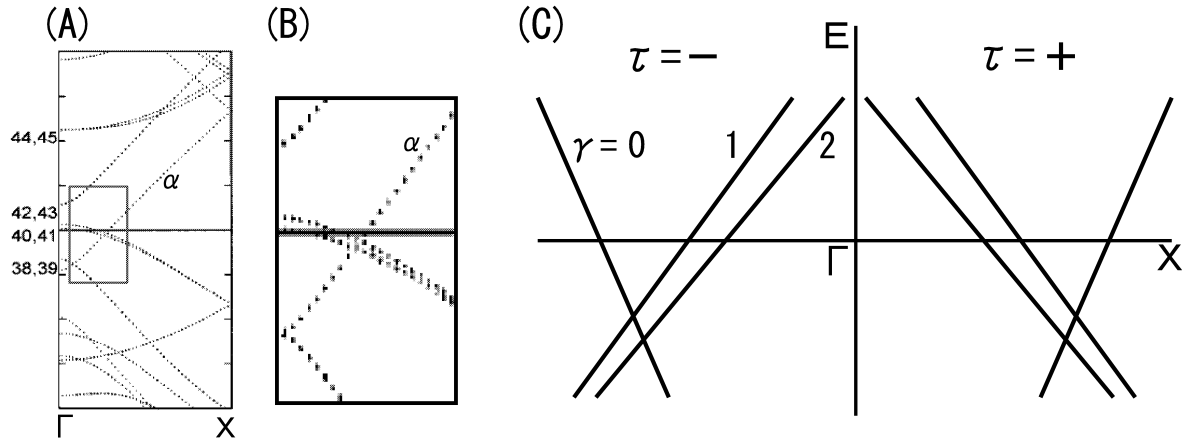

Figure 2.1: (A)(B) Band structure of (5,0) CN and its magnification taken from [37]. (C) Three linear bands of (5,0) CN. Electrons are labeled by band $\gamma \in \{0, 1, 2\}$, Fermi point $\tau = \pm$, angular momentum $L_\gamma = \pm\hbar|n_\gamma|$ and spin $\sigma = \pm$.

electrons,

$$H_I = \sum g^{\tau_1,\tau_2,\tau_3,\tau_4}_{\gamma_1,\gamma_2,\gamma_3,\gamma_4} \quad \psi^\dagger_{\gamma_1,\tau_1,l_1,\sigma}(k+q)\psi^\dagger_{\gamma_2,\tau_2,l_2,\sigma'}(k'-q) \times \psi_{\gamma_3,\tau_3,l_3,\sigma'}(k')\psi_{\gamma_4,\tau_4,l_4,\sigma}(k). \tag{2.2}$$

Keeping the momentum transfer in mind both in the circumferential direction as well as in the axial direction, we abbreviate interaction constants as g^j_i where i and j represent the types of scattering processes in axial and circumferential direction respectively: 1 =backward, 2 =inter-branch forward, 3 =Umklapp and 4 =intra-branch forward. We neglect the intra-branch forward scatterings g^j_4 because they are irrelevant within the one-loop RG framework. We also neglect Umklapp processes g^j_3 because (5,0) CN systems are far from the half-filling for any bands.

We divide six channels into three groups by considering the types of scattering processes. We denote the channel between the electrons in band γ and band γ' by (γ, γ').

Group 1 : (0,0),(0,1),(0,2)

These channels contain only two types of interactions ($b_{0,\gamma}$, $f_{0,\gamma}$) because of the restriction in momentum conservation. The backscattering $b_{0,\gamma}$ exchanges the Fermi points of the incident electrons, and in contrast, the forward scattering $f_{0,\gamma}$ does not.

Group 2 : (1,1),(2,2)

These channels contain backward processes (g_1^1, g_2^1) in the circumferential direction, which exchange angular momentum between electrons. We will consider six interactions (g_1^1, g_1^2, g_1^4, g_2^1, g_2^2, g_2^4) here.

Group 3 : (1,2) If $|n_1| + |n_2| = 5$, these channels contain Umklapp processes (g_1^3, g_2^3), which conserve the total momentum along the axial direction but does not conserve the total angular momentum along the circumferential direction. We have to allow the shift in the total angular momentum by a reciprocal lattice vector. We will consider six interactions (g_1^1, g_1^3, g_1^4, g_2^2, g_2^3, g_2^4). If $|n_1| + |n_2| \neq 5$, then we shall put $g_1^3 = g_2^3 = 0$.

2.3 Scaling Equations

Our RG calculations are straightforward generalization of the method of Sólyom [18] and performed by summing up all one-loop diagrams i.e. Cooper-channels and Peierls-channels.

2.3.1 Group 1

These channels have two types of scattering processes (b; backward) and (f; forward). RG analysis of these channels is the same as pure one-dimensional system. RG equations for coupling constants are

$$(\tilde{b}_{0,\gamma})' = 2\tilde{b}_{0,\gamma}^2, \tag{2.3}$$

$$(\tilde{f}_{0,\gamma})' = \tilde{b}_{0,\gamma}^2. \tag{2.4}$$

Here $\tilde{b}_{0,\gamma} = b_{0,\gamma}/2\pi v_{0,\gamma}$ and $\tilde{f}_{0,\gamma} = f_{0,\gamma}/2\pi v_{0,\gamma}$ are normalized dimensionless coupling constants where $v_{0,\gamma} \equiv (v_{F,0} + v_{F,\gamma})/2$. The prime denotes differentiation with respect to x, where $x \equiv \ln \frac{T}{E_c}$ with E_c being an energy cutoff. In these channels four types of two-particle correlations are produced. They are

$$\hat{O}_{0,\gamma,l}^{\mathrm{cdw}}(q_1^+) = \frac{1}{\sqrt{L}} \sum_{k,\sigma=\pm} \psi_{\gamma,-,l,\sigma}^\dagger(k)\psi_{0,+,\sigma}(k+q_1^+), \tag{2.5}$$

$$\hat{O}_{0,\gamma,l}^{\mathrm{sdw}}(q_1^+) = \frac{1}{\sqrt{L}} \sum_{k,\sigma=\pm} \sigma\psi_{\gamma,-,l,\sigma}^\dagger(k)\psi_{0,+,\sigma}(k+q_1^+), \tag{2.6}$$

$$\hat{O}_{0,\gamma,l}^{\mathrm{ssc}}(q_1^-) = \frac{1}{\sqrt{L}} \sum_{k,\sigma=\pm} \sigma\psi_{\gamma,-,l,\sigma}(k)\psi_{0,+,\sigma}(q_1^- - k), \tag{2.7}$$

$$\hat{O}_{0,\gamma,l}^{\mathrm{tsc}}(q_1^-) = \frac{1}{\sqrt{L}} \sum_{k,\sigma=\pm} \psi_{\gamma,-,l,\sigma}(k)\psi_{0,+,\sigma}(q_1^- - k), \tag{2.8}$$

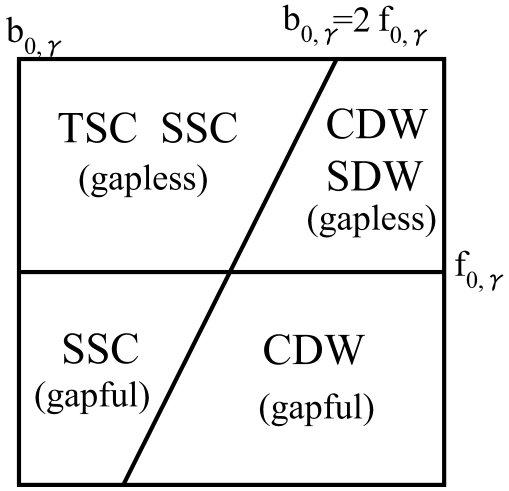

Figure 2.2: Phase diagram for group 1 in $(f_{0,\gamma}, b_{0,\gamma})$ plane, whose phase boundaries are given by the two lines $b_{0,\gamma} = 2f_{0,\gamma}$ and $b_{0,\gamma} = 0$.

where $q_1^{\pm} \equiv k_{F,0} \pm k_{F,\gamma}$ represents the total momentum of the two-particle correlation. In their suffixes, cdw, sdw, ssc and tsc stand for charge-density wave (CDW), spin-density wave (SDW), singlet superconductor (SSC) and triplet superconductor (TSC), respectively. We can also derive scaling equations for these two-particle correlation functions $\tilde{\chi}_m$ where $\chi_m \equiv \langle \hat{O}_m^\dagger \hat{O}_m \rangle$ and $\tilde{\chi}_m \equiv \pi v_m \frac{d}{dx} \chi_m$ and m stands for a kind of two-particle correlation.

$$\frac{d}{dx} \log \tilde{\chi}_m = K_m, \tag{2.9}$$

$$K_{\rm cdw}^{0,\gamma} = 4\tilde{b}_{0,\gamma} - 2\tilde{f}_{0,\gamma}, \tag{2.10}$$

$$K_{\rm sdw}^{0,\gamma} = -2\tilde{f}_{0,\gamma}, \tag{2.11}$$

$$K_{\rm ssc}^{0,\gamma} = 2\tilde{b}_{0,\gamma} + 2\tilde{f}_{0,\gamma}, \tag{2.12}$$

$$K_{\rm tsc}^{0,\gamma} = -2\tilde{b}_{0,\gamma} + 2\tilde{f}_{0,\gamma}. \tag{2.13}$$

We determine the most divergent two-particle correlation by solving these scaling equations. The phase diagram for group 1 is the same as that of a pure one-dimensional system with backward and forward scatterings as shown in Fig. 2.2. When we have $b_{0,\gamma} < 0$ initially, it is scaled towards negative large quantity and diverges at finite temperature. We call this region gapful because gap opens in the excitation spectrum at this temperature.

2.3.2 Group 2

These channels have six scattering processes shown in Fig. 2.3. Scaling equations for these six couplings are

$$
\begin{aligned}
(\tilde{g}_1^1)' &= 2(\tilde{g}_1^1)^2 + 2\tilde{g}_1^2\tilde{g}_2^1, && (2.14)\\
(\tilde{g}_1^2)' &= (4\tilde{g}_1^4 + 2\tilde{g}_2^2 - 2\tilde{g}_2^4)\tilde{g}_1^2 + (2\tilde{g}_1^1 - 2\tilde{g}_1^4)\tilde{g}_2^1, && (2.15)\\
(\tilde{g}_1^4)' &= 2(\tilde{g}_1^2)^2 + 2(\tilde{g}_1^4)^2 - 2\tilde{g}_1^2\tilde{g}_2^1, && (2.16)\\
(\tilde{g}_2^1)' &= 2\tilde{g}_1^1\tilde{g}_1^2 + 2(\tilde{g}_2^2 - \tilde{g}_2^4)\tilde{g}_2^1, && (2.17)\\
(\tilde{g}_2^2)' &= (\tilde{g}_1^1)^2 + (\tilde{g}_1^2)^2 + \tilde{g}_1^2\tilde{g}_2^1, && (2.18)\\
(\tilde{g}_2^4)' &= (\tilde{g}_1^4)^2 - (\tilde{g}_2^1)^2, && (2.19)
\end{aligned}
$$

where $\tilde{g}_i^j = g_i^j/2\pi v_{F,\gamma}$ are normalized coupling constants. Couplings are scaled towards the large values and diverge at some finite temperature except for the case of $\tilde{g}_1^1 = \tilde{g}_2^1 = 0$. This suggests that the channel from group 2 tends to produce gapful phases when it contains interactions with angular momentum transfer.

There are several types of two-particle correlations in these channels and these orders have either zero or $\pm 2n_\gamma$ total angular momentum. Symmetry in the spin space and in the circumferential direction characterize each two-particle correlation; either of symmetric or antisymmetric order with respect to inversion will appear both in the spin and the circumferential direction. We denote all the twelve types of two-particle correlations as;

$$\hat{O}^{dw}_{\gamma,\mu_1,\mu_2}(2k_{F,\gamma},0) = \frac{1}{\sqrt{2L}}\sum_{k,\sigma,\sigma',l,l'} \psi^\dagger_{\gamma,-,l,\sigma}(k)\ (\sigma^{\sigma,\sigma'}_{\mu_1}\otimes M^{l,l'}_{\mu_2})\ \psi_{\gamma,+,l',\sigma'}(k+2k_{F,\gamma}), \tag{2.20}$$

$$\hat{O}^{dw}_{\gamma,\mu_1}(2k_{F,\gamma},2l\mathrm{L}_\gamma) = \frac{1}{\sqrt{L}}\sum_{k,\sigma,\sigma'} \psi^\dagger_{\gamma,-,l,\sigma}(k)\ \sigma^{\sigma,\sigma'}_{\mu_1}\ \psi_{\gamma,+,-l,\sigma'}(k+2k_{F,\gamma}), \tag{2.21}$$

$$\hat{O}^{sc}_{\gamma,\mu_1}(0,2l\mathrm{L}_\gamma) = \frac{1}{\sqrt{L}}\sum_{k,\sigma,\sigma'} \psi_{\gamma,-,l,\sigma}(-k)\ \tilde{\sigma}^{\sigma,\sigma'}_{\mu_1}\ \psi_{\gamma,+,l,\sigma'}(k), \tag{2.22}$$

$$\hat{O}^{sc}_{\gamma,\mu_1,\mu_2}(0,0) = \frac{1}{\sqrt{2L}}\sum_{k,\sigma,\sigma',l,l'} \psi_{\gamma,-,l,\sigma}(-k)\ (\tilde{\sigma}^{\sigma,\sigma'}_{\mu_1}\otimes \tilde{M}^{l,l'}_{\mu_2})\ \psi_{\gamma,+,l',\sigma'}(k), \tag{2.23}$$

$$\mu_1,\mu_2 = \pm,\ \mathrm{L}_\gamma = \hbar n_\gamma, \tag{2.24}$$

$$\sigma_\pm, M_\pm = \begin{pmatrix} 1 & 0 \\ 0 & \pm 1 \end{pmatrix},\ \tilde{\sigma}_\pm, \tilde{M}_\pm = \begin{pmatrix} 0 & 1 \\ \pm 1 & 0 \end{pmatrix}. \tag{2.25}$$

We have abbreviated density wave and superconductor as dw and sc in the superscript.

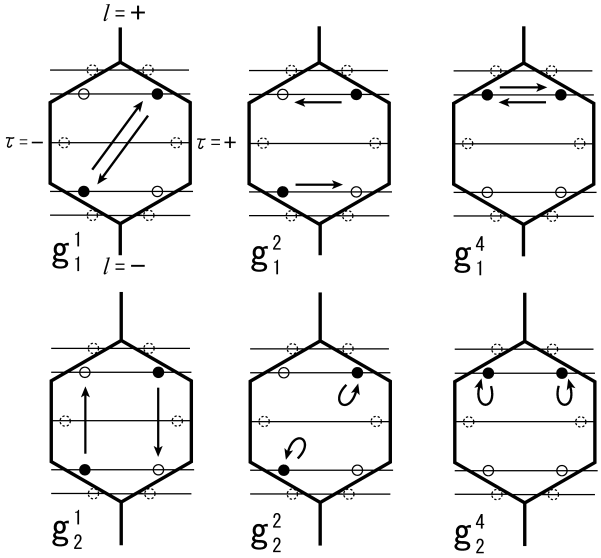

Figure 2.3: Six scattering processes in channels of group 2 are shown in momentum space when $(n_0, n_1, n_2) = (0, 3, 2)$. Hexagon represents the Brillouin zone.

μ_1 represents symmetry in spin space and μ_2 represents symmetry with respect to circumferential direction. We use + for symmetric orders and − for antisymmetric orders. Therefore $\mu_1 = +$ means CDW and TSC and $\mu_1 = -$ represents SDW and SSC. Scaling equations for these two-particle correlation functions have the same form as the first line in Eqs. (2.9)−(2.13). K_i for each orders can be calculated as

$$
\begin{aligned}
K^{\rm cdw}_{\mu_2}(0) &= (4\tilde{g}^4_1 - 2\tilde{g}^4_2) + \mu_2(4\tilde{g}^2_1 - 2\tilde{g}^1_2), && (2.26)\\
K^{\rm sdw}_{\mu_2}(0) &= -2(\tilde{g}^4_2 + \mu_2\tilde{g}^1_2), && (2.27)\\
K^{\rm cdw}(2ln_\gamma) &= 4\tilde{g}^1_1 - 2\tilde{g}^2_2, && (2.28)\\
K^{\rm sdw}(2ln_\gamma) &= -2\tilde{g}^2_2, && (2.29)\\
K^{\rm ssc}(2ln_\gamma) &= 2\tilde{g}^4_1 + 2\tilde{g}^4_2, && (2.30)\\
K^{\rm tsc}(2ln_\gamma) &= -2\tilde{g}^4_1 + 2\tilde{g}^4_2, && (2.31)\\
K^{\rm ssc}_{\mu_2}(0) &= (2\tilde{g}^1_1 + 2\tilde{g}^2_2) + \mu_2(2\tilde{g}^2_1 + 2\tilde{g}^1_2), && (2.32)\\
K^{\rm tsc}_{\mu_2}(0) &= (-2\tilde{g}^1_1 + 2\tilde{g}^2_2) + \mu_2(-2\tilde{g}^2_1 + 2\tilde{g}^1_2). && (2.33)
\end{aligned}
$$

By substituting the solution for Eqs. (2.14)−(2.19) into Eqs. (2.26)−(2.33), we obtain the temperature dependences of two-particle correlation functions. We then obtain the

phase diagram in coupling space by specifying the most divergent correlation function. The phase diagrams are shown in Fig. 2.4. If we assume that the bare values for couplings depend only on the momentum transfer, we can put "$\tilde{g}_1^2 = \tilde{g}_1^4 \equiv b$, $\tilde{g}_2^2 = \tilde{g}_2^4 \equiv f$" and get four independent parameters "$b, f, \tilde{g}_1^1, \tilde{g}_2^1$".

For the special case "$\tilde{g}_1^1 = \tilde{g}_2^1 = 0$", we can solve the Eqs. (2.14)−(2.19) exactly, and the solution is

$$\tilde{b}(x) = \frac{\tilde{b}(0)}{1 - 4\tilde{b}(0)x}, \tag{2.34}$$

$$\tilde{b}(x) - 4\tilde{f}(x) = \tilde{b}(0) - 4\tilde{f}(0). \tag{2.35}$$

When $\tilde{b}(0) < 0$, $\tilde{b}$ diverges at a finite temperature $T_c = E_c \exp(1/4\tilde{b}(0))$. In one dimension, such an anomaly at the finite temperature is an artifact of the one-loop approximation, and higher-order terms will shift it to $T = 0$. Nevertheless, this T_c suggests to us the temperature where the system crosses over from the weak-coupling to the strong-coupling regime.

The phase diagram for this special case is shown in Fig. 2.4 (a). In gapless phases, all the DWs and SCs are degenerate and have the same temperature dependence of the correlation function. The DW phase and the SC phase are separated by a phase boundary $b - 4f = 0$. In the gapful phase, only $\mathrm{CDW}_+(0)$ phase appears, where + and (0) represent the symmetry $\mu_2 = +$ and angular momentum $\mathrm{L} = 0$ respectively.

In general, $\tilde{g}_1^1$ and $\tilde{g}_2^1$ are some finite values, and other gapful phases emerge in the phase diagram as shown in Fig. 2.4 (b). The effect of $\tilde{f}$ on the phase diagram is negligible. Independent of the values of $\tilde{b}$ and $\tilde{f}$, there exist four gapful phases in which the most divergent order of each is $\mathrm{SSC}_+(0)$, $\mathrm{SSC}_-(0)$, $\mathrm{CDW}_+(0)$ and $\mathrm{CDW}_-(0)$ respectively. There is no gapless phase except for the original point $(\tilde{g}_1^1, \tilde{g}_2^1) = (0, 0)$ even when $\tilde{b} > 0$. Four gapful phases are characterized by the asymptotic behaviors of the couplings near a critical temperature T_c [63], which are given by

$$\tilde{g}_i^j = g_i^{j*}\Lambda/[1 + \Lambda x], \tag{2.36}$$

$$T_c = E_c \exp(-\Lambda^{-1}). \tag{2.37}$$

All the couplings are proportional to $\Lambda/[1+\Lambda x]$, which diverges at T_c given above. Sets of g_i^{j*} are universal in each phase as in [63], and are shown in Table 2.1. Eqs. (2.14)−(2.19) are invariant under the transformation $(\tilde{g}_1^2, \tilde{g}_2^1) \to (-\tilde{g}_1^2, -\tilde{g}_2^1)$. The two sets of solutions $(g_1^{1*}, g_1^{2*}, g_1^{4*}, g_2^{1*}, g_2^{2*}, g_2^{4*})$ and $(g_1^{1*}, -g_1^{2*}, g_1^{4*}, -g_2^{1*}, g_2^{2*}, g_2^{4*})$ correspond to two phases with different symmetry ($\mu_2 = \pm$) as seen in Table 2.1. The asymptotic solutions lead to

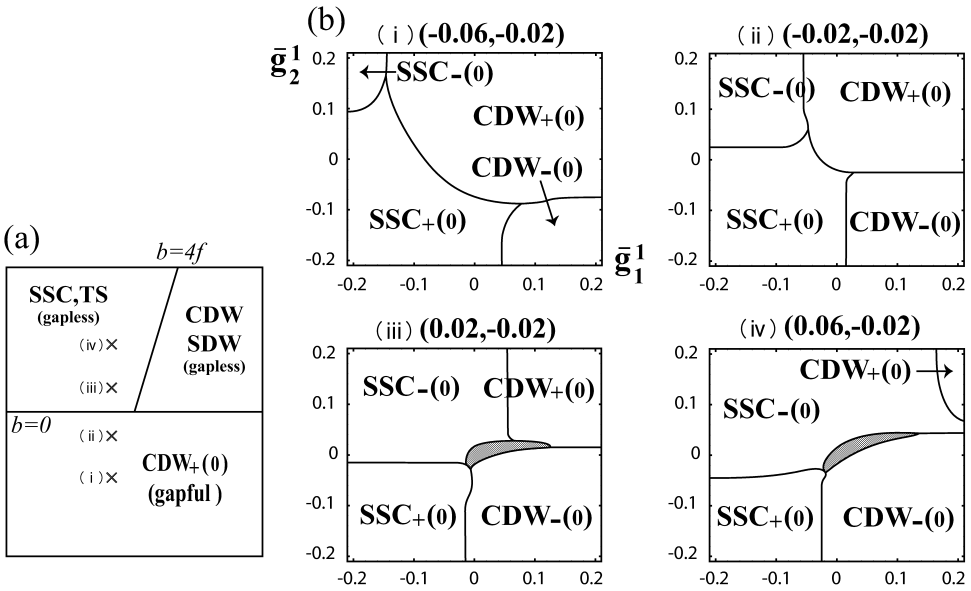

Figure 2.4: (a) Phase diagram for group 2 in $(\tilde{f}, \tilde{b})$ plane is exactly obtained for the special case $\tilde{g}_1^1 = \tilde{g}_2^1 = 0$. (b) Phase diagram for group 2 in $(\tilde{g}_1^1, \tilde{g}_2^1)$ plane. Fixed $(\tilde{b}, \tilde{f})$ values are shown above each diagram. In the shaded region [64], we cannot determine which two-particle correlation is the most divergent since couplings diverge at very low temperature.

the behaviors of two-particle correlations,

$$\chi_m \propto \left| \ln \frac{T}{T_c} \right|^{\alpha_m+1} \propto \left(\frac{1}{T - T_c} \right)^{-\alpha_m-1} , \tag{2.38}$$

where α_m determines the critical exponent for the two-particle correlation functions of type m and is calculated from the value of g_i^{j*} using $\alpha_m = K_m|_{\tilde{g}_i^j = g_i^{j*}}$. Correlation functions diverge at T_c if the exponents are positive, and are suppressed if they are negative. These exponents in each phase are listed in Table 2.2.

It can be seen from Table 2.1 that scattering processes with angular momentum transfer g_1^1 and g_2^1 are renormalized to 0 in the two CDW phases; on the other hand they are renormalized to large values in the two SSC phases. This means such scattering processes become strong attractions between electrons in a SC pair and give rise to divergence of SCC. We should note that all the dominant two-particle correlations in these channels carry zero angular momentum, though they have the same correlation function as two-

Table 2.1: Strong-coupling fixed-point parameters for each gapful phase in group 2

phase	g_1^{1*}	g_1^{2*}	g_1^{4*}	g_2^{1*}	g_2^{2*}	g_2^{4*}
$CDW_+(0)$	0	-1/4	-1/4	0	-1/16	-1/16
$CDW_-(0)$	0	1/4	-1/4	0	-1/16	-1/16
$SSC_+(0)$	-1/4	-1/4	0	-1/4	-3/16	1/16
$SSC_-(0)$	-1/4	1/4	0	1/4	-3/16	1/16

Table 2.2: Exponents $-(\alpha_m + 1)$ in group 2

phase	$CDW_+(0)$ $SSC_+(0)$	$CDW_-(0)$ $SSC_-(0)$	$CDW(2L_\gamma)$ $SSC(2L_\gamma)$	$SDW_+(0)$ $TSC_+(0)$	$SDW_-(0)$ $TSC_-(0)$	$SDW(2L_\gamma)$ $TSC(2L_\gamma)$
$CDW_+(0)$	7/8	-9/8	-9/8	-9/8	-9/8	-9/8
	-3/8	-11/8	-3/8	-11/8	-3/8	-11/8
$CDW_-(0)$	-9/8	7/8	-9/8	-9/8	-9/8	-9/8
	-11/8	-3/8	-3/8	-3/8	-11/8	-11/8
$SSC_+(0)$	-3/8	-11/8	-3/8	-11/8	-3/8	-11/8
	7/8	-9/8	-9/8	-9/8	-9/8	-9/8
$SSC_-(0)$	-11/8	-3/8	-3/8	-3/8	-11/8	-11/8
	-9/8	7/8	-9/8	-9/8	-9/8	-9/8

particle correlation with angular momentum $\pm 2\hbar n_\gamma$ in the non-interacting case. Only one type of two-particle correlation diverges and all others are suppressed in every phase.

We see from the numerical calculations that T_c exponentially depends on backscatterings $\tilde{b}$ and T_c becomes higher with negative large $\tilde{b}$. However T_c will be quickly suppressed in case of positive $\tilde{b}$. Therefore, a phase transition can occur at 15K in these channels only when the backscatterings $\tilde{b}$ are attracting forces. However, T_c tends to be higher than that of group 1's for two reasons; (i) double degeneracy of opposite angular momenta and (ii) smaller curvature of the bands ($v_{F,1} \sim v_{F,2} = 2.8 \times 10^5\ m/s < v_{F,0} = 6.9 \times 10^5\ m/s$) result in the large density of states compared to that for band 1.

2.3.3 Group 3

This channel has six independent scattering processes shown in Fig. 2.5. Scaling equations for these six couplings are

$$
\begin{aligned}
(\tilde{g}_1^1)' &= 2(\tilde{g}_1^1)^2 - 2\tilde{g}_1^3\tilde{g}_2^3, && (2.39)\\
(\tilde{g}_1^3)' &= (4\tilde{g}_1^1 + 2\tilde{g}_2^4 - 2\tilde{g}_2^2)\tilde{g}_1^3 + (2\tilde{g}_1^4 - 2\tilde{g}_1^1)\tilde{g}_2^3, && (2.40)\\
(\tilde{g}_1^4)' &= 2(\tilde{g}_1^4)^2 + 2\tilde{g}_1^3\tilde{g}_2^3, && (2.41)\\
(\tilde{g}_2^2)' &= (\tilde{g}_1^1)^2 - (\tilde{g}_2^3)^2, && (2.42)\\
(\tilde{g}_2^3)' &= 2\tilde{g}_1^3\tilde{g}_1^4 + (2\tilde{g}_2^4 - 2\tilde{g}_2^2)\tilde{g}_2^3, && (2.43)\\
(\tilde{g}_2^4)' &= (\tilde{g}_1^3)^2 + (\tilde{g}_1^4)^2 + (\tilde{g}_2^3)^2, && (2.44)
\end{aligned}
$$

where $\tilde{g}_i^j = g_i^j/\pi(v_{F,1} + v_{F,2})$ in Eq. (2.36) are normalized scattering amplitudes. All couplings are scaled to large values except for the case $\tilde{g}_1^3 = \tilde{g}_2^3 = 0$. This suggests that the channel from group 3 tends to produce gapful phases when it contains Umklapp processes $\tilde{g}_1^3, \tilde{g}_2^3$.

There are twelve types of two-particle correlations:

$$\hat{O}^{dw}_{\mu_1}(q_3^+, l\mathrm{L}^-) = \frac{1}{\sqrt{L}} \sum_{k,\sigma,\sigma'} \psi^\dagger_{2,-,l,\sigma}(k)\ \sigma^{\sigma,\sigma'}_{\mu_1}\ \psi_{1,+,l,\sigma'}(k + q_3^+), \tag{2.45}$$

$$\hat{O}^{dw}_{\mu_1,\mu_2}(q_3^+, \mathrm{L}^+) = \frac{1}{\sqrt{2L}} \sum_{k,\sigma,\sigma',l,l'} \psi^\dagger_{2,-,l,\sigma}(k)\ (\sigma^{\sigma,\sigma'}_{\mu_1} \otimes \tilde{M}^{l,l'}_{\mu_2})\ \psi_{1,+,l',\sigma'}(k + q_3^+), \tag{2.46}$$

$$\hat{O}^{sc}_{\mu_1}(q_3^-, \mathrm{L}^+) = \frac{1}{\sqrt{2L}} \sum_{k,\sigma,\sigma',l,l'} \psi_{2,-,l,\sigma}(q_3^- - k)\ (\tilde{\sigma}^{\sigma,\sigma'}_{\mu_1} \otimes M^{l,l'}_{\mu_2})\ \psi_{1,+,l',\sigma'}(k), \tag{2.47}$$

$$\hat{O}^{sc}_{\mu_1,\mu_2}(q_3^-, l\mathrm{L}^-) = \frac{1}{\sqrt{L}} \sum_{k,\sigma,\sigma'} \psi_{2,-,-l,\sigma}(q_3^- - k)\ \tilde{\sigma}^{\sigma,\sigma'}_{\mu_1}\ \psi_{1,+,l,\sigma'}(k). \tag{2.48}$$

We use symbols $\sigma_{\mu 1}, \tilde{\sigma}_{\mu 1}, M_{\mu 2}$ and $\tilde{M}_{\mu 2}$ which are the same as the ones in Eq. (2.25). Two-particle correlations carry momentum in the axis direction $q_3^\pm = k_{F,1} \pm k_{F,2}$. They carry angular momentum L^+ or L^-, where $\mathrm{L}^+ = \hbar(n_1 + n_2) = 5\hbar$ and $\mathrm{L}^- = \hbar(n_1 - n_2)$. The Umklapp processes induce the transition between the two-particle correlation with $-\mathrm{L}^+$ and the two-particle correlation with L^+ in the first order correction, therefore bonding or anti-bonding states are formed. In other words, $\tilde{g}_1^3$ and $\tilde{g}_2^3$ produce the symmetric or anti-symmetric states with respect to the inversion of circumferential direction.

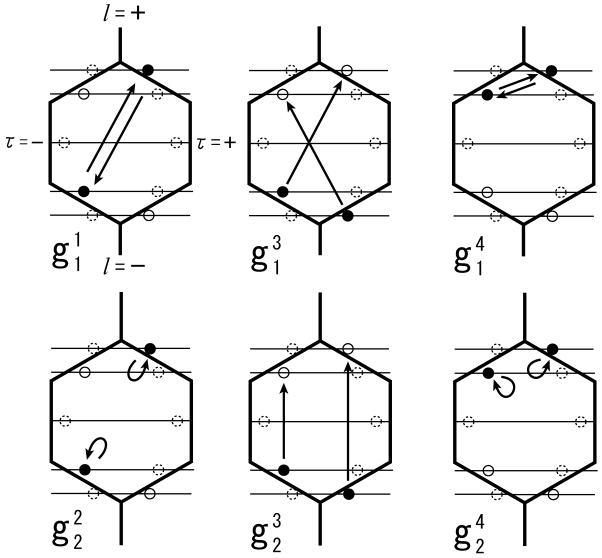

Figure 2.5: Six scattering processes in channels of group 3 are shown in momentum space when $(n_0, n_1, n_2) = (0, 3, 2)$. Hexagon represents the Brillouin zone.

K_i in the scaling equations for these two-particle correlation functions are given by

$$K^{\rm cdw}(\mathrm{L}^-) = 4\tilde{g}_1^4 - 2\tilde{g}_2^4, \tag{2.49}$$
$$K^{\rm sdw}(\mathrm{L}^-) = -2\tilde{g}_2^4, \tag{2.50}$$
$$K^{\rm cdw}_{\mu_2}(\mathrm{L}^+) = (4\tilde{g}_1^1 - 2\tilde{g}_2^2) + \mu_2(4\tilde{g}_1^3 - 2\tilde{g}_2^3), \tag{2.51}$$
$$K^{\rm sdw}_{\mu_2}(\mathrm{L}^+) = -2(\tilde{g}_2^2 + \mu_2\tilde{g}_2^3), \tag{2.52}$$
$$K^{\rm ssc}_{\mu_2}(\mathrm{L}^+) = (2\tilde{g}_1^4 + 2\tilde{g}_2^4) + \mu_2(2\tilde{g}_1^3 + 2\tilde{g}_2^3), \tag{2.53}$$
$$K^{\rm tsc}_{\mu_2}(\mathrm{L}^+) = (-2\tilde{g}_1^4 + 2\tilde{g}_2^4) + \mu_2(-2\tilde{g}_1^3 + 2\tilde{g}_2^3), \tag{2.54}$$
$$K^{\rm ssc}(\mathrm{L}^-) = 2\tilde{g}_1^1 + 2\tilde{g}_2^2, \tag{2.55}$$
$$K^{\rm tsc}(\mathrm{L}^-) = -2\tilde{g}_1^1 + 2\tilde{g}_2^2. \tag{2.56}$$

If we have $\tilde{g}_1^3 = \tilde{g}_2^3 = 0$ initially, these equations can be solved and phase diagram becomes

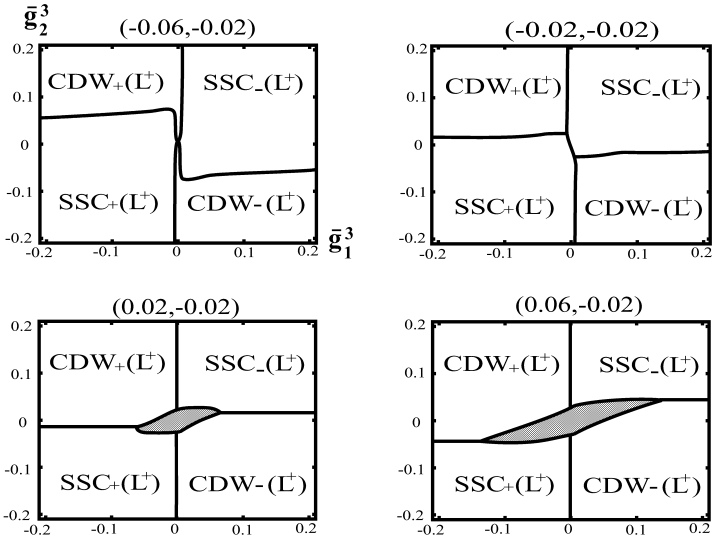

Figure 2.6: Phase diagram for group 3 in $(\tilde{g}_1^3, \tilde{g}_2^3)$ plane. Fixed $(\tilde{b}, \tilde{f})$ values are shown above each diagram. In the shaded region, we cannot determine which two-particle correlation is the most divergent since couplings diverge only at very low temperatures, where our calculation becomes less reliable.

equivalent to that of group 1. In this case scaling equations $(-)$ are reduced to

$$(\tilde{g}_1^1)' = 2(\tilde{g}_1^1)^2, \tag{2.57}$$
$$(\tilde{g}_2^2)' = (\tilde{g}_1^1)^2, \tag{2.58}$$
$$(\tilde{g}_1^4)' = 2(\tilde{g}_1^4)^2, \tag{2.59}$$
$$(\tilde{g}_2^4)' = (\tilde{g}_1^4)^2. \tag{2.60}$$

$\tilde{g}_1^1$ and $\tilde{g}_1^4$ diverge at the different temperatures $T_c = E_c \exp(1/2\tilde{g}_1^1)$ and $T_c' = E_c \exp(1/2\tilde{g}_1^4)$ respectively. Gapless phases appear for $\tilde{g}_1^1, \tilde{g}_1^4 > 0$, and gapful phases appear for $\tilde{g}_1^1, \tilde{g}_1^4 < 0$.

By solving $(-)$ and $(-)$ numerically, we obtain phase diagrams (Fig. 2.6) for the case where Umklapp processes have some finite value $(\tilde{g}_1^3, \tilde{g}_2^3 \neq 0)$.

We have taken $\tilde{g}_1^1 = \tilde{g}_1^4 = \tilde{b}$ and $\tilde{g}_2^2 = \tilde{g}_2^4 = \tilde{f}$ for simplicity. The effect of $\tilde{f}$ on the phase diagram is negligible. Independent of $\tilde{b}, \tilde{f}$ values, phase diagram mainly consists of four large gapful regions $\{\mathrm{CDW}_\pm(\mathrm{L}^+), \mathrm{SSC}_\pm(\mathrm{L}^+)\}$, and there is no gapless phase when we have non-zero Umklapp processes $(\tilde{g}_1^3, \tilde{g}_2^3)$. These gapful phases are characterized by the asymptotic solutions Eqs. (2.36) and (2.38) as well as in group 2. We show the values of g_i^{j*} in Table 2.3, and exponents $-(\alpha_m + 1)$ in Table 2.4. Equations $(-)$ are invariant under

Table 2.3: Strong coupling fixed point parameters for each gapful phase in group 3

phase	g_1^{1*}	g_1^{3*}	g_1^{4*}	g_2^{2*}	g_2^{3*}	g_2^{4*}
$\mathrm{CDW}_+(\mathrm{L}^+)$	-0.1258	-0.4219	0.0810	-0.0034	0.1116	-0.1970
$\mathrm{CDW}_-(\mathrm{L}^+)$	-0.1258	0.4219	-0.0810	-0.0034	-0.1116	-0.1970
$\mathrm{SSC}_+(\mathrm{L}^+)$	0.1026	-0.2302	-0.2764	0.0616	-0.2685	-0.2015
$\mathrm{SSC}_-(\mathrm{L}^+)$	0.1026	0.2302	-0.2764	0.0616	0.2685	-0.2015

Table 2.4: Exponents $-(\alpha_m + 1)$ in group 3

phase	$\mathrm{CDW}_+(\mathrm{L}^+)$ $\mathrm{SSC}_+(\mathrm{L}^+)$	$\mathrm{CDW}_-(\mathrm{L}^+)$ $\mathrm{SSC}_-(\mathrm{L}^+)$	$\mathrm{CDW}(\mathrm{L}^-)$ $\mathrm{SSC}(\mathrm{L}^-)$	$\mathrm{SDW}_+(\mathrm{L}^+)$ $\mathrm{TSC}_+(\mathrm{L}^+)$	$\mathrm{SDW}_-(\mathrm{L}^+)$ $\mathrm{TSC}_-(\mathrm{L}^+)$	$\mathrm{SDW}(\mathrm{L}^-)$ $\mathrm{TSC}(\mathrm{L}^-)$
$\mathrm{CDW}_+(\mathrm{L}^+)$	1.407	-2.414	-1.718	-0.784	-1.230	-1.394
	-0.147	-1.389	-0.742	-1.511	0.623	-1.245
$\mathrm{CDW}_-(\mathrm{L}^+)$	-2.414	1.407	-1.718	-1.230	-0.784	-1.394
	-1.389	-0.147	-0.742	0.623	-1.511	-1.245
$\mathrm{SSC}_+(\mathrm{L}^+)$	-0.903	-1.671	-0.297	-1.414	-0.340	-1.403
	0.953	-1.042	-1.328	-1.073	-1.227	-0.918
$\mathrm{SSC}_-(\mathrm{L}^+)$	-1.671	-0.903	-0.297	-0.340	-1.414	-1.403
	-1.042	0.953	-1.328	-1.227	-1.073	-0.918

a transformation $(\tilde{g}_1^3, \tilde{g}_2^3) \to (-\tilde{g}_1^3, -\tilde{g}_2^3)$. The two solutions $(g_1^{1*}, g_1^{3*}, g_1^{4*}, g_2^{2*}, g_2^{3*}, g_2^{4*})$ and $(g_1^{1*}, -g_1^{3*}, g_1^{4*}, g_2^{2*}, -g_2^{3*}, g_2^{4*})$ correspond to two phases with different symmetry ($\mu_2 = \pm$) as seen from Table 2.3.

In $\mathrm{CDW}_{\mu_2}(\mathrm{L}^+)$ phase, the correlation function for both $\mathrm{CDW}_{\mu_2}(\mathrm{L}^+)$ and $\mathrm{TSC}_{-\mu_2}(\mathrm{L}^+)$ diverges at T_c and all others are suppressed. Correlation function for $\mathrm{SSC}_{\mu_2}(\mathrm{L}^+)$ alone diverges in $\mathrm{SSC}_{\mu_2}(\mathrm{L}^+)$ phase. Every divergent two-particle correlations carry angular momentum $\mathrm{L}^+ = 5\hbar$. Umklapp processes $(\tilde{g}_1^3, \tilde{g}_2^3)$ are scaled toward large values in any case, which implies that they play an important role for two-particle correlations with angular momentum L^+ to develop. T_c is exponentially dependent on the value of backscatterings $\tilde{b}$ as in the case of group 2. When $\tilde{b} > 0$, the T_c is suppressed to a very small energy scale. This seems to be a trace of the gapless phase in the special case $\tilde{g}_1^3 = \tilde{g}_2^3 = 0$. When $\tilde{b} < 0$, however, T_c will be higher than that of the gapful phase in group 1 for the same reason stated in group 2.

2.4 Summary

We have discussed possible phase transitions in (5,0) CNs, which are quasi one-dimensional systems with angular momentum, by evaluating the most divergent two-particle correlation function.

We have found new types of superconducting phases, where a Cooper pair carries non-zero angular momentum and Umklapp processes play significant roles. All other dominant two-particle correlations are singlet-superconducting or charge-density wave with zero or $5\hbar$ angular momentum, which are caused by backscattering or Umklapp scattering. Back scatterings in the circumferential direction strengthen the correlation between electrons with opposite angular momentum and produce the divergent two-particle correlation with zero angular momentum. On the other hand Umklapp processes strengthen the correlation between electrons with angular momentum in the same direction, and produce the divergent two-particle correlation with angular momentum.

The critical temperature T_c evaluated from the RG equations become quite low with repulsive interactions between electrons. So we need a large reduction of Coulomb interactions or strong attractions by electron-phonon interactions for the phase transition to occur at 15K. However, in group 2 and 3, T_c will be higher than that of group 1 because they have higher density of states at Fermi level. Therefore it seems that group 2 and group 3 play a critical role in the superconductivity observed in (5,0) CN. Recent works [41, 62] have shown that the acoustic-phonon exchanges result in strong attractive interactions in nanotubes with smaller diameters. Thus, there may be some possibility of understanding the unusually high transition temperature (15K) with our result.

In our study we have not considered the effects of pair-tunneling processes such as $\{(\gamma, \pm\tau), (\gamma, \mp\tau)\} \rightarrow \{(\gamma', \pm\tau), (\gamma', \mp\tau)\}$. Such processes are known to be important for the formation of SCC in (n, n) CNs [55, 57, 58] and in two- and three-leg ladder systems [65] as well. Therefore it is also important to study the effects of pair-tunneling processes. However things will be more difficult since the pair-tunneling processes will mix with the two-particle correlations in all channels and we cannot treat the three groups independently. Effects of the pair-tunneling processes are discussed in details in a recent publication by Ganzalez *et al.* [66].

Chapter 3

Spin-Charge Mixing Effects in Polarized TL Liquid

3.1 Introduction

Spin-charge separation and interaction dependent power-laws of correlation functions have been known as non-Fermi-liquid behavior of Tomonaga-Luttinger (TL) liquid, which is expected to describe the low energy physics of one-dimensional interacting electron systems [20]. In the past ten years, experimental evidences for the realization of TL states have been reported in many systems such as carbon nanotube devices [14, 67, 68], quantum wires in semiconductor heterostructures [10, 11] and fractional quantum Hall systems [69, 70], as predicted by theories [71, 72]. The power-law temperature dependencies of the tunneling density of states [67, 68, 69, 70], and the bulk spectral density near the Fermi level [73] have been the key signatures of TL states in these experiments. On the other hand, there are only a few experiments on the direct observation of spin-charge separation [74, 75]. In order to obtain such low energy spectral profiles, we need to resolve local density of states in large distances from a scatterer or a boundary edge, by scanning tunneling microscope (STM) [75], which seems rather difficult to obtain high resolution data. Instead, experiments on resonant tunneling [14, 76, 77] seems to be a more suitable procedure to detect the spin-charge separation, since they probe the energy level spacings in the quantum island.

The resonant tunneling in TL liquid has been studied for more than a decade since Kane and Fisher's work [43, 45]. The charge transport is a main focus in their work. Meanwhile, the spin transport in presence of external magnetic field, which is closely linked to detecting spin-charge separation, has not been studied enough. There are some

theoretical works concerned with this issue [79, 80, 81]. They consider the quantum wire forms the quantum dot between ferromagnetic contacts. There the spin and the charge transport can be controlled by the relative angle between the magnetization orientations of the ferromagnets [80]. In their results, the qualitative change due to the spin-charge separation can be seen. However, the quantitative determination of the spin-charge separation in the excitation spectrum seems to be difficult.

In this chapter, we study the resonant tunneling through double impurities in a spinful TL liquid under magnetic fields [50, 51]. A schematic picture of the system is shown in Fig. 3.1; a strong field B is applied to the entire one-dimensional system. The charge and the spin in the region between double impurities are changed by a gate voltage $V_{\rm g}$ and a weak field $B_{\rm g}$, respectively. Applying a strong magnetic field breaks the spin rotational symmetry and violate spin-charge separation in the spectral peaks [82], due to the Fermi velocity differences between two spins. As a result, the spin and the charge sector mix with each other [46, 47]. It is shown that the spin-charge mixing effects can clearly be seen in the resonant oscillation patterns of zero bias conductance in $(V_{\rm g}, B_{\rm g})$ plane. The spin dependent scaling behavior of a single impurity potential, due to Zeeman effect, has been discussed by previous works [47, 48, 49, 52]. We also discuss a spin-charge mixing effects on the impurity scaling in the resonant tunneling.

Zero bias conductance is calculated by standard bosonization technique [43, 45, 78] as a function of a gate voltage, gate magnetic field, temperature T and the strong magnetic field. The impurity potential $V(x) = V\left(\delta(x-d) + \delta(x+d)\right)$ is assumed to be either very weak ($V/v_{\rm F} \ll 1$) or very strong ($V/v_{\rm F} \gg 1$). When $B \neq 0$, changing the gate voltage does affect the spin density together with the charge density due to the spin-charge mixing, leading to noticeable deformation in the lattice pattern of the conductance peaks [50]. Moreover contour shapes at low temperatures are divided into three types, depending on the bulk parameters such as B, interaction parameters $K_{\rho,s}$, where the impurity potentials are scaled towards "perfect reflection", "perfect transmission" and magnetic field induced "spin-filtering", respectively. These three behaviors are explained by a renormalization group (RG) analysis of a single impurity potential in spin-charge mixed systems.

3.2 Tomonaga-Luttinger Liquid under a Magnetic Field

We consider a system illustrated in Fig. 3.1. An infinite TL liquid, under a strong magnetic field $\overrightarrow{B}$ perpendicular to the wire, has two impurities (or barriers) of the strength V at $x = \pm d$. Hereafter we take the spin quantization axis in the direction of $\overrightarrow{B}$, and denote the strength of $\overrightarrow{B}$ by $B \equiv |\overrightarrow{B}|$. Zeeman effect due to B is incorporated into Hamiltonian as the difference in Fermi velocity between two spin species. For simplicity,

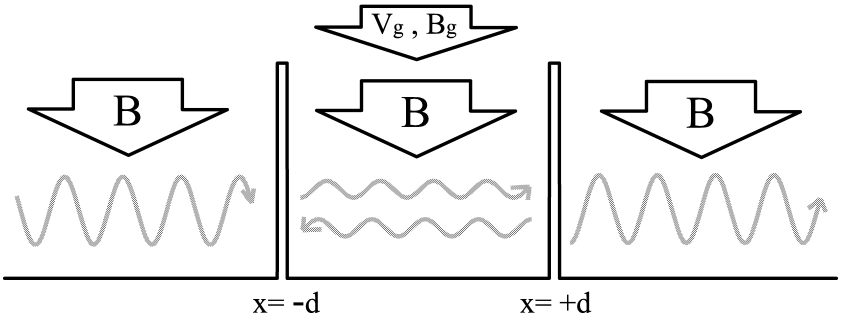

Figure 3.1: Schematic figure of spin polarized Tomonaga-Luttinger liquid with two impurities under magnetic field.

we take into account the Zeeman effect only on spins with neglecting the orbital effects. This is allowed when the magnetic length $l_{\rm B} = \sqrt{1/eB}$ is longer than a width of the TL wire, as discussed in [83]. In the effective mass approximation $\varepsilon = k^2/2m^*$, the velocity difference is given by,

$$2\Delta = v_{\rm F}(\sqrt{1 + \frac{g\mu_B B}{2\varepsilon_{\rm F}}} - \sqrt{1 - \frac{g\mu_B B}{2\varepsilon_{\rm F}}}). \tag{3.1}$$

For not too strong fields, Δ is approximately linear in B. For simplicity, we set $v_\sigma = v_{\rm F} + \sigma\Delta$, where the sign $\sigma = +(-)$ represents up (down) spin. We shall call the region $-d < x < d$ an island. In the island, chemical potential of spin σ electrons can be controlled by gate voltage $V_{\rm g}$ and gate magnetic field $B_{\rm g}$; $\delta\mu_\sigma = -eV_{\rm g} + \sigma\frac{g\mu_B}{2}B_{\rm g}$. We consider the situation where Zeeman energies due to strong magnetic field B and due to gate magnetic field $B_{\rm g}$ are, respectively, on the order of Fermi energy and energy level spacing in the island; i.e. $\varepsilon_{\rm F} \geq \frac{g\mu_B B}{2} \gg \frac{g\mu_B B_{\rm g}}{2} \sim v_{\rm F}\frac{2\pi}{2d}$. Then the Fermi velocity change due to $B_{\rm g}$ can be neglected.

The Hamiltonian of the system consists of four parts,

$$H \equiv H_0 + H_{\rm int} + H_{\rm island} + H_{\rm b} \ , \tag{3.2}$$

where $H_0, H_{\rm int}, H_{\rm island}$ and $H_{\rm b}$ are the Hamiltonian for free electrons, two-body interaction, electrons on the island, and barrier potential, respectively. They are given in terms of the

fermion field operators,

$$H_0 = \sum_\sigma \frac{v_\sigma}{i} \int dx \left[\psi^\dagger_{+,\sigma}\partial_x\psi_{+,\sigma} - \psi^\dagger_{-,\sigma}\partial_x\psi_{-,\sigma}\right], \tag{3.3}$$

$$H_{\rm int} = \frac{1}{2}\sum_{\sigma,\sigma'} \int dxdy\ n_\sigma(x)\mathcal{U}_{\sigma,\sigma'}(x-y)n_{\sigma'}(y), \tag{3.4}$$

$$H_{\rm island} = \int_{-d}^{d} dx \left[-eV_{\rm g}\left(\sum_\sigma n_\sigma\right) + \frac{1}{2}g\mu_B\overrightarrow{B_{\rm g}}\cdot(\psi^\dagger_\alpha\vec{\sigma}_{\alpha,\beta}\psi_\beta)\right], \tag{3.5}$$

$$H_{\rm b} = V\sum_\sigma \left[n_\sigma(-d) + n_\sigma(d)\right], \tag{3.6}$$

where $\psi_\sigma \equiv \psi_{+,\sigma}e^{ik_{{\rm F},\sigma}x} + \psi_{-,\sigma}e^{-ik_{{\rm F},\sigma}x}$ and $n_\sigma = \psi^\dagger_\sigma\psi_\sigma$ are the annihilation operator and the density operator for electrons with spin σ. We neglect the charging energy of the island (U in [45]), which can be incorporated into $H_{\rm int}$. $H_0 + H_{\rm int}$ are written in terms of bosonic phase fields [20],

$$\begin{aligned} H_0 + H_{\rm int} &= \sum_{i=\rho,s}\frac{\pi v_i}{2}\int dx\left[K_i^{-1}(\frac{1}{\pi}\partial_x\phi_i)^2 + K_i\Pi_i^2\right] \\ &\quad +\pi\Delta\int dx\left[(\frac{1}{\pi}\partial_x\phi_\rho)(\frac{1}{\pi}\partial_x\phi_s) + \Pi_\rho\Pi_s\right], \end{aligned} \tag{3.7}$$

Here, a is the inverse of the Fermi wave number: ϕ_i and Π_i are conjugate pairs of bosonic field with commutation relations $[\phi_i(x), \Pi_j(x')] = i\delta_{i,j}\delta(x-x')$, where $i = \rho$ (s) represent charge (spin) variables.

To diagonalize $H_0 + H_{\rm int}$, we use the linear transformation [47, 48] (see also Appendix B for the expression in ladder operators of TL bosons)

$$\begin{pmatrix}\phi_\rho\\ \phi_s\end{pmatrix} = \begin{pmatrix}\cos\alpha & -\frac{1}{y}\sin\alpha\\ y\sin\alpha & \cos\alpha\end{pmatrix}\begin{pmatrix}\tilde{\phi}_\rho\\ \tilde{\phi}_s\end{pmatrix}, \tag{3.8}$$

$$\begin{pmatrix}\Pi_\rho\\ \Pi_s\end{pmatrix} = \begin{pmatrix}\cos\alpha & -y\sin\alpha\\ \frac{1}{y}\sin\alpha & \cos\alpha\end{pmatrix}\begin{pmatrix}\tilde{\Pi}_\rho\\ \tilde{\Pi}_s\end{pmatrix}. \tag{3.9}$$

Commutation relations are preserved under this transformation $[\tilde{\phi}_i(x), \tilde{\Pi}_j(x')] = i\delta_{i,j}\delta(x-x')$. Parameters α and y are, respectively, a rotation angle and a scale factor in "spin-

charge space" given by,

$$y = \sqrt{\frac{v_\rho K_\rho^{-1} + v_s K_s}{v_\rho K_\rho + v_s K_s^{-1}}}, \tag{3.10}$$

$$\tan 2\alpha = \frac{2\Delta}{v_\rho K_\rho y - v_s K_s y^{-1}}. \tag{3.11}$$

The rotation angle α is proportional to Δ, and thus to B, for small Δ. After the transformation, $H_{\rm TL} \equiv H_0 + H_{\rm int}$ becomes,

$$H_{\rm TL} = \sum_{i=\rho,s} \frac{\pi \tilde{v}_i}{2} \int dx \left[\tilde{K}_i^{-1} (\frac{1}{\pi} \partial_x \tilde{\phi}_i)^2 + \tilde{K}_i \tilde{\Pi}_i^2 \right]. \tag{3.12}$$

The expression of $\tilde{v}_i$ and $\tilde{K}_i$ are given in Appendix A.

As discussed in [47, 48, 52, 49], in a polarized TL liquid, the scaling dimensions of a single impurity potential split between two spins. Renormalization group equations for small backscattering amplitude V_σ and small tunneling amplitude t_σ are given

$$\frac{dV_\sigma}{dl} = (1 - \frac{\eta_\sigma}{2}) V_\sigma \quad \text{for} \quad V_\sigma \ll v_{\rm F}, \tag{3.13}$$

$$\frac{dt_\sigma}{dl} = (1 - \frac{\lambda_\sigma}{2}) t_\sigma \quad \text{for} \quad V_\sigma \gg v_{\rm F}, \tag{3.14}$$

with $l = \ln \Lambda/\Lambda'$ and an initial (running) energy cutoff Λ (Λ'). The scaling dimensions η_σ and λ_σ are given by

$$\eta_\sigma = \tilde{K}_\rho B_{\rho,\sigma}^2 + \tilde{K}_s B_{s,\sigma}^2, \tag{3.15}$$

$$\lambda_\sigma = \tilde{K}_\rho^{-1} D_{\rho,\sigma}^2 + \tilde{K}_s^{-1} D_{s,\sigma}^2. \tag{3.16}$$

where $B_{\rho,\sigma} = \cos\alpha + \sigma y \sin\alpha$, $B_{s,\sigma} = -y^{-1}\sin\alpha + \sigma\cos\alpha$, $D_{\rho,\sigma} = \cos\alpha + \sigma y^{-1}\sin\alpha$, and $D_{s,\sigma} = \sigma\cos\alpha - y\sin\alpha$. Thus the ratio of reflection amplitudes and tunneling amplitudes scale like, respectively, $V_\uparrow/V_\downarrow \propto (T/\Lambda)^{\frac{\eta_\uparrow - \eta_\downarrow}{2}}$ and $t_\uparrow/t_\downarrow \propto (T/\Lambda)^{\frac{\lambda_\uparrow - \lambda_\downarrow}{2}}$. The differences of the exponents $\delta\eta = (\eta_\uparrow - \eta_\downarrow)/2$ and $\delta\lambda = (\lambda_\uparrow - \lambda_\downarrow)/2$ are given by

$$\delta\eta = (\tilde{K}_\rho y - \tilde{K}_s y^{-1}) \sin 2\alpha, \tag{3.17}$$

$$\delta\lambda = \frac{\tilde{K}_s y^{-1} - \tilde{K}_\rho y}{\tilde{K}_\rho \tilde{K}_s} \sin 2\alpha. \tag{3.18}$$

This expression tells us that the split of the scaling dimensions between two spins become large when the spin-charge mixing angle is large. Due to the split of exponents, we expect

the spin current with large polarization $P = \frac{t_\uparrow - t_\downarrow}{t_\uparrow + t_\downarrow}$ at low temperature in the strong barrier limit. This scaling effect with the exponents η_σ and λ_σ also appears in the conductance for double barrier structure.

3.3 Weak Barrier Limit ($V \to 0$)

We consider first the weak barrier limit $V \to 0$, where the electron transfer is due to the coherent tunneling of the spin-charge mixed density wave. The zero bias conductance is calculated perturbatively with respect to the small barrier potential $\frac{V}{\pi a}$. The Hamiltonian for the island and for the barriers in Eq. (3.5) and Eq. (3.6) are written in terms of the bosonic phase at $x = \pm d$,

$$H_{\rm island} = \frac{-2eV_g}{\pi}\theta_\rho^- + \frac{g\mu_B B_g}{\pi}\theta_s^-, \tag{3.19}$$

$$H_{\rm b} = \frac{V}{\pi a}\sum_{\sigma=\pm}\sin(\theta_\rho^+ + \sigma\theta_s^+)\cos(2k_{{\rm F},\sigma}d + \theta_\rho^- + \sigma\theta_s^-). \tag{3.20}$$

$\theta_i^\pm = (\phi_i(d) \pm \phi_i(-d))/\sqrt{2}$ is the linear combination of phases at $x = \pm d$. According to our assumption that the magnetic field B is strong enough that $(k_{{\rm F},\uparrow} - k_{{\rm F},\downarrow})d \gg \pi$, only z-component of $\overrightarrow{B_{\rm g}}$ remains after the integration of (3.5) with neglecting the fast oscillating terms. Hereafter, we denote $(\overrightarrow{B_{\rm g}})_{\rm z}$ by $B_{\rm g}$.

To make calculations easier, it is helpful to construct an effective action [42] obtained by integrating out the TL field except for the positions of the barriers $x = \pm d$, since charge (spin) current through barriers depends only on the local variables, $j_{\rho(s)} = (2/\pi)\partial_t\theta^+_{\rho(s)}$. The integrated effective action is calculated as,

$$S_{\rm eff} = \sum_{\omega_n, j=\pm, i=\rho,s}\tilde{\epsilon}_i^j(\omega_n)\tilde{\theta}_i^j(\omega_n)\tilde{\theta}_i^j(-\omega_n) + \int_0^\beta d\tau\left[H_{\rm island} + H_{\rm b}\right], \tag{3.21}$$

$$\tilde{\epsilon}_i^\pm(\omega_n) = \frac{1}{\pi\tilde{K}_i}\frac{|\omega_n|}{1 \pm \exp\{-(2d/\tilde{v}_i)|\omega_n|\}}. \tag{3.22}$$

Here we have defined new variables $\tilde{\theta}_i^\pm \equiv (\tilde{\phi}_i(d) \pm \tilde{\phi}_i(-d))/\sqrt{2}$. $\tilde{\theta}$ and θ are related to each other by the same linear transformation between $\tilde{\phi}$ and ϕ. We will calculate zero bias conductance for charge (spin) current following Kubo formula,

$$G_{\rho(s)} = \lim_{\omega\to 0}\frac{2e^2}{\omega_n}\left\langle j_{\rho(s)}(x,\omega_n)j_\rho(y,-\omega_n)\right\rangle\Big|_{i\omega_n=\omega+i\delta}, \tag{3.23}$$

where analytic continuation is to be taken before taking the limit. The effective action $S_{\rm eff}$ is used for taking thermal average such that

$$\langle A \rangle = \frac{\int \prod_{i,j} D\tilde{\theta}_i^j A \exp\{-S_{\rm eff}\}}{\int \prod_{i,j} D\tilde{\theta}_i^j \exp\{-S_{\rm eff}\}} \ . \tag{3.24}$$

Hamiltonian for the island $H_{\rm island}$ is given after canonical transformation Eq. (3.8) and Eq. (3.9) as

$$H_{\rm island} \ = \ A_1\tilde{\theta}_\rho^- + A_2\tilde{\theta}_s^-, \tag{3.25}$$

with the coefficients,

$$A_1 = -\frac{2eV_g}{\pi}\cos\alpha + \frac{g\mu_B B_{\rm g}}{\pi} y \sin\alpha, \tag{3.26}$$

$$A_2 = \frac{2eV_g}{\pi}\frac{1}{y}\sin\alpha + \frac{g\mu_B B_{\rm g}}{\pi}\cos\alpha. \tag{3.27}$$

Thus, the terms other than barrier potentials, quadratic in $\tilde{\theta}_i^{\pm}$, can be treated exactly in $S_{\rm eff}$.

After straightforward calculation, we obtain an explicit form of the conductance to the second order in $\frac{V}{\pi a}$; $G_i = G_i^{(0)} + G_i^{(2)}$ for $i = \rho, s$. The unperturbed conductance $G_\rho^{(0)}$ and $G_s^{(0)}$ are [47],

$$G_\rho^{(0)} \ = \ \frac{e^2}{\pi}(\tilde{K}_\rho \cos^2\alpha + \tilde{K}_s y^{-2}\sin^2\alpha), \tag{3.28}$$

$$G_s^{(0)} \ = \ \frac{e^2}{2\pi}(\tilde{K}_\rho y - \tilde{K}_s y^{-1})\sin 2\alpha \ . \tag{3.29}$$

This expression implies that the spin polarized current can flow in a clean, infinite TL liquid due to spin-charge mixing effect, since $G_s^{(0)} = 0$ when $\Delta = 0$ for all interaction parameters. However, such a violation of the conductance quantization is shown to be an artifact for infinite system as previous works pointed out for unpolarized system [84, 85, 86]. We show in Appendix C that the prefactors of conductance should vanish i.e. $G_\uparrow^{(0)} = G_\downarrow^{(0)} = \frac{e^2}{2\pi}$ also for spin polarized system, by taking into account the effects of Fermi liquid reservoirs. Thus the spin polarized current cannot be generated in a clean system, even when a magnetic field is applied.

The second order correction $G_i^{(2)}$ is

$$G_i^{(2)} = -\frac{e^2}{4}\left(\frac{V}{\pi a}\right)^2 \sum_\sigma C_\sigma^i \lim_{\omega_n\to 0}\int_0^\beta d\tau \ \left[\frac{1-\cos\omega_n\tau}{\omega_n}R_\sigma \right. \tag{3.30}$$
$$\left. \times \exp\left(-\frac{1}{2\beta}\sum_{\omega_n'}\left(\frac{B_{\rho,\sigma}^2}{\tilde{\epsilon}_\rho^+(\omega_n')}+\frac{B_{s,\sigma}^2}{\tilde{\epsilon}_s^+(\omega_n')}\right)(1-\cos\omega_n'\tau)\right)\right],$$

$$R_\sigma = \cos\Omega_\sigma \exp\left(-\sum_{\omega_n'} f_\sigma(\omega_n')(1+\cos\omega_n'\tau)\right) \tag{3.31}$$
$$+\exp\left(-\sum_{\omega_n'} f_\sigma(\omega_n')(1-\cos\omega_n'\tau)\right),$$

$$\Omega_\sigma = -4k_{\mathrm{F},\sigma}d + \left(\frac{-\cos\alpha B_{\rho,\sigma}}{\pi\tilde{\epsilon}_\rho^-(0)}+\frac{y^{-1}\sin\alpha B_{s,\sigma}}{\pi\tilde{\epsilon}_s^-(0)}\right)2eV_g \tag{3.32}$$
$$+\left(\frac{y\sin\alpha B_{\rho,\sigma}}{\pi\tilde{\epsilon}_\rho^-(0)}+\frac{\cos\alpha B_{s,\sigma}}{\pi\tilde{\epsilon}_s^-(0)}\right)g\mu_B B_g,$$

$$f_\sigma(\omega_n') = \frac{1}{2\beta}\left(\frac{B_{\rho,\sigma}^2}{\tilde{\epsilon}_\rho^-(\omega_n')}+\frac{B_{s,\sigma}^2}{\tilde{\epsilon}_s^-(\omega_n')}\right), \tag{3.33}$$

with $\beta = 1/T$ and the constants given by,

$$C_\sigma^\rho = \left(\cos\alpha\ B_{\rho,\sigma}\tilde{K}_\rho - y^{-1}\sin\alpha\ B_{s,\sigma}\tilde{K}_s\right)^2, \tag{3.34}$$

$$C_\sigma^s = \left(\cos\alpha\ B_{\rho,\sigma}\tilde{K}_\rho - y^{-1}\sin\alpha\ B_{s,\sigma}\tilde{K}_s\right) \tag{3.35}$$
$$\times\left(y\sin\alpha\ B_{\rho,\sigma}\tilde{K}_\rho + \cos\alpha\ B_{s,\sigma}\tilde{K}_s\right).$$

The second order correction $G_i^{(2)}$ gives us some information about the resonant oscillation in (V_g, B_g) plane; the exponential terms determine the temperature dependent amplitude, and Ω_σ determines the period. As seen in the above expression, the conductance oscillation comes from a sum of two independent contributions; resonant tunneling of spin-up electrons and spin-down electrons. This is because the average of a product of cosine terms for up spin and down spin always vanishes; $\left\langle \sin\left(\theta_\rho^+(\tau)+\theta_s^+(\tau)\right)\sin\left(\theta_\rho^+(0)-\theta_s^+(0)\right)\right\rangle = 0$.

At low temperature $T \ll \tilde{\epsilon}_\rho^-(0), \tilde{\epsilon}_s^-(0)$, it is given

$$G_i^{(2)} = -\frac{e^2}{2\pi}\left(\frac{V}{a\Lambda}\right)^2 \sum_\sigma C_\sigma^i \frac{\Gamma(\frac{\eta_\sigma}{2})}{\Gamma(\frac{\eta_\sigma+1}{2})/\Gamma(\frac{3}{2})} \times (1+\cos\Omega_\sigma)\left(\frac{\pi T}{\Lambda}\right)^{\eta_\sigma-2}, \tag{3.36}$$

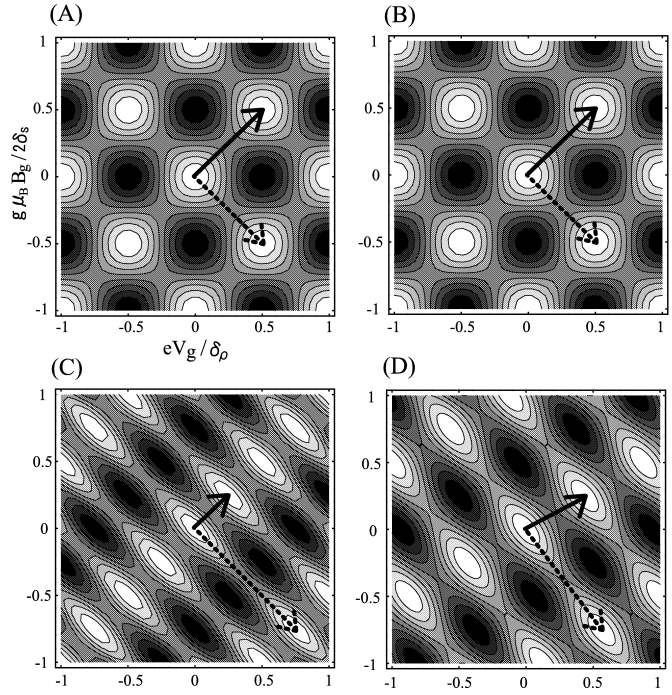

Figure 3.2: Second order conductance correction $G_\rho^{(2)}$ are plotted as a function of gate voltage and magnetic field normalized by $\delta_i = \frac{v_i}{K_i}\frac{\pi}{2d}$ for Hubbard model. $K_\rho = v_F/v_\rho$, $K_s = v_F/v_s = 1$; (A) $K_\rho = 1,\ \Delta/v_F = 0$, (B) $K_\rho = 0.5,\ \Delta/v_F = 0$, (C) $K_\rho = 1,\ \Delta/v_F = 0.5$, (D) $K_\rho = 0.5,\ \Delta/v_F = 0.5$. The temperature is fixed at $T/\Lambda = 0.1$ in all figures. Solid (broken) arrow indicates the direction of peak line of the conductance deviation due to up (down) spin resonant tunneling.

where Λ is the high energy cut-off. At high temperature $T \gg \tilde{\epsilon}_\rho^-(0), \tilde{\epsilon}_s^-(0)$, the term proportional to $\cos\Omega_\sigma$ is exponentially suppressed as increasing temperature, while the other terms remain unchanged in Eq. (3.36). Thus, the conductance oscillation disappears and the double impurity structure can be viewed as a single impurity whose scaling law is given in Eq. (3.13) for $\frac{\pi v_F}{2d} \ll T \ll \Lambda$.

Fig. 3.2 shows the contour plot of the conductance correction as a function of gate voltage and gate magnetic field. Conductance peaks form a lattice in $(V_g\ , B_g)$ plane and spin-charge mixing effect causes the deformation of the lattice. For an unpolarized Fermi liquid $\Delta = 0$ and $K_\rho = K_s = 1$ in Fig. 3.2 (A), conductance peaks form a rectangular lattice with periods $(eV_g)_0 = (\frac{1}{2}\mu_B B_g)_0 = \frac{\pi v_F}{2d}$. Changing the interaction parameter from $K_\rho = 1$ to $K_\rho = 0.5$ (from Fig. 3.2 (A) to Fig. 3.2 (B)), the lattice shape does not

change but with a shift in the period $(eV_{\rm g})_0 = \frac{\pi v_\rho}{2dK_\rho}$ due to the change in charge- and spin- susceptibility of the island $\delta_\rho = \frac{\pi v_\rho}{2dK_\rho}$ and $\delta_s = \frac{\pi v_s}{2dK_s}$. As increasing Δ from $\Delta = 0$ to $\Delta = 0.5v_{\rm F}$ in the Fermi liquid case (from Fig. 3.2 (A) to Fig. 3.2 (C)), stretch in the primary unit-vector of the lattice (arrows in figures), by a factor ($\sim 1 + \sigma\frac{\Delta}{v_{\rm F}}$) for spin σ electrons, is seen. It reflects the change in the level spacing due to Zeeman effect given by $\sigma\frac{2\pi\Delta}{2d}$. Then, increasing the interaction from $K_\rho = 1$ to $K_\rho = 0.5$ (from Fig. 3.2 (C) to Fig. 3.2 (D)), the primary unit-vectors rotate reflecting the rotations of spin-charge space. This is exactly due to spin-charge mixing effect. For $K_\rho = K_s$, the rotation cannot be seen in Fig. 3.2 (C) since the principal axis in spin-charge space stay in the direction $\pm\frac{\pi}{4}$ independent of Δ. The rotation angle $\delta\vartheta$ is proportional to "spin-charge mixing angle α" for small Δ,

$$\delta\vartheta = \frac{1}{2}\big(y + y^{-1} - y\frac{v_s/K_s}{v_\rho/K_\rho} - y^{-1}\frac{v_\rho/K_\rho}{v_s/K_s}\big)\alpha + \mathcal{O}(\alpha^2), \tag{3.37}$$

when there are only density-density interactions between electrons $H_{\rm int} \propto g_\rho(\frac{1}{\pi}\partial_x\phi_\rho)^2 + g_s(\frac{1}{\pi}\partial_x\phi_s)^2$ i.e. TL parameters satisfy $K_\rho v_\rho = K_s v_s = v_{\rm F}$,

$$\delta\vartheta = \frac{K_\rho^2 - K_s^2}{2}\frac{\Delta}{v_{\rm F}} + \mathcal{O}\left((\Delta/v_{\rm F})^2\right). \tag{3.38}$$

When the temperature decreases, the amplitude of oscillation for two spins follow power laws with different exponents. In the case of spin isotropic interaction ($K_s = 1$ i.e. $g_s = 0$), depending on whether the interaction between charges $g_\rho = \frac{1}{2}(K_\rho^{-2} - 1)$ is repulsive or attractive, impurity potentials are scaled toward perfect reflection or perfect transmission. Extending the parameter space to spin anisotropic interaction ($K_s \neq 1$ i.e. $g_s \neq 0$), "spin-filter phase" where $\eta_\uparrow > 2, \eta_\downarrow < 2$, emerges between the two phases "perfect transmission" and "perfect reflection". In this phase, the impurity potential scales toward perfect transmission for up spin (majority spin), and perfect reflection for down (minority) spin. The conductance correction at different temperatures are plotted with TL parameters in spin-filter phase in Fig. 3.3. The peaks of the conductance correction changes from a lattice structure to one plane wave, as lowering temperature from Fig. 3.3 (A) to Fig. 3.3 (B). This is due to the strong suppression of backscattering current of the majority spins, and the enhancement for the minority spin at low temperature. These results suggest the possibility of generating and modulating spin current with large polarization by gate voltage and gate magnetic field.

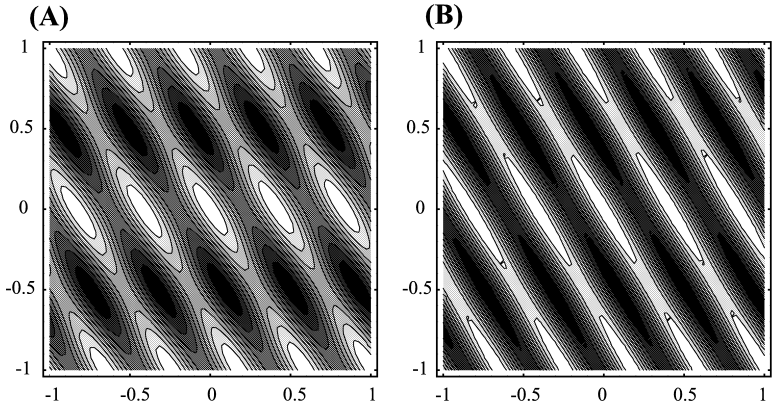

Figure 3.3: $G_\rho^{(2)}$ are plotted as a function of gate voltage and magnetic field normalized by $\delta_i = \frac{v_i}{K_i}\frac{\pi}{2d}$ for spin anisotropic interaction parameters. $K_\rho = v_{\rm F}/v_\rho = 0.6$, $K_s = v_{\rm F}/v_s = 1.4$, $\Delta/v_{\rm F} = 0.5$; (A) $T/\Lambda = 10^{-2}$, (B) $T/\Lambda = 10^{-6}$.

3.4 Weak Link Limit ($V \to \infty$)

In this section, we consider the weak link limit ($V \to \infty$), where the tunneling amplitudes t_σ satisfies $t_\sigma/v_{\rm F} \ll 1$ and the electron transport is described by a sequential tunneling picture [45, 78]. We will calculate zero-bias conductance perturbatively to the lowest order within a master equation framework. The higher order contributions, such as cotunneling (COT) [45, 78] and correlated sequential tunneling (CST) [87], are neglected. Contributions from COT and CST become important, respectively, away from the resonance peaks and for rather transparent barriers [87]. Thus, they do not seem to make major changes in the discussions here focusing on the peak positions and the height in the weak link limit.

We consider a quantum island with length $2d$, weakly linked to the semiinfinite TL wires at the both ends. The Hamiltonian for the semiinfinite wires $H_{\rm wires}$ are the same as Eq. (3.12). We represent electron field operators of the island, the right (R) and the left (L) wire by $\psi_\sigma = \sum_\tau \psi_{\tau,\sigma}$, $\psi_\sigma^{\rm R} = \sum_\tau \psi_{\tau,\sigma}^{\rm R}$ and $\psi_\sigma^{\rm L} = \sum_\tau \psi_{\tau,\sigma}^{\rm L}$, respectively. They obey the open boundary condition $\psi_\sigma(\pm d) = \psi_\sigma^{\rm R}(d) = \psi_\sigma^{\rm L}(-d) = 0$. The chemical potentials of the right and the left wire are set $\mu_{\rm R} = -eV_{\rm bias}$ and $\mu_{\rm L} = 0$, and we take the limit $eV_{\rm bias} \to 0$ at the last stage of the calculations for the zero bias conductance. In the sequential tunneling regime, the number of excess electrons on the island N_σ becomes a

good quantum number, which enters in the zero mode Hamiltonian $H_{\rm zero} = H_{\rm d} + H_{\rm island}$,

$$H_{\rm d} = \frac{\pi v_{\rm F}}{4d} \sum_{\sigma} \left(\frac{K_\rho^{-2} + K_s^{-2}}{2} + \sigma \frac{\Delta}{v_{\rm F}} \right) N_\sigma^2 + \frac{\pi v_{\rm F}}{2d} \left(\frac{K_\rho^{-2} - K_s^{-2}}{2} \right) N_\uparrow N_\downarrow, \tag{3.39}$$

$$H_{\rm island} = \sum_{\sigma} \left(-eV_g + \sigma \frac{g\mu_B B_g}{2} \right) N_\sigma. \tag{3.40}$$

The Hamiltonian for non-zero mode $H_{\rm fluc}$ is the same as in Eq. (3.12);

$$H_{\rm fluc} = \sum_{i=\rho,s,n>0} \tilde{v}_i k_n (\tilde{\alpha}_{i,n}^\dagger \tilde{\alpha}_{i,n} + 1/2), \tag{3.41}$$

where $k_n = \pi n/2d$. Under the boundary condition, the mode expansion of the electron field operator ψ_σ becomes [48, 88, 89, 90],

$$\psi_{\tau,\sigma} = \sqrt{\frac{k_{{\rm F},\sigma}}{\pi}} e^{i\tau k_{{\rm F},\sigma}(x+d) + i\tau(\chi^0_{\tau,\sigma} + \chi_{\tau,\sigma})}, \tag{3.42}$$

$$\chi^0_{\tau,\sigma} = \frac{\pi}{2} + \frac{\pi N_\sigma (x+d)}{2d} + \tau\theta_\sigma, \tag{3.43}$$

$$\chi_{\tau,\sigma} = \sum_{i=\rho,s} \frac{\tilde{K}_i^{1/2} B_{i,\sigma} \tilde{\phi}_i^+ + \tau \tilde{K}_i^{-1/2} D_{i,\sigma} \tilde{\phi}_i^-}{2}, \tag{3.44}$$

where θ_σ is the zero-mode phase satisfying $[N_\sigma, \theta_\sigma] = i$. Non-zero mode phase $\tilde{\phi}_i^\pm$ is given

$$\tilde{\phi}_i^+ = \sum_{n=1}^{\infty} \sqrt{\frac{2}{n}} \sin k_n (x+d) \left(\tilde{\alpha}_{i,n} + \tilde{\alpha}_{i,n}^\dagger \right), \tag{3.45}$$

$$\tilde{\phi}_i^- = \sum_{n=1}^{\infty} \sqrt{\frac{2}{n}} \frac{\cos k_n (x+d)}{i} \left(\tilde{\alpha}_{i,n} - \tilde{\alpha}_{i,n}^\dagger \right). \tag{3.46}$$

The mode expansion of $\psi_\sigma^{\rm R,L}$ are similarly obtained. Using the boundary operators, the tunnel Hamiltonian $H_{\rm T} = H_{\rm T}^{\rm R} + H_{\rm T}^{\rm L}$ is given

$$H_{\rm T}^{\rm R} = \sum_{\sigma} t_\sigma^{\rm R} \psi_{-,\sigma}^\dagger(d) \psi_{-,\sigma}^{\rm R}(d) + {\rm h.c.}, \tag{3.47}$$

$$H_{\rm T}^{\rm L} = \sum_{\sigma} t_\sigma^{\rm L} \psi_{+,\sigma}^\dagger(-d) \psi_{+,\sigma}^{\rm L}(-d) + {\rm h.c.}. \tag{3.48}$$

The transition rate $P^{\mathrm{R(L)}}_{i\to f}$ from a initial state $|i\rangle \equiv |N_\sigma, N_{-\sigma}\rangle$ to a final state $|f\rangle \equiv |N_\sigma + q, N_{-\sigma}\rangle$ ($q = \pm 1$), via tunneling processes at the right (left) end of the island, can be calculated perturbatively. To the lowest order, it becomes

$$P^{\mathrm{R(L)}}_{i\to f} = \int_{-\infty}^{\infty} dt\ \langle\langle i|H_{\mathrm{T}}^{\mathrm{R(L)}}(t)|f\rangle\langle f|H_{\mathrm{T}}^{\mathrm{R(L)}}(0)|i\rangle\rangle, \tag{3.49}$$

where the time evolution of operators is given in interaction representation $A(t) = U^\dagger(t)AU(t)$ with $U = \exp[-it(H_{\mathrm{zero}} + H_{\mathrm{fluc}} + H_{\mathrm{wires}})]$. We obtain the expression for $P^j_{i\to f}$ ($j = \mathrm{R}, \mathrm{L}$) as,

$$P^j_{i\to f} = \frac{1}{\beta}\exp[-\frac{\beta\varepsilon^j_\sigma}{2}]\gamma^j(\varepsilon^j_\sigma, \beta), \tag{3.50}$$

$$\gamma^j(\varepsilon^j_\sigma, \beta) \sim \frac{1}{\pi}\left(\frac{t^j_\sigma}{v_{\mathrm{F},\sigma}}\right)^2\left(\frac{\pi}{\beta\Lambda}\right)^{\frac{\lambda_\sigma}{2}-2}\prod_{i=\rho,s}\left(\frac{3\tilde{v}_i/d}{\Lambda}\right)^{\frac{D^2_{i,\sigma}}{2K_i}} \times 2^{\lambda_\sigma - 1}B\left[\frac{\lambda_\sigma + i\beta\varepsilon^j_\sigma/\pi}{2}, \frac{\lambda_\sigma - i\beta\varepsilon^j_\sigma/\pi}{2}\right], \tag{3.51}$$

where $\varepsilon^j_\sigma \equiv \langle f|H_{\mathrm{zero}}|f\rangle - \langle i|H_{\mathrm{zero}}|i\rangle - q\mu_j$ is the energy difference between the two states. The line shape of the conductance near the peak is roughly given by the beta function in Eq. (3.51), and the peak height scales like $\propto (T/\Lambda)^{\lambda_\sigma/2-2}$ as lowering temperature. The probability P_i to find the system in $|i\rangle$, and the current of spin σ electrons I_σ are obtained by solving a set of master equations,

$$\frac{d}{dt}P_i = \sum_{i'} P_{i'\to i}P_{i'} - P_{i\to i'}P_i = 0, \tag{3.52}$$

$$I_\sigma = e\sum_{i,q} qP_i(P^{\mathrm{R}}_{i\to f} - P^{\mathrm{L}}_{i\to f}), \tag{3.53}$$

where $P_{i\to i'} = P^{\mathrm{R}}_{i\to i'} + P^{\mathrm{L}}_{i\to i'}$.

The zero bias conductance $G_\rho = G_\uparrow + G_\downarrow$ is evaluated from Eqs. (3.50)$-$(3.53) and plotted as a function of gate voltage and gate magnetic field in Fig. 3.4. The conductance peak form a lattice in $(V_{\mathrm{g}}, B_{\mathrm{g}})$ plane, and one can see the spin-charge mixing effect on the shape as well as in the case of weak barriers. Arrows in figures are the primary unit vectors, and a translation by a solid (dotted) arrow corresponds to a change in the average particle number of down (up) spin electrons in the island by one. When spin and charge excitations are degenerate ($K_\rho = K_s$), the primary unit vectors of the lattice

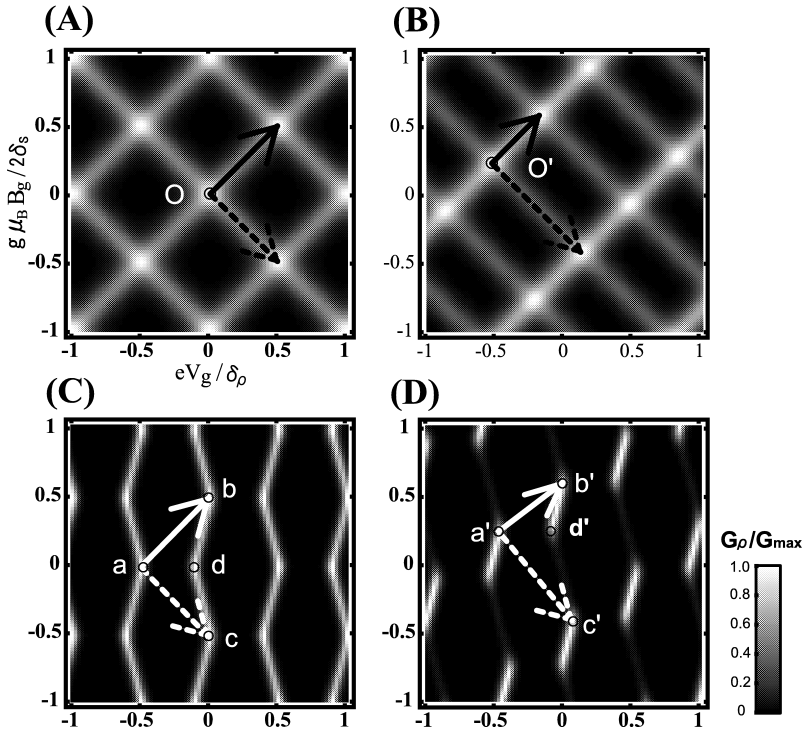

Figure 3.4: Zero bias conductance G_ρ is plotted as a function of gate voltage and magnetic field normalized by $\delta_i = \frac{v_i}{K_i}\frac{\pi}{2d}$, with $T = 10^{-1}\frac{\pi v_F}{4d} = 10^{-3}\Lambda$ and $(t_\sigma^j/v_{F,\sigma})^2/\pi = 10^{-2}$. Different values of interaction and magnetic field are taken as; (A) $K_\rho = K_s = 1$, $\Delta/v_F = 0$, (B) $K_\rho = K_s = 1$, $\Delta/v_F = 0.3$, (C) $K_\rho = 0.5$, $K_s = 1$, $\Delta/v_F = 0$, and (D) $K_\rho = 0.5$, $K_s = 1$, $\Delta/v_F = 0.3$.

pattern are in the direction of $\pm\frac{\pi}{4}$ independently of the magnetic field Δ as shown in Fig. 3.4 (A) and Fig. 3.4 (B). On the other hand, when spin-charge separation does hold ($K_\rho, K_s \neq 1$), the vectors rotate as increasing Δ as seen in Fig. 3.4 (C) and Fig. 3.4 (D). From Eqs. (3.39)−(3.40), one can ensure that the angle of the solid (dotted) arrow $\vartheta_\downarrow$ ($\vartheta_\uparrow$) is given

$$\vartheta_\sigma = \tan^{-1}\frac{-\sigma - K_s^2\Delta/v_F}{1 + \sigma K_\rho^2\Delta/v_F}. \tag{3.54}$$

Thus the expansion of the rotation angle $\delta\vartheta$ to the linear order in Δ, yields the same result as Eq. (3.38) obtained for the weak barrier case. This could indicate that applying

a magnetic field causes a rotation of the lattice of conductance peaks by the same angle for entire range of barrier strength to the linear order. Of course, being similar to the weak barrier case, the splits of scaling dimensions for tunneling amplitudes between two spins result in strong suppression of the peak height along the resonant line $\overline{\mathrm{d'c'}}$, compared to $\overline{\mathrm{b'd'}}$ in Fig. 3.4 (D). Another interesting result in the strong barrier limit is that for $K_\rho \neq K_s$ there are no resonance points of four number states (say $|n,m\rangle$, $|n+1,m\rangle$, $|n,m+1\rangle$ and $|n+1,m+1\rangle$) like O and O$'$. Instead, such a resonance point splits into two; one like a and a$'$ where the three states $|n,m\rangle$, $|n+1,m\rangle$ and $|n,m+1\rangle$ degenerate, and the other like d and d$'$ where $|n+1,m+1\rangle$, $|n+1,m\rangle$ and $|n,m+1\rangle$ degenerate. The length between the separated resonance points $\overline{\mathrm{ad}}$ and $\overline{\mathrm{a'd'}}$, corresponds to $eV_\mathrm{g} = \frac{\pi v_\mathrm{F}}{4d}(K_\rho^{-2} - K_s^{-2})$. It can thus be a measure for the strength of spin-charge separation.

3.5 Summary

We have discussed the spin-charge mixing effect on the resonant tunneling in spin-polarized Tomonaga-Luttinger liquid under magnetic fields. The zero bias conductance is calculated as a function of gate voltage V_g and gate magnetic field B_g. Conductance peaks form a lattice structure in $(V_\mathrm{g}, B_\mathrm{g})$ plane. We find two effects of the spin-charge mixing in the plot of zero bias conductance; (i) The primary unit vectors of the lattice pattern rotate as increasing magnetic field due to the "spin-charge mixing". (ii) The amplitude of conductance oscillation differs significantly at low temperature between two spins, which originates from the split of the scaling dimension of impurity potential. For systems with appropriate interaction parameters, the impurity potential can become a spin-filter that selects electrons of one spin orientation to pass through. We should note that such spin-filtering phase appears only for the systems with spin-anisotropic interaction ($K_s \neq 1$), whose candidates in real systems haven't been found yet. However, recent studies predict that spin-orbit interactions in a quantum wire, whose strength is controllable by the gate voltage, can also cause spin-charge mixing [91] as the Zeeman effect does. Moreover Gritsev *et al.* [92] show that an interaction parameter K_s can be renormalized and shift from $K_s = 1$ in the presence of Rashba coupling. These facts may suggest a possibility to lead such spin-filtering phase to an experimentally accessible region.

Finally we would like to address the possibility for the experimental test of our theory. If one uses armchair carbon nanotube as a TL wire, there arise two difficulties to observe the spin-charge mixing. Armchair nanotubes are described as TL liquids with the four components (spinful TL liquid with two bands $p = \pm$), having a symmetry in the band structure $v_{\mathrm{F},p} = v_{\mathrm{F},-p}$ at the Fermi level $\epsilon_\mathrm{F} = 0$ [71]. Due to this unique band structure,

the symmetry between up and down spins will not be broken even when a magnetic field is applied. Hense the spin-charge mixing does not occur for $\epsilon_{\rm F} = 0$. This is one difficulty. However, for doped carbon nanotubes ($\epsilon_{\rm F} \neq 0$) with the band structure symmetry broken $v_{{\rm F},p} \neq v_{{\rm F},-p}$, the spin-charge mixing occurs when a strong magnetic field is applied. Another difficulty is in the realization of such a strong magnetic fields that the spin-charge mixing effect can be measured. In our case, a significant change in the Fermi velocity about $\frac{\Delta}{v_{\rm F}} = \frac{v_{{\rm F},\uparrow} - v_{{\rm F},\downarrow}}{2v_{\rm F}} \geq 0.1$ is needed. Such a situation may be difficult to prepare in carbon nanotubes with a band width $t \sim 2.5$ eV [93] since g-factor for electrons in carbon nanotubes is $g \sim 2$ [94], which means a magnetic field 1T amounts to $g\mu_B B \sim 0.12$ meV. To make velocity difference $\Delta/v_{\rm F} = 0.1$, $B \sim 1.25 \times 10^4$ tesla is needed in the case of carbon nanotubes. And the preparation of the local magnetic field $B_{\rm g}$ with a submicron meter scale is also an open issue, though there are some works reporting magnetic fields with a micron meter scale [95]. However, if one uses a quantum wire with a small Fermi energy and a large g-factor *e.g.* an InSb quantum wire with $g \sim -50$, two problems lying on carbon nanotubes are cleared, and our predictions can possibly be verified in experiments. Ultracold fermionic atoms in optical lattices [96], which show remarkable progress in experiments, with controllable parameters such as interaction parameters, lattice shapes, and the potential height, will also give us another conceivable stage to test our theory.

It is the more important issue of spintronics to suggest new ways of creating spin filters i.e. the way to modify the split of scaling dimensions between two spin channels in more realistic models. However, the concepts of "spin-charge mixing effect" will play one key role in this matter.

Chapter 4

Finite Barrier Scaling in Tomonaga-Luttinger Liquid

4.1 Introduction

One-dimensional interacting fermions with a local potential show a crucial difference from those of non-interacting fermions in the transport properties at low temperature. As already seen in the previous section, the tunneling amplitude through a single impurity potential and local density of states (LDOS) near the local potential, have power law dependences on temperatures with interaction-dependent anomalous exponents [19, 20, 21], which is understood in terms of the renormalization of effective impurity potential strength. The scaling behavior is known as one of the key signatures of TL liquid, and observed in the tunneling conductance through junctions of carbon nanotubes [67, 68] and the quantum point contact in fractional quantum Hall systems [69, 70].

The scaling of a local potential in TL liquid has been extensively studied for more than a decade after pioneering works based on perturbative renormalization group (RG) analysis [42, 44]. Calculations presented in the previous chapter are also based on the perturbative RG theory. Roughly speaking, it was shown that the backscattering by an impurity potential is a relevant (irrelevant) perturbation when interparticle interaction is repulsive (attractive) for a spinless TL liquid. One can trust these scaling flows just around the two fixed points, weak or strong potential limits due to the theoretical limits of perturbative treatment. Another theory confirmed the scaling flows at arbitrary strength of barrier potential [97, 98]; however, their results based on Fermi liquid picture i.e. perturbation theory on interparticle interaction, are less reliable when interparticle interactions are not weak, e.g. for carbon nanotubes. Exact conductance for arbitrary

barrier strength is calculated for special values of interaction parameters ($g = 1/2$ for spinless TL model, and $\nu = 1/3$ case in the fractional quantum Hall edge states) based on the Bethe-ansatz calculation [99, 100, 101]; however the application of these theories to general TL liquid with arbitrary interaction parameters seems difficult. Therefore, the scaling problem of a single impurity in TL liquid of arbitrary interaction parameters and arbitrary transmission, remain unsolved yet, even after 15 years from the first pioneering work [42, 44]. In this chapter, we propose a non-perturbative approach both in the strength of an impurity potential and interparticle interactions [53]. Bosonization formula derived for arbitrary barrier strength is used to calculate LDOS and zero bias conductance.

Before formulating the theory for arbitrary strength of barrier potential, we briefly see RG flows of a single impurity potential in the two limits ($V \to 0, \infty$) [42, 44]. The scaling equations for the backscattering operator $\hat{V}=V(\psi^\dagger_{\mathrm{R},\sigma}(0)\psi_{\mathrm{L},\sigma}(0) + \mathrm{h.c.})$ and the tunneling operator $\hat{T}=t(\psi^\dagger_{\mathrm{R},\sigma}(0)\psi_{\mathrm{R},\sigma}(0) + \mathrm{h.c.})$ were derived as

$$\frac{dV}{dl} = \left(\frac{2 - K_\rho - K_s}{2}\right) V, \text{ for } V \ll v_{\mathrm{F}}, \tag{4.1}$$

$$\frac{dt}{dl} = \left(\frac{2 - 1/K_\rho - 1/K_s}{2}\right) t, \text{ for } V \gg v_{\mathrm{F}}, \tag{4.2}$$

where $l = \ln \beta\Lambda$ with the high energy cutoff $\Lambda = v_{\mathrm{F}} k_{\mathrm{F}}$ and inverse temperature β. From the perturbative RG equations, a zero temperature phase diagram in the interaction parameter space is determined as shown in Fig.4.1. The scaling flow diagrams at the cross sections (indicated in the phase diagram) are shown in Fig. 4.1 (A) and Fig. 4.1 (B). In the figures, scaling flows obtained and predicted are represented by solid arrows and dotted lines. The fixed point of scaling flows around small reflection and small transmission amplitudes are given by K_ρ+K_{S}=2 and $1/K_\rho$+$1/K_{\mathrm{S}}$=2 respectively. For spin independent models ($K_s = 1$), the fixed points for the weak-reflection regime and for the weak-tunneling regime are given by an unique value $K_\rho = 1$. Since the directions of the scaling flows towards zero temperature are the same for the two limits, one can safely predict that the effective impurity potential flows towards a strong reflection for repulsive interaction $K_\rho < 1$, and towards a weak reflection for attractive interaction $K_\rho > 1$, independent of the impurity potential. However, for spin dependent models ($K_s \neq 1$), the fixed points given in the two limits become different. Thus, it is predicted naively that the direction of scaling flows change at some critical value of the potential strength in a regime of interaction parameter $2 - K_s < K_\rho < (2 - K_s^{-1})^{-1}$.

In order to obtain complete flow diagrams for arbitrary barrier strength for a spinful TL model, we have to develop a non-perturbative method.

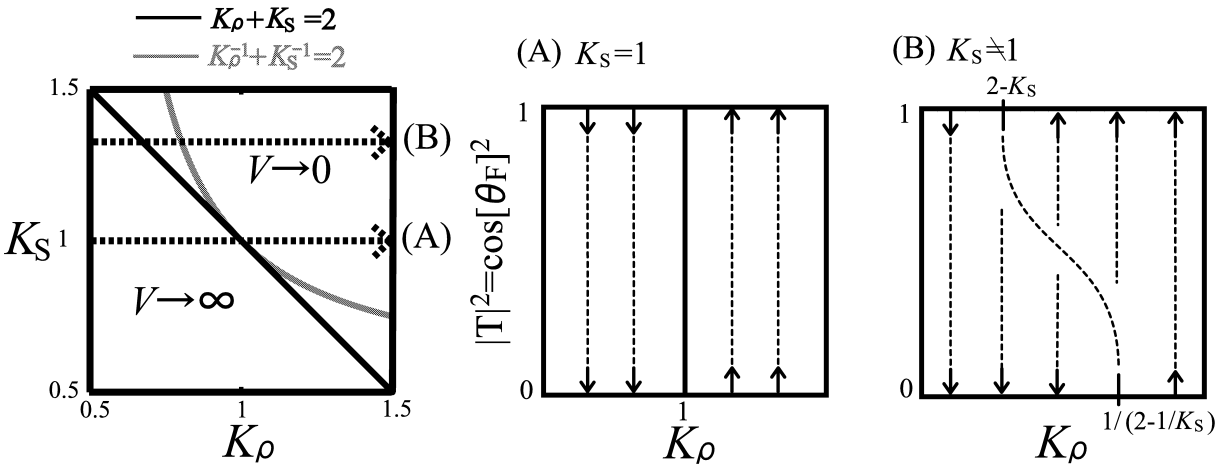

Figure 4.1: Phase diagram of TL liquid with a single impurity potential shown in the references [42, 44], and the flow diagrams along the broken arrows (A) $K_S = 1$, and (B) $K_S \neq 1$. In (A) and (B), the unknown flows are represented by broken lines.

4.2 Boundary Bosonization for Finite Barrier

4.2.1 Free Fermions

Firstly, we construct the bosonization formula for spinless fermions with a single impurity of arbitrary strength. After that, we apply the discussions to the spinful fermions. The bosonization procedure is the same for spinful fermions with the only difference in additional spin degrees of freedom. And as a first step to this problem, we assume that the potential barrier is repulsive, localized, symmetric in spin rotation, and has an inversion symmetry: $V_\uparrow(x) = V_\downarrow(x) = V\delta(x)$ and $V > 0$, for simplicity.

Let's start with a scattering problem of a one-dimensional system of length L with a single impurity potential $V(x)=V\delta(x)$ at the center.

$$\left(-\frac{\partial_x^2}{2m} + V\delta(x)\right)\phi = \epsilon\phi, \tag{4.3}$$

where $V > 0$. The boundary condition at the scattering center is read as,

$$\phi(+0) = \phi(-0), \tag{4.4}$$

$$\left.\frac{\partial_x\phi(x)}{2m}\right|_{-0}^{+0} = V\phi(0). \tag{4.5}$$

The solutions for one-body scattering problem are given,

$$\phi_{\mathrm{P}=-1,k} = \sqrt{\frac{2}{L}} \sin(kx), \tag{4.6}$$

$$\phi_{\mathrm{P}=+1,k} = \sqrt{\frac{2}{L}} \cos(|kx| - \theta_k), \tag{4.7}$$

where P denotes the parity, even parity for $\mathrm{P} = +1$ and odd parity for $\mathrm{P} = -1$. The phase shift by the potential is given by $0 < \theta_k = \arctan[mV/k] < \pi/2$. The boundary condition at the end of the system, fixes the momentum. We choose here the periodic boundary condition (we will take the limit $L \to \infty$ in the calculation, and hence the result does not depend on the choice of the boundary condition far from impurity site $x = 0$.) as,

$$\phi(L/2) = \phi(-L/2), \tag{4.8}$$

$$\partial_x \phi(L/2) = \partial_x \phi(-L/2), \tag{4.9}$$

which determines the momentum for even-parity and odd-parity wave functions as,

$$k = \frac{2\pi n}{L} \text{ for } \mathrm{P} = -1, \tag{4.10}$$

$$k = \frac{2n\pi + 2\theta_k}{L} \text{ for } \mathrm{P} = +1. \tag{4.11}$$

The momentum distribution is schematically shown in Fig.4.2(A). Surely, only even parity states suffer from the momentum shift. One sees that odd-parity and even-parity states have the same momenta and are degenerate in the weak barrier limit $k \gg mV$, meaning that there are no restrictions between the right-moving and the left-moving components. For the strong barrier limit $k \ll mV$, one sees that even parity states suffer momentum shift by π/L, indicating that the right-moving and the left-moving components are in one-to-one correspondence. When considering the low temperature physics, we can safely approximate the phase shift $\theta_k \sim \theta_{\mathrm{F}} = \arctan[mV/k_{\mathrm{F}}]$, which will produce the corrections of order $O(T/\epsilon_{\mathrm{F}})$. With the wave functions of free fermions in Eqs. (4.6)−(4.7), the fermion field operator is defined by

$$\psi(x) = \sum_{\mathrm{P}=\pm 1, k>0} \phi_{\mathrm{P},k}(x) c_{\mathrm{P}}(k), \tag{4.12}$$

where $c_{\mathrm{P}}(k)$ is an annihilation operator of fermions;

$$\left[c_{\mathrm{P}}(k), c^{\dagger}_{\mathrm{P}'}(k')\right]_{+} = \delta_{\mathrm{P},\mathrm{P}'}\delta_{k,k'}. \tag{4.13}$$

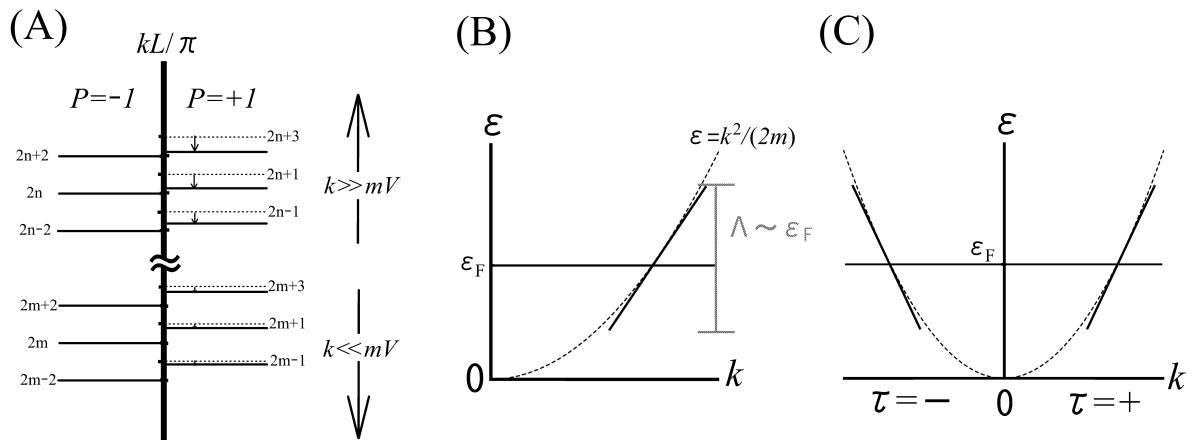

Figure 4.2: (A) Momenta of the solution for one-body scattering problem Eqs. (4.10)−(4.11), and energy band diagrams (B) before and (C) after the decomposition of the fermions into right and left movers, where the linearization is allowed near the Fermi level.

The field operator satisfies $\psi(x)$ the usual anticommutation relations and commutation relations,

$$\left[\psi(x), \psi^\dagger(y)\right]_+ = \delta(x-y), \tag{4.14}$$

$$\left[\psi^\dagger(y)\psi(y), \psi(x)\right]_- = -\delta(x-y)\psi(x). \tag{4.15}$$

In the second quantized representation, the Hamiltonian for free fermions are given by,

$$H_0 = \int_{-L/2}^{L/2} dx \left[\psi^\dagger \left(-\frac{\partial_x^2}{2m} + V\delta(x) - \epsilon_{\rm F}\right)\psi\right] \tag{4.16}$$

$$= \sum_{{\rm P},k>0} \left[\left(\frac{k^2}{2m} - \epsilon_{\rm F}\right) c_{\rm P}^\dagger(k) c_{\rm P}(k)\right] \tag{4.17}$$

$$\sim \sum_{{\rm P},k>0} \left[v_{\rm F}(k-k_{\rm F}) c_{\rm P}^\dagger(k) c_{\rm P}(k)\right]. \tag{4.18}$$

The energy band is schematically shown in Fig. 4.2 (B). We note that the band lies in the half momentum space $k > 0$.

As is also done in the open boundary bosonization [20, 88], we will extend the Hilbert space to a full momentum space allowing the right and the left movers, but with a constraint between them. In the full momentum space shown in Fig. 4.2 (C), we will construct

the bosonization formula, and the boundary conditions between the right-movers and the left-movers are finally put. The decomposition of the free wave functions are:

$$\begin{aligned}
\phi_{+1,k}c_{+1}(k) &= \sqrt{\frac{1}{2L}}\left(e^{ikx-i\mathrm{sign}x\theta_k}+e^{-ikx+i\mathrm{sign}x\theta_k}\right)c_{+1}(k) && (4.19)\\
&\to \sum_{\tau=\pm}\sqrt{\frac{1}{2}}\tilde{\phi}_{+1,\tau k}\tilde{c}_{+1}(\tau k). && (4.20)\\
\phi_{-1,k}c_{-1}(k) &= \sqrt{\frac{1}{2L}}\left(e^{ikx-i\pi/2}+e^{-ikx+i\pi/2}\right)c_{+1}(k) && (4.21)\\
&\to \sum_{\tau=\pm}\sqrt{\frac{1}{2}}\tilde{\phi}_{-1,\tau k}\tilde{c}_{-1}(\tau k). && (4.22)
\end{aligned}$$

Here, operators after the decomposition into right ($\tau=+$) and left ($\tau=-$) movers, are symbolically denoted by the tilde. The new wave functions after the decomposition are given,

$$\begin{aligned}
\tilde{\phi}_{+1,\tau k} &= \sqrt{\frac{1}{L}}e^{i\tau kx-i\tau\mathrm{sign}x\theta_k}\sim\sqrt{\frac{1}{L}}e^{i\tau kx-i\tau\mathrm{sign}x\theta_{\mathrm{F}}}, && (4.23)\\
\tilde{\phi}_{-1,\tau k} &= \sqrt{\frac{1}{L}}e^{i\tau(kx-\pi/2)}. && (4.24)
\end{aligned}$$

In Eq. (4.23), we approximate the phase shift by the value at the Fermi level θ_{F}. The constraints on the new fermion operators, and their anticommutation relations are given by,

$$\begin{aligned}
&\tilde{c}_{\mathrm{P}}(k)=\tilde{c}_{\mathrm{P}}(-k), && (4.25)\\
&\left[\tilde{c}_{\mathrm{P}}(k),\tilde{c}^{\dagger}_{\mathrm{P}'}(k')\right]_{+}=\delta_{\mathrm{P},\mathrm{P}'}\delta_{k,k'}. && (4.26)
\end{aligned}$$

By using the wave functions in Eqs. (4.19)−(4.24), the fermion field operators for the right and the left-movers are given as

$$\begin{aligned}
\psi(x) &= \sqrt{\frac{1}{2}}\sum_{\tau=\pm}\tilde{\psi}_{\tau}(x)e^{i\tau k_{\mathrm{F}}x}, && (4.27)\\
\tilde{\psi}_{\tau}(x) &= \sum_{\mathrm{P},k>0}\left(\tilde{\phi}_{\mathrm{P},\tau k}e^{-i\tau k_{\mathrm{F}}x}\right)\tilde{c}_{\mathrm{P}}(\tau k), && (4.28)
\end{aligned}$$

and follow the commutation relation and the anticommutation relation, which are the same as Eq. (4.14) and Eq. (4.15),

$$\left[\tilde{\psi}_\tau(x), \tilde{\psi}^\dagger_{\tau'}(y)\right]_+ = \delta_{\tau,\tau'}\delta(x-y), \tag{4.29}$$

$$\left[\tilde{\psi}^\dagger_\tau(y)\tilde{\psi}_\tau(y), \tilde{\psi}_{\tau'}(x)\right]_- = -\delta_{\tau,\tau'}\delta(x-y)\tilde{\psi}_\tau(x). \tag{4.30}$$

The Hamiltonian for free fermions in extended Hilbert space, after the linearization near the Fermi level as shown in Fig. 4.2 (C), is then written as

$$H_0 \to \tilde{H}_0 = \sum_{\mathrm{P},k>0,\tau} \left[v_\mathrm{F}(k-k_\mathrm{F})\tilde{c}^\dagger_\mathrm{P}(\tau k)\tilde{c}_\mathrm{P}(\tau k)\right]. \tag{4.31}$$

For fermions in one dimension, the linearized Hamiltonian is rewritten in terms of long-wavelength density fluctuations defined by,

$$:\psi^\dagger\psi: = \delta n(k\sim 0) + \delta n(k\sim 2k_\mathrm{F}), \tag{4.32}$$

$$\delta n(k\sim 0) = \frac{1}{2}\sum_\tau :\tilde{\psi}^\dagger_\tau\tilde{\psi}_\tau: = \frac{1}{2}\sum_\tau J_\tau(x), \tag{4.33}$$

$$\delta n(k\sim 2k_\mathrm{F}) = \frac{1}{2}\sum_\tau :\tilde{\psi}^\dagger_\tau\tilde{\psi}_{-\tau}: e^{-i\tau 2k_\mathrm{F}x}. \tag{4.34}$$

From here, we focus on the long-wavelength density fluctuation $\delta n(k\sim 0)$, and construct TL bosons from them, keeping the constraints in Eq. (4.25).

$$J_\tau(x) = \sum_{\mathrm{P},\mathrm{P}'} J^{\mathrm{P},\mathrm{P}'}_\tau(x) \tag{4.35}$$

$$= \frac{1}{L}\sum_{\mathrm{P},\mathrm{P}',q} e^{iqx-i\tau\theta_{\mathrm{P},\mathrm{P}'}} J^{\mathrm{P},\mathrm{P}'}_\tau(q), \tag{4.36}$$

where the fermion phase shift enters the expression like

$$\theta_{\mathrm{P},\mathrm{P}'} = \delta_{\mathrm{P},-\mathrm{P}'} \times \mathrm{P} \times (\mathrm{sign}x\theta_\mathrm{F} - \pi/2). \tag{4.37}$$

The Fourier components of the density fluctuation

$$J^{\mathrm{P},\mathrm{P}'}_\tau(q) = \sum_k \tilde{c}_\mathrm{P}(\tau k - q)\tilde{c}^\dagger_{\mathrm{P}'}(\tau k), \tag{4.38}$$

satisfies the bosonic commutation relations as conventional bosonization manners,

$$\left[J_{\tau}^{\mathrm{P}_1,\mathrm{P}_2}(q), J_{\tau'}^{\mathrm{P}_3,\mathrm{P}_4}(-q')\right]_- = \delta_{\tau,\tau'}\delta_{\mathrm{P}_1,\mathrm{P}_4}\delta_{\mathrm{P}_2,\mathrm{P}_3}\delta_{q,q'}\frac{\tau q}{2\pi/L}, \tag{4.39}$$

$$\left[\tilde{H}_0, J_{\tau}^{\mathrm{P},\mathrm{P}'}(q)\right]_- = -\tau v_{\mathrm{F}} q J_{\tau}^{\mathrm{P},\mathrm{P}'}(q). \tag{4.40}$$

This yields the boson representation of the Hamiltonian in Eq. (4.31), using the operator identities.

$$\tilde{H}_0 = \frac{2\pi v_{\mathrm{F}}}{L}\sum_{\tau,q,\mathrm{P},\mathrm{P}'} J_{\tau}^{\mathrm{P},\mathrm{P}'}(q)J_{\tau}^{\mathrm{P}',\mathrm{P}}(-q) \tag{4.41}$$

Here, we neglect the zero mode contributions for simplicity, which do not change the physics in systems of infinite length. From Eq. (4.25), the density operator must satisfy

$$J_{\tau}^{\mathrm{P},\mathrm{P}'}(q) = J_{-\tau}^{\mathrm{P},\mathrm{P}'}(-q) \tag{4.42}$$

Introducing an appropriate normalization condition to the commutation relation Eq. (4.39), one can define the creation and annihilation operators of TL bosons $b_{\mathrm{P},\mathrm{P}'}$ and $b_{\mathrm{P},\mathrm{P}'}^{\dagger}$;

$$\left[b_{\mathrm{P}_1,\mathrm{P}_2}(q), b_{\mathrm{P}_3,\mathrm{P}_4}^{\dagger}(q')\right]_- = \delta_{\mathrm{P}_1,\mathrm{P}_3}\delta_{\mathrm{P}_2,\mathrm{P}_4}\delta_{q,q'}, \tag{4.43}$$

where the relation between $b_{\mathrm{P},\mathrm{P}'}(q)$ and $J_{\tau}^{\mathrm{P},\mathrm{P}}(q)$ is given by

$$J_{\tau}^{\mathrm{P},\mathrm{P}}(q) = \sqrt{\left|\frac{qL}{2\pi}\right|}\left(Y(\tau q)b_{\mathrm{P},\mathrm{P}}(q) + Y(-\tau q)b_{\mathrm{P},\mathrm{P}}^{\dagger}(-q)\right), \tag{4.44}$$

$$J_{\tau}^{\mathrm{P},-\mathrm{P}}(q) = \sqrt{\left|\frac{qL}{2\pi}\right|}\left(Y(\tau q)b_{\mathrm{P},-\mathrm{P}}(q) + Y(-\tau q)b_{-\mathrm{P},\mathrm{P}}^{\dagger}(-q)\right). \tag{4.45}$$

$Y(x)$ is step function: $Y(x>0)=1$ and $Y(x<0)=0$. From Eq. (4.42), it must be kept in mind,

$$b_{\mathrm{P},\mathrm{P}'}(q) = b_{\mathrm{P},\mathrm{P}'}(-q). \tag{4.46}$$

For convenience, we use symmetric and antisymmetric combinations of them,

$$b_1(q) = \frac{1}{\sqrt{2}}\left(b_{+1,+1}(q) + b_{-1,-1}(q)\right). \tag{4.47}$$

$$b_2(q) = \frac{1}{\sqrt{2}}\left(b_{+1,+1}(q) - b_{-1,-1}(q)\right). \tag{4.48}$$

$$b_3(q) = \frac{1}{\sqrt{2}}\left(b_{+1,-1}(q) + b_{-1,+1}(q)\right). \tag{4.49}$$

$$b_4(q) = \frac{1}{\sqrt{2}}\left(b_{+1,-1}(q) - b_{-1,+1}(q)\right). \tag{4.50}$$

The Hamiltonian Eq. (4.41) is expressed in terms of the TL bosons as,

$$\begin{aligned}\tilde{H}_0 &= \frac{1}{2}\sum_{q,\mathrm{P},\mathrm{P}'} v_{\mathrm{F}}|q|\left(b^{\dagger}_{\mathrm{P},\mathrm{P}'}(q)b_{\mathrm{P},\mathrm{P}'}(q) + 1/2\right) \\ &= \sum_{q>0,\mathrm{P},\mathrm{P}'} v_{\mathrm{F}}|q|\left(b^{\dagger}_{\mathrm{P},\mathrm{P}'}(q)b_{\mathrm{P},\mathrm{P}'}(q) + 1/2\right). \\ &= \sum_{q>0,l=1\sim 4} v_{\mathrm{F}}|q|\left(b^{\dagger}_{l}(q)b_{l}(q) + 1/2\right).\end{aligned} \tag{4.51}$$

From Eqs. (4.30), (4.36) and (4.39), one gets the bosonic representation of the fermion field operators as usual bosonization formula,

$$\tilde{\psi}_{\tau}(x) = \sqrt{\frac{k_{\mathrm{F}}}{\pi}}\exp\left[i\tau\chi_{\tau}(x)\right]. \tag{4.52}$$

$$\chi_{\tau}(x) = 2\pi\int^{x} J_{\tau}(y)dy \tag{4.53}$$

By substituting Eqs. (4.36)−(4.50) into Eq. (4.53), we finally arrive at the bosonization formula of the fermion field operator for spinless fermions,

$$\chi_{\tau}(x) = \sum_{q>0,l}\left(\sqrt{\frac{\pi}{qL}}f^{l}_{\tau,q}(x)b_l(q) + \mathrm{h.c.}\right), \tag{4.54}$$

$$f^{1}_{\tau,q} = -i\tau e^{i\tau qx}, \tag{4.55}$$

$$f^{2}_{\tau,q} = 0, \tag{4.56}$$

$$f^{3}_{\tau,q} = -i\tau\mathrm{sign}[x]\sin[\theta_{\mathrm{F}}]e^{i\tau qx}, \tag{4.57}$$

$$f^{4}_{\tau,q} = \cos[\theta_{\mathrm{F}}]e^{i\tau qx}. \tag{4.58}$$

Next we will derive a formula for spinful fermions. But the formulation of the bosonization is quite the same as the spinless case except for spin degrees of freedom. The Hamiltonian is given by

$$\begin{aligned} H_0 &= \sum_{\sigma} \int_{-L/2}^{L/2} dx \ \left[\psi_\sigma^\dagger \left(-\frac{\partial_x^2}{2m} + V\delta(x) - \epsilon_{\rm F} \right) \psi_\sigma \right] && (4.59) \\ &\sim \sum_{{\rm P},\sigma,k>0} \left[v_{\rm F}(k-k_{\rm F}) c_{{\rm P},\sigma}^\dagger(k) c_{{\rm P},\sigma}(k) \right] && (4.60) \\ &= \sum_{q>0,\sigma,l=1\sim 4} v_{\rm F}|q| \left(b_{\sigma,l}^\dagger(q) b_{\sigma,l}(q) + 1/2 \right), && (4.61) \end{aligned}$$

where $\sigma = +1 = \uparrow$ and $\sigma = -1 = \downarrow$ stand for up-spin and down-spin fermions, respectively. $b_{\sigma,l}$ are similarly defined as in Eq. (4.47)−(4.50). For spin symmetric systems in consideration, it is convenient to switch to the separate spin-charge representation, given by

$$\begin{aligned} b_{\rho,l}(q) &= \frac{1}{\sqrt{2}} \left(b_{\uparrow,l}(q) + b_{\downarrow,l}(q) \right). && (4.62) \\ b_{s,l}(q) &= \frac{1}{\sqrt{2}} \left(b_{\uparrow,l}(q) - b_{\downarrow,l}(q) \right). && (4.63) \end{aligned}$$

Then the Hamiltonian is written as

$$\begin{aligned} H_0 &= \frac{2\pi v_{\rm F}}{L} \sum_{\tau,\sigma,q,{\rm P},{\rm P}'} J_{\sigma,\tau}^{{\rm P},{\rm P}'}(q) J_{\sigma,\tau}^{{\rm P}',{\rm P}}(-q) && (4.64) \\ &= \sum_{q>0,l,j=\rho,s} v_{\rm F}|q| \left(b_{j,l}^\dagger(q) b_{j,l}(q) + 1/2 \right). && (4.65) \end{aligned}$$

The boson representation of the fermion field operators are similarly given,

$$\tilde{\psi}_{\sigma,\tau}(x) = \sqrt{\frac{k_{\rm F}}{\pi}} \exp\left[i\tau\chi_{\sigma,\tau}(x) \right], \qquad (4.66)$$

where the phase field $\chi_{\sigma,\tau}$ is obtained by putting $b_l \to b_\sigma = (b_{\rho,l} + \sigma b_{s,l})/\sqrt{2}$ into the

expression for spinless fermions Eq. (4.54),

$$\chi_{\sigma,\tau}(x) = \sum_{q>0,j,l} \sqrt{\frac{\pi}{2qL}} \left(f^{\rho,l}_{\tau,q}(x) b_{\rho,l}(q) + \sigma f^{s,l}_{\tau,q}(x) b_{s,l}(q) + \text{h.c.} \right), \tag{4.67}$$

$$f^{j,1}_{\tau,q} = -i\tau e^{i\tau q x}, \tag{4.68}$$

$$f^{j,2}_{\tau,q} = 0, \tag{4.69}$$

$$f^{j,3}_{\tau,q} = -i\tau \text{sign}[x] \sin[\theta_{\text{F}}] e^{i\tau q x}, \tag{4.70}$$

$$f^{j,4}_{\tau,q} = \cos[\theta_{\text{F}}] e^{i\tau q x}. \tag{4.71}$$

4.2.2 Interacting Fermions

In this section, we will include the interparticle interaction, coming from long wavelength fluctuations. Diagonalization of total Hamiltonian is performed by following the usual bosonization techniques, but with additional parity indices. Firstly, we will solve the spinless model, and later the spinful model will be considered.

The interaction Hamiltonian for spinless model is given by,

$$H_{\text{int}} = g \int dx \left[\delta n(k \sim 0) \right]^2 \tag{4.72}$$

$$= \frac{g}{4} \sum_{\tau,\tau'} \int dx \left[J_\tau(x) J_{\tau'}(x) \right] \tag{4.73}$$

$$= \frac{g}{4} \sum_{\tau,\tau'} \sum_{\text{P}_1,\text{P}_2,\text{P}_3,\text{P4}} \int dx \left[J^{\text{P}_1,\text{P}_2}_\tau(x) J^{P_3,P4}_{\tau'}(x) \right]. \tag{4.74}$$

Terms remaining after integration must satisfy the parity conservation, $\text{P}_1 \times \text{P}_2 \times \text{P}_3 \times \text{P}_4 = 1$. Keeping in mind the parity conservation, one can write the interaction Hamiltonian as,

$$\begin{aligned} H_{\text{int}} &= \frac{g}{4} \sum_{\tau,\tau'} \sum_{\text{P},\text{P}'} \int dx \left[J^{\text{P},\text{P}}_\tau(x) J^{\text{P}',\text{P}'}_{\tau'}(x) \right] + \frac{g}{4} \sum_{\tau,\text{P}} \int dx \left[J^{\text{P},-\text{P}}_\tau(x) J^{\text{P},-\text{P}}_\tau(x) \right] \\ &+ \frac{g}{4} \sum_{\tau,\text{P}} \int dx \left[J^{\text{P},-\text{P}}_\tau(x) J^{\text{P},-\text{P}}_{-\tau}(x) \right] + \frac{g}{4} \sum_{\tau,\text{P}} \int dx \left[J^{\text{P},-\text{P}}_\tau(x) J^{-\text{P},\text{P}}_\tau(x) \right] \\ &+ \frac{g}{4} \sum_{\tau,\text{P}} \int dx \left[J^{\text{P},-\text{P}}_\tau(x) J^{-\text{P},\text{P}}_{-\tau}(x) \right]. \end{aligned} \tag{4.75}$$

The effects of the potential barrier enter in the second term and the fifth term of the right-hand side of Eq. (4.75). After the integration, they are given,

$$\frac{g}{4}\sum_{\tau,\mathrm{P}}\int dx\,\left[J_{\tau}^{\mathrm{P},-\mathrm{P}}(x)J_{\tau}^{\mathrm{P},-\mathrm{P}}(x)\right] = -\frac{g\cos[2\theta_{\mathrm{F}}]}{4L}\sum_{\tau,q,\mathrm{P}} J_{\tau}^{\mathrm{P},-\mathrm{P}}(q)J_{\tau}^{\mathrm{P},-\mathrm{P}}(-q), \quad (4.76)$$

$$\frac{g}{4}\sum_{\tau,\mathrm{P}}\int dx\,\left[J_{\tau}^{\mathrm{P},-\mathrm{P}}(x)J_{-\tau}^{-\mathrm{P},\mathrm{P}}(x)\right] = -\frac{g\cos[2\theta_{\mathrm{F}}]}{4L}\sum_{\tau,q,\mathrm{P}} J_{\tau}^{\mathrm{P},-\mathrm{P}}(q)J_{-\tau}^{-\mathrm{P},\mathrm{P}}(-q). \quad (4.77)$$

All other terms in Eq. (4.75) are unaffected by the potential barriers, and have the form like,

$$\frac{g}{4L}\sum_{q} J_{\tau}^{\mathrm{P}_1,\mathrm{P}_2}(q)J_{\tau'}^{\mathrm{P}_3,\mathrm{P}_4}(-q), \quad (4.78)$$

The total Hamiltonian is expressed in terms of creation and annihilation operators of TL bosons defined in the previous section as,

$$\begin{aligned} H_0 + H_{\mathrm{int}} &= \sum_{q}|q|\left[(v_{\mathrm{F}}+\frac{g}{\pi})(b_1^{\dagger}(q)b_1(q)+1/2)+\left(\frac{g}{2\pi}b_1(q)b_1(-q)+\mathrm{h.c.}\right)\right] \quad (4.79)\\ &+ \sum_{q}|q|\left[v_{\mathrm{F}}(b_2^{\dagger}(q)b_2(q)+1/2)\right]\\ &+ \sum_{q}|q|\left[(v_{\mathrm{F}}+\frac{g\sin[\theta_{\mathrm{F}}]^2}{\pi})(b_3^{\dagger}(q)b_3(q)+1/2)+\left(\frac{g\sin[\theta_{\mathrm{F}}]^2}{2\pi}b_3(q)b_3(-q)+\mathrm{h.c.}\right)\right]\\ &+ \sum_{q}|q|\left[(v_{\mathrm{F}}+\frac{g\sin[\theta_{\mathrm{F}}]^2}{\pi})(b_4^{\dagger}(q)b_4(q)+1/2)+\left(\frac{g\cos[\theta_{\mathrm{F}}]^2}{2\pi}b_4(q)b_4(-q)+\mathrm{h.c.}\right)\right]. \end{aligned}$$

As seen clearly, interaction parameters for density fluctuations $J^{\mathrm{P},-\mathrm{P}}$ with different combination of the parity indices, depend on the barrier strength through the fermion phase shift. This is understood as such density fluctuation produce the density fluctuation with odd parity, which changes the relative number of the fermions in the left side and the right side of the potential barrier. In order to make such fluctuations, fermions must tunnel through the barrier. Thus, the effects of a barrier potential enter the TL parameters for the mode $J^{\mathrm{P},-\mathrm{P}}$. On the other hand, producing the density fluctuation with even parity $J^{\mathrm{P},\mathrm{P}}$, does not involve the tunneling processes through the barrier. Thus, the interaction parameters for the mode $J^{\mathrm{P},\mathrm{P}}$ are unaffected by the barrier potential.

Finally, we can diagonalize the total Hamiltonian by performing Bogoliubov transformation,

$$\begin{pmatrix} b_l(q) \\ b_l^{\dagger}(q) \end{pmatrix} = \begin{pmatrix} \cosh\varphi_l & \sinh\varphi_l \\ \sinh\varphi_l & \cosh\varphi_l \end{pmatrix}\begin{pmatrix} \tilde{b}_l(q) \\ \tilde{b}_l^{\dagger}(q) \end{pmatrix}, \quad (4.80)$$

with the Bogoliubov rotation angle φ_l given by

$$\tanh 2\varphi_1 = \frac{-g}{\pi v_{\rm F} + g}, \tag{4.81}$$

$$\tanh 2\varphi_2 = 0 \tag{4.82}$$

$$\tanh 2\varphi_3 = \frac{-g \sin[\theta_{\rm F}]^2}{\pi v_{\rm F} + g \sin[\theta_{\rm F}]^2}, \tag{4.83}$$

$$\tanh 2\varphi_4 = \frac{-g \cos[\theta_{\rm F}]^2}{\pi v_{\rm F} + g \cos[\theta_{\rm F}]^2}. \tag{4.84}$$

The Hamiltonian $H_{\rm TL} = H_0 + H_{\rm int}$ is

$$H_{\rm TL} = \sum_{q,l} v_l |q| (\tilde{b}_l^\dagger(q) \tilde{b}_l(q) + 1/2), \tag{4.85}$$

where the TL parameters are given by

$$v_{\rm F}/v_1 = K_1 = e^{2\varphi_1} = \sqrt{\frac{1}{1 + 2g/\pi v_{\rm F}}}, \tag{4.86}$$

$$v_{\rm F}/v_2 = K_2 = e^{2\varphi_2} = 1, \tag{4.87}$$

$$v_{\rm F}/v_3 = K_3 = e^{2\varphi_3} = \sqrt{\frac{1}{1 + 2g \sin[\theta_{\rm F}]^2/\pi v_{\rm F}}}, \tag{4.88}$$

$$v_{\rm F}/v_4 = K_4 = e^{2\varphi_4} = \sqrt{\frac{1}{1 + 2g \cos[\theta_{\rm F}]^2/\pi v_{\rm F}}}. \tag{4.89}$$

The fermion field operators are expressed in terms of TL bosons which diagonalize the Hamiltonian as,

$$\chi_\tau(x) = \sum_{q>0,l} \left(\sqrt{\frac{\pi}{qL}} \tilde{f}^l_{\tau,q}(x) \tilde{b}_l(q) + \text{h.c.} \right), \tag{4.90}$$

$$\tilde{f}^1_{\tau,q} = \sqrt{K_1} \sin[qx] - i\tau \sqrt{1/K_1} \cos[qx], \tag{4.91}$$

$$\tilde{f}^2_{\tau,q} = 0, \tag{4.92}$$

$$\tilde{f}^3_{\tau,q} = \text{sign}[x] \sin[\theta_{\rm F}] \left(\sqrt{K_3} \sin[qx] - i\tau \sqrt{1/K_3} \cos[qx] \right), \tag{4.93}$$

$$\tilde{f}^4_{\tau,q} = \cos[\theta_{\rm F}] \left(\sqrt{K_4} \cos[qx] + i\tau \sqrt{1/K_4} \sin[qx] \right). \tag{4.94}$$

Now we have a diagonal TL Hamiltonian and the TL boson representation of the fermion field operator, and can calculate any correlation functions exactly.

The diagonalization procedures are the same for spinful models. We express the coupling parameters following the conventional manners: interaction parameter for charge densities is $g_\rho = (g_\parallel + g_\perp)/2$, and spin densities is $g_s = (g_\parallel - g_\perp)/2$. With these parameters, in the similar way in the spinless case, TL Hamiltonian is

$$H_{\rm TL} = \sum_{j,q,l} v_{j,l}|q|(\tilde{b}^\dagger_{j,l}(q)\tilde{b}_{j,l}(q) + 1/2), \tag{4.95}$$

where the TL parameters are given by

$$v_{\rm F}/v_{j,1} = K_{j,1} = e^{2\varphi_{j,1}} = \sqrt{\frac{1}{1+2g_j/\pi v_{\rm F}}}, \tag{4.96}$$

$$v_{\rm F}/v_{j,2} = K_{j,2} = e^{2\varphi_{j,2}} = 1, \tag{4.97}$$

$$v_{\rm F}/v_{j,3} = K_{j,3} = e^{2\varphi_{j,3}} = \sqrt{\frac{1}{1+2g_j \sin[\theta_{\rm F}]^2/\pi v_{\rm F}}}, \tag{4.98}$$

$$v_{\rm F}/v_{j,4} = K_{j,4} = e^{2\varphi_{j,4}} = \sqrt{\frac{1}{1+2g_j \cos[\theta_{\rm F}]^2/\pi v_{\rm F}}}. \tag{4.99}$$

And the phase field of the fermion operators are,

$$\chi_{\sigma,\tau}(x) = \sum_{q>0,j,l} \sqrt{\frac{\pi}{2qL}} \left(\tilde{f}^{\rho,l}_{\tau,q}(x)\tilde{b}_{\rho,l}(q) + \sigma \tilde{f}^{s,l}_{\tau,q}(x)\tilde{b}_{s,l}(q) + \text{h.c.} \right), \tag{4.100}$$

$$\tilde{f}^{j,1}_{\tau,q} = \sqrt{K_{j,1}}\sin[qx] - i\tau\sqrt{1/K_{j,1}}\cos[qx], \tag{4.101}$$

$$\tilde{f}^{j,2}_{\tau,q} = 0, \tag{4.102}$$

$$\tilde{f}^{j,3}_{\tau,q} = \text{sign}[x]\sin[\theta_{\rm F}]\left(\sqrt{K_{j,3}}\sin[qx] - i\tau\sqrt{1/K_{j,3}}\cos[qx] \right), \tag{4.103}$$

$$\tilde{f}^{j,4}_{\tau,q} = \cos[\theta_{\rm F}]\left(\sqrt{K_{j,4}}\cos[qx] + i\tau\sqrt{1/K_{j,4}}\sin[qx] \right). \tag{4.104}$$

Using these bosonization formulas, we will discuss the scaling properties of impurity potential, by calculating the temperature dependencies of the local density of states (LDOS) as a function of distance from the impurity site, and the zero bias conductance. Before the calculation, it is worthwhile to see the validity of these formula in the weak barrier ($\theta_{\rm F} = 0$) and the strong barrier ($\theta_{\rm F} = \pi/2$) limits.

In the weak barrier limit $\theta_{\rm F} = 0$ ($V \ll v_{\rm F}, g_j$), we have $K_{j,1} = K_{j,4} \equiv K_j$ and $v_{j,1} = v_{j,4} \equiv v_j$ from Eq. (4.96) and Eq. (4.99). Then, the phase field of the fermions moving in a direction $\tau = \pm$ can be written as

$$\chi_{\sigma,\tau}(x) = \sum_{q>0,j} \varepsilon_{j,\sigma} \sqrt{\frac{\pi}{qL}} \left[\left(\frac{K_j^{1/2} + K_j^{-1/2}}{2} \right) \acute{b}_j(\tau q) e^{i\tau q x} + \left(\frac{K_j^{1/2} - K_j^{-1/2}}{2} \right) \acute{b}_j(-\tau q) e^{-i\tau q x} + \text{h.c.} \right], \tag{4.105}$$

where $\varepsilon_{j,\sigma} = \delta_{j,\rho} + \sigma \delta_{j,s}$. The new operator $\acute{b}_j$ is defined by $\acute{b}_j(\tau q) \equiv \left[i\tau \tilde{b}_{j,1}(q) + \tilde{b}_{j,4}(q) \right] / \sqrt{2}$ and the Hamiltonian is given in the ordinal form: $h_j = \sum_{q \neq 0} v_j |q| (\acute{b}_j^\dagger(q) \acute{b}_j(q) + 1/2)$. This expression is exactly the same as that of the homogeneous system.

In the strong barrier limit $\theta_{\rm F} = \pi/2$ ($V \gg v_{\rm F}, g_j$), we have $K_{j,1} = K_{j,3} \equiv K_j$ and $v_{j,1} = v_{j,3} \equiv v_j$ from Eq. (4.96) and Eq. (4.98). The phase field of the fermions moving in the $\tau = \pm$ direction can be written as

$$\chi_{\sigma,\tau}(x) = \sum_{q>0,j} \varepsilon_{j,\sigma} \sqrt{\frac{\pi}{qL}} \left[\left(K_j^{1/2} \sin[qx] - i\tau K_j^{-1/2} \cos[qx] \right) \grave{b}_j \left(xq/|x| \right) + \text{h.c.} \right]. \tag{4.106}$$

The new operator $\grave{b}_j$ is defined by $\grave{b}_j(\pm q) \equiv \left[\tilde{b}_{j,1}(q) \pm \tilde{b}_{j,3}(q) \right] / \sqrt{2}$ and the Hamiltonian is given by $h_j = \sum_{q \neq 0} v_j |q| (\grave{b}_j^\dagger(q) \grave{b}_j(q) + 1/2)$. This expression reproduces the formula of open boundary bosonization. It is interesting in the strong barrier limit to note that two independent wires were naturally introduced from a single TL liquid in the operator level: it is clearly shown $\langle \chi_{\sigma,\tau}(x > 0, t) \chi_{\sigma,\tau}(y < 0, 0) \rangle = 0$. Within both limits, the parameters governing the physics are K_ρ and K_s.

4.3 Results

4.3.1 Local Density of States

First, we will calculate the local density of states (LDOS) for spinful TL liquid, since it is closely related to the tunneling probability of TL bosons at the fixed energy level, as was discussed for the strong barrier case in [88, 89, 90]. In the strong barrier limit, LDOS near the impurity ($|x| \ll v_{\rm F}\beta$) gives a tunneling density of states, which determines the zero bias conductance in the tunneling limit. Thus, we will be able to extract the scaling behavior of the impurity potential from LDOS.

LDOS at the energy from the Fermi level $\hbar\omega = E - E_{\rm F}$ is defined as

$$N(x,\beta,\omega) = \frac{1}{4\pi}\sum_{\sigma,\tau}\int_{-\infty}^{\infty} dt\ \langle\left[\tilde{\psi}^{\dagger}_{\sigma,\tau}(x,t),\tilde{\psi}_{\sigma,\tau}(x,0)\right]_{+}\rangle \exp[i\omega t], \tag{4.107}$$

where the time evolution of the fermion operator is given in the interaction representation $\tilde{\psi}_{\sigma,\tau}(x,t) = e^{iH_{\rm TL}t/\hbar}\tilde{\psi}_{\sigma,\tau}(x)e^{-iH_{\rm TL}t/\hbar}$. From the bosonization formula in Eqs. (4.100)−(4.104), LDOS for zero frequency $\omega \ll 1/\beta$ is calculated as

$$\begin{aligned} N(x,\beta,0) &= \frac{2}{\pi v_{\rm F}}\left(\frac{\pi}{\beta\Lambda}\right)^{(\sum_{j,l=1,3,4}A_{j,l}+B_{j,l})/8-1}\int_0^{\infty} dq\ \cos[\gamma(q)] \\ &\quad\times\left[\prod_{\substack{j=\rho,s,\\ l=1,3,4}}|\sinh[\pi q]|^{-\frac{A_{j,l}+B_{j,ll}}{8}}\left|\frac{\sinh[r_{j,l}-\pi q]\sinh[r_{j,l}+\pi q]}{\sinh[r_{j,l}]^2}\right|^{-\frac{A_{j,l}-B_{j,l}}{16}}\right. \\ &\quad\left.-\prod_{\substack{j=\rho,s,\\ l=1,3,4}}|\pi q|^{-\frac{A_{j,l}+B_{j,ll}}{8}}\left|1-\left(\frac{\pi q}{r_{j,l}}\right)^2\right|^{-\frac{A_{j,l}-B_{j,l}}{16}}\right], \end{aligned} \tag{4.108}$$

$$\gamma(q) = \frac{\pi}{16}\sum_{j,l=1,3,4}\left[(A_{j,l}+B_{j,l})+(A_{j,l}-B_{j,l})Y(\pi q - r_{j,l})\right], \tag{4.109}$$

where

$$r_{j,l} = 2\pi|x|/(v_{j,l}\beta), \tag{4.110}$$

$$(A_{j,1},A_{j,3},A_{j,4}) = (K_{j,1}^{-1},\sin[\theta_{\rm F}]^2K_{j,3}^{-1},\cos[\theta_{\rm F}]^2K_{j,4}), \tag{4.111}$$

$$(B_{j,1},B_{j,3},B_{j,4}) = (K_{j,1},\sin[\theta_{\rm F}]^2K_{j,3},\cos[\theta_{\rm F}]^2K_{j,4}^{-1}). \tag{4.112}$$

The straight forward calculation yields the asymptotic expressions for the exponents in the bulk $N(|x| \gg v_{\rm F}\beta) \equiv N_{\rm bulk}$, and near the potential barrier $N(|x| \ll v_{\rm F}\beta) \equiv N_{\rm bound}$ as :

$$N_{\rm bound} = \frac{2}{\pi v_{\rm F}}\left(\frac{\pi}{\beta\Lambda}\right)^{\lambda_{\rm bound}-1}C(\lambda_{\rm bound})\prod_{j,l}\left(\frac{2k_{\rm F}|x|}{v_{j,l}/v_{\rm F}}\right)^{\frac{A_{j,l}-B_{j,l}}{8}}, \tag{4.113}$$

$$N_{\rm bulk} = \frac{2}{\pi v_{\rm F}}\left(\frac{\pi}{\beta\Lambda}\right)^{\lambda_{\rm bulk}-1}C(\lambda_{\rm bulk}). \tag{4.114}$$

$C(\lambda)$ is non-universal constants of order of unity given by

$$C(\lambda) = \cos[\pi\lambda/2] \int_0^\infty dq \left[\sinh[\pi q]^{-\lambda} - (\pi q)^{-\lambda}\right], \tag{4.115}$$

which is convergent for $1 < \lambda < 3$. From the asymptotic expressions, LDOS follows power law dependencies on temperature with exponents $\lambda_{\rm bulk} - 1$ in the bulk and $\lambda_{\rm bound} - 1$, respectively. The exponents are given by

$$\lambda_{\rm bound} = \frac{\sum_j \left[K_{j,1}^{-1} + \sin[\theta_{\rm F}]^2 K_{j,3}^{-1} + \cos[\theta_{\rm F}]^2 K_{j,4}\right]}{4}, \tag{4.116}$$

$$\lambda_{\rm bulk} = \frac{\sum_j \left[(K_{j,1} + K_{j,1}^{-1}) + \sin[\theta_{\rm F}]^2 (K_{j,3} + K_{j,3}^{-1}) + \cos[\theta_{\rm F}]^2 (K_{j,4} + K_{j,4}^{-1})\right]}{8}. \tag{4.117}$$

In Fig. 4.3 (A)−(B), LDOS is plotted as a function of temperature with the position x fixed, for different values of interaction parameters. As seen clearly, the slope of the logarithmic plot crossovers from $\lambda_{\rm bulk} - 1$ to $\lambda_{\rm bound} - 1$ as lowering the temperature from bulk regime ($|x| \gg v_{\rm F}\beta$) to boundary dominated regime ($|x| \ll v_{\rm F}\beta$), meaning that their temperature dependencies crossovers from $T^{\lambda_{\rm bulk}-1}$ to $T^{\lambda_{\rm bound}-1}$. As already discussed in the previous works for open boundary problem [88, 89], the physics of two regimes are subjected to the different classes with the scaling dimensions $\lambda_{\rm bound}$ and $\lambda_{\rm bulk}$ in the presence of the impurity potential of arbitrary strength. When interaction parameters are in the strong repulsion [Fig. 4.3 (A)], the slope is sharper in the boundary regime than in the bulk regime. As moving towards the attractive interaction [Fig. 4.3 (B)], the slope is slower in the boundary regime than in the bulk regime, on the other hand.

In Fig. 4.4 (A)−(D), LDOS is plotted as a function of distance from the barrier x with the temperature fixed. Changes in LDOS are seen in boundary regime $|x| \lesssim v_{\rm F}\beta$, and their behaviors near boundary are classified into four types: (A), (B), (C), (D). For interparticle interactions are strong repulsion as in Fig. 4.4 (A), LDOS is suppressed near the boundary, independent of the strength of impurity potential except for the case $V = 0$. In contrast, when the interparticle interactions are strong attraction as in Fig. 4.4 (B), the enhancement of the LDOS near the impurity site is seen, which is independent of the strength of impurity potential except for $V = 0$. For intermediate interaction strength, which satisfies $K_\rho + K_s > 2$ and $K_\rho^{-1} + K_s^{-1} > 2$, the behavior of LDOS near the boundary changes at some critical value of the potential strength $V = V_{\rm c}$ as in Fig. 4.4 (C): for strong barrier $V > V_{\rm c}$ LDOS is suppressed near the boundary, and for weak barrier $V < V_{\rm c}$ LDOS is enhanced near the boundary. These behaviors of LDOS can be interpreted from the asymptotic forms at the boundary and in the bulk. The behavior of LDOS near boundary are determined by the magnitude relation between $\lambda_{\rm bound}$ and $\lambda_{\rm bulk}$: at sufficiently low

temperature, for $\lambda_{\rm bound} > \lambda_{\rm bulk}$ LDOS should be strongly suppressed near the boundary, compared with the bulk value according to Eq. (4.113) and Eq. (4.114), and in contrast, for $\lambda_{\rm bound} < \lambda_{\rm bulk}$ the LDOS should be enhanced near the boundary.

Therefore, if one relates the scaling behavior of LDOS with that of impurity potentials, the phase boundary is given by $\lambda_{\rm bulk} = \lambda_{\rm bound}$ (the phase boundary in Fig. 4.6 is determined by this equation). In the next section, we will relate the scaling behaviors of LDOS with zero bias conductance, i.e. renormalized transmission probability at the Fermi level.

4.3.2 Zero Bias Conductance

The zero bias conductance can be calculated from the Kubo formula,

$$G = \lim_{\omega\to 0} \frac{2e^2}{\omega_n} \langle j_\rho(x,\omega_n) j_\rho(y,-\omega_n)\rangle \Big|_{i\omega_n=\omega+i\delta}, \tag{4.118}$$

where the current operator is defined as

$$j_\rho(x,t) = \frac{1}{\sqrt{8}\pi} \sum_{\sigma,\tau} \partial_t \chi_{\sigma,\tau}(x,t), \tag{4.119}$$

$$j_\rho(x,t) = \frac{1}{\sqrt{\beta}} \sum_n j_\rho(x,\omega_n) e^{i\omega_n t}. \tag{4.120}$$

We obtain the zero bias conductance as,

$$G = \frac{e^2}{\pi} K_{1,\rho} \cos[\theta_{\rm F}]^2. \tag{4.121}$$

The zero bias conductance of infinite TL liquid, with effects of contacts neglected, is known to be

$$G = \frac{e^2}{\pi} K_{1,\rho}. \tag{4.122}$$

Compare Eq. (4.121) with Landauer formula for free electrons;

$$G = \frac{e^2}{\pi} |t|^2, \tag{4.123}$$

where $|t|^2$ is the transmission probability. One may think that the transmission probability of TL liquid through a potential barrier is likely to be given by $|t|^2 = \cos[\theta_{\rm F}]^2$ independent

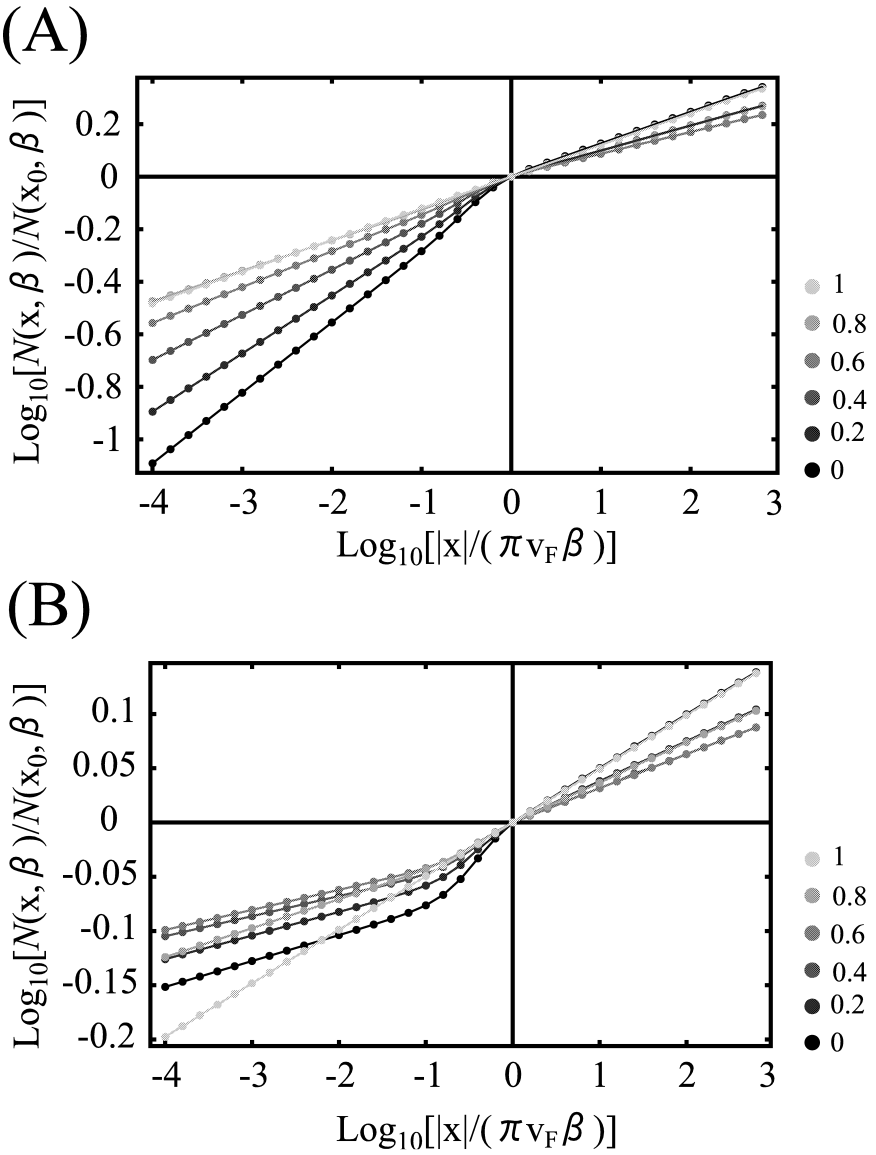

Figure 4.3: Local Density of States normalized by the value at $x_0 = \pi v_{\rm F}\beta$ are plotted as a function of temperature $T = 1/\beta$ for different sets of interaction parameters: (A) $K_\rho = 0.55$, $K_s = 1.4$, (B) $K_\rho = 0.75$, $K_s = 1.4$. Colors of dots indicate the strength of the barrier potential with the numbers ($= \cos^2[\theta_{\rm F}]$). The distance from the impurity x is held fixed at $x = (\pi/k_{\rm F}) \times 10^3$, and sets the scales.

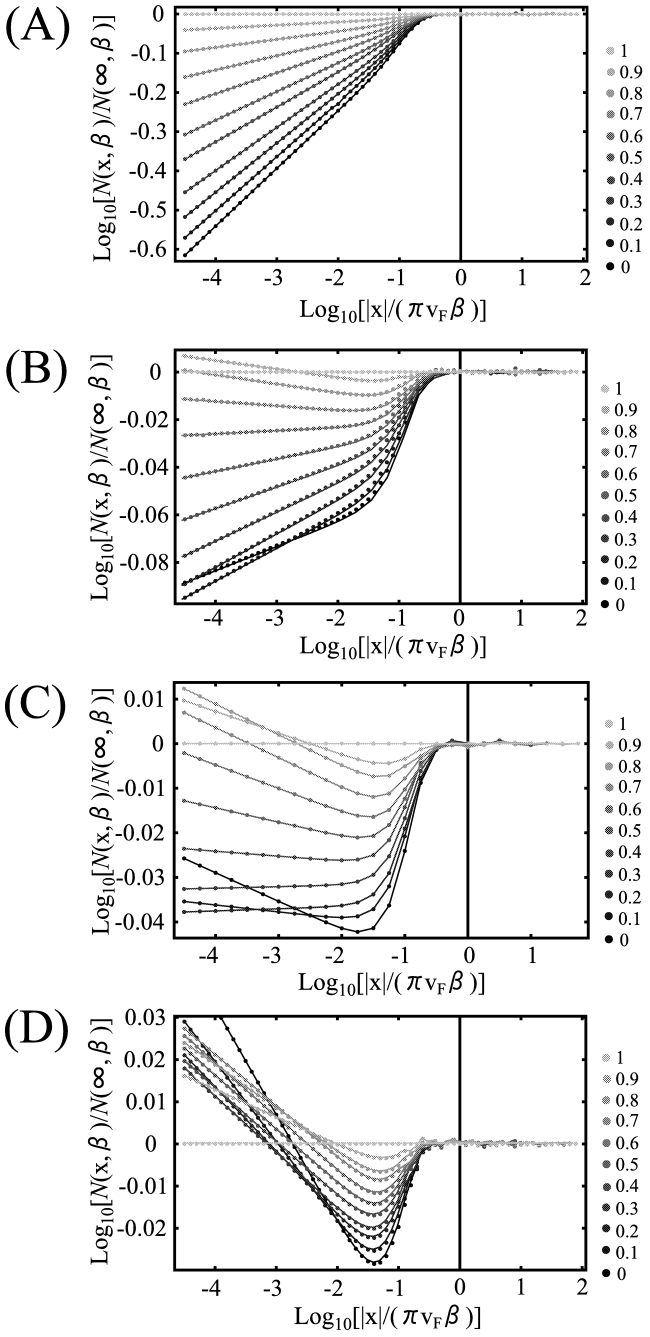

Figure 4.4: Local Density of States are plotted as a function of normalized distance from the impurity position $|x|/(\pi v_{\rm F}\beta)$ for various interaction parameters: (A) $K_\rho = 0.55$, $K_s = 1.4$, (B) $K_\rho = 0.7$, $K_s = 1.4$, (C) $K_\rho = 0.723$, $K_s = 1.4$, (C) $K_\rho = 0.75$, $K_s = 1.4$. Colors of dots indicate the strength of the barrier potential with the numbers ($= \cos^2[\theta_{\rm F}]$). The temperature T is held fixed at $T/E_{\rm F} = 10^{-4}$, and sets the scales. The slope for $|x|/(\pi v_{\rm F}\beta) \ll 1$ is given by $\lambda_{\rm bound} - \lambda_{\rm bulk}$ defined in the texts.

of temperature. Based on Kubo formula in the zero bias limit, the system is assumed to be uniform except for the impurity position. For sufficiently low temperature, however, the thermal coherence length becomes very large and most of the system is in the boundary regime. Thus, the system cannot be regarded as uniform anymore as shown in the behavior of LDOS in Fig. 4.4 at low temperature. Thus, one can trust the expression $|t|^2 = \cos[\theta_{\rm F}]^2$, which is the same expression for free fermions, only at relatively high temperature. It is consistent with our knowledge that particles for sufficiently high temperatures, one can neglect the interaction effects.

Then, in order to derive a correct expression for the conductance formula that works at low temperature, we relate the scaling behaviors of LDOS to the conductance. At relatively high temperature $T \sim \Lambda = v_{\rm F} k_{\rm F}$,

$$|t_0|^2 = \cos[\theta_{\rm F}]^2, \tag{4.124}$$

where it is understood that there is no scaling factor since $T/\Lambda \sim 1$, and the ratio $N_{\rm bound}/N_{\rm bulk}$ is simply given by the solution of one body scattering problem. Eq. (4.124) gives the initial condition of the scaling equation for the zero bias conductance. From the asymptotic expression for LDOS in Eq. (4.113) and Eq. (4.114), one can derive the scaling equation

$$\frac{d}{dl}\left[N_{\rm bound}/N_{\rm bulk}\right] = (\lambda_{\rm bound} - \lambda_{\rm bulk})\left[N_{\rm bound}/N_{\rm bulk}\right], \tag{4.125}$$

which can be read as the scaling equation for temperature-dependent transmission amplitude $|t|$:

$$d|t|/dl = (\lambda_{\rm bound} - \lambda_{\rm bulk})|t|. \tag{4.126}$$

In this way, the scaling equation for zero bias conductance $G(T)/(e^2/\pi) = |t|^2 = \cos[\theta_F(T)]^2$ (the renormalization factor $K_{1,\rho}$ should disappear including the effect of reserver) is derived as

$$\frac{d}{dl}\left[G(T)/(e^2/\pi)\right] = 2(\lambda_{\rm bound} - \lambda_{\rm bulk})\left[G(T)/(e^2/\pi)\right]. \tag{4.127}$$

The numerical solution of Eq. (4.127) are shown in Fig. 4.5 (A)−(D). The scaling behavior of the conductance is similar to that of LDOS. For repulsive interaction as in Fig. 4.5 (A), zero bias conductance is suppressed at low temperature towards 0, independent of the strength of impurity potential unless $V = 0$. In contrast, for attractive interaction Fig. 4.5 (D), zero bias conductance is enhanced towards $G_0 = e^2/\pi$ at low

temperature, independent of the strength of impurity potential unless $V = 0$. For intermediate interaction strength roughly given by $K_\rho + K_s > 2$ and $K_\rho^{-1} + K_s^{-1} > 2$ as in Fig. 4.5 (B), the directions of the scaling flows of zero bias conductance towards zero temperature change at some critical value of the potential strength $V = V_c$: for strong barrier $V > V_c$ zero bias conductance is suppressed, and for weak barrier $V < V_c$ zero bias conductance is enhanced. There is another interesting regime as shown in Fig. 4.5 (C) around the intermediate interaction strength, where the zero bias conductance flows towards some finite value $0 < G^*/(e^2/\pi) < 1$. This interesting behavior is understood from the reentrance structure of the phase diagram shown in Fig. 4.6, as discussed in the next section.

In the last of this section, it is important to note that, Eq. (4.127) derived from the scaling properties of LDOS, coincides with the RG equation derived by Yu, Glazman and Matveev [97, 98], which is based on the scattering theory with interparticle interactions treated in the perturbation theory, within the weak interaction limit ($g_\rho, g_s \ll V, v_F$):

$$\frac{d}{dl}|t|^2 = \frac{g_\rho + g_s - g_1}{\pi v_F}(1 - |t|^2)|t|^2, \tag{4.128}$$

which can be easily checked by expanding the Eq. (4.127) with respect to small g_j and then putting $g_j \to g_j - g_1/2$ to incorporate the effect of $g_1^{\parallel}$ term [18]. The same result is derived from the completely different approaches: interparticle interactions are incorporated in a nonperturbative method in our theory.

4.3.3 Phase Diagram

The phase diagram for impurity scaling obtained from the scaling feature of LDOS and zero bias conductance. Following the discussions in the previous sections, the suppression and the enhancement of LDOS in the boundary regime ($|x| \ll v_F\beta$) correspond, respectively, to the suppression and the enhancement of tunneling probability through potential barrier. Thus, the phase boundary is given by $\lambda_{\rm bulk} = \lambda_{\rm bound}$ from Eqs. (4.113)−(4.114) and (4.125)−(4.127). Just on the phase boundary, the scaling dimensions in the bulk and in the boundary regime coincide with each other, and we cannot distinguish between them.

For spinless fermions and spin independent model ($K_s = 1$) of spinful fermions, the phase boundary is given by $K_\rho = 1$, independently of the barrier strength. This is easily checked from $\lambda_{\rm bound} = \lambda_{\rm bulk}$. Thus, we can ensure the complete phase diagram at arbitrary barrier strength shown in Fig. 4.1 (A).

The phase diagram for spin dependent models ($K_s \neq 1$), is shown in Fig. 4.6. The scaling flows toward zero temperature are indicated by arrows in the figure. The phase

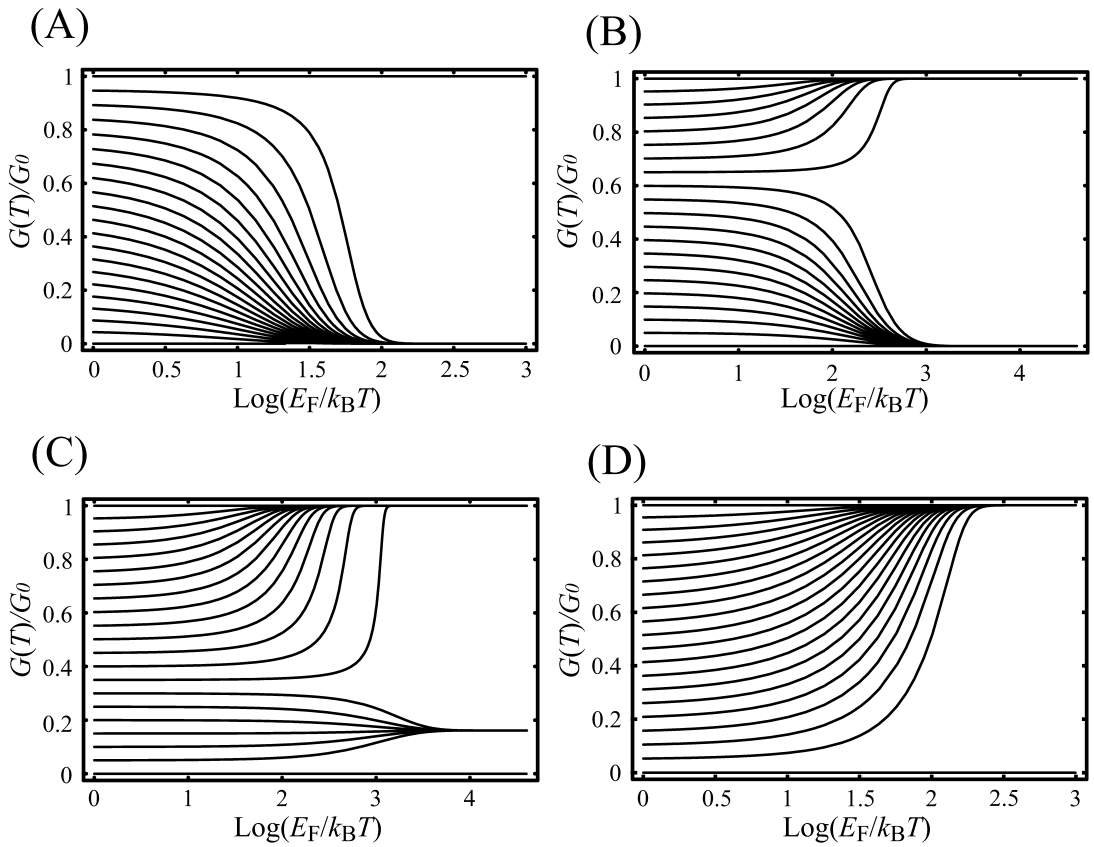

Figure 4.5: Zero bias conductance G normalized by $G_0 = 2e^2/h$, calculated from the RG equation, is plotted as function of $\log E_{\rm F}/k_{\rm B}T$, varying the strength of a potential barrier. (A) $K_\rho = 0.55$, $K_s = 1.4$, (B) $K_\rho = 0.7$, $K_s = 1.4$, (C) $K_\rho = 0.723$, $K_s = 1.4$, (D) $K_\rho = 0.8$, $K_s = 1.4$.

diagram is classified into four phases (A), (B), (C), (D), which respectively correspond to (A), (B), (C), (D) in Fig. 4.5 and Fig. 4.4. In a regime (A), transmission amplitude is renormalized towards zero at any strength of potential barrier. In a regime (D), transmission amplitude is renormalized towards $|t|^2 = 1$ at any strength of potential barrier. In regime (B), the directions of scaling flow change at some critical potential strength. In regime (C), due to the existence of reentrance in the phase boundary, there arises the fixed point of transmission probability at finite amplitude, as seen in Fig. 4.5 (C).

The phase boundary starts from $K_\rho \sim 2 - K_s$ in the weak barrier limit, to $K_\rho = 1/K_s$ in the strong barrier limit. Those fixed points (phase boundary) are different from the previous results [42, 44], which do not take into account the power-law temperature dependence of LDOS in the bulk. One can certainly recover the conventional results of the scaling dimensions for the tunneling operators and the backscattering operators within the two limits in our theory, since our bosonization formula yields the conventional form in weak and strong barrier limits, as seen in Sec. 4.2.2. The difference originates from the way of evaluating the scaling of potential barrier. In order to extract the scaling property of transmission probability, it will be a natural assumption that the transmission amplitude should be determined by $N_{\rm bound}/N_{\rm bulk}$ in terms of the normalization condition for the wave functions similar to one-body scattering problems. For weakly interacting systems $g_\rho, g_s \ll v_{\rm F}$, the bulk exponent of LDOS $((K_\rho + 1/K_\rho + K_s + 1/K_s)/4 - 1)$ is quadratic in g's, while the boundary exponent is linear in g's. Thus one can neglect the scaling of bulk density of states for weakly interacting systems. Actually, the phase boundary $g_\rho + g_s = 0$ to the linear order (g_1 term is neglected here), can be derived from both theories of ours and perturbative RG theory [42, 44]. However, the neglection cannot be allowed in strongly correlated systems anymore.

4.4 Summary

To summarize this chapter, we studied the scaling properties of a single potential barrier of arbitrary strength in a Tomonaga-Luttinger liquid:

- The boundary bosonization formula is developed to include arbitrary barrier potential.
- With our new formula, the local density of states is calculated, and a scaling equation of zero bias conductance is derived.
- Phase diagram is determined, where the phase boundary shows the reentrance suggesting the existence of stable fixed points at the finite transmission probability.

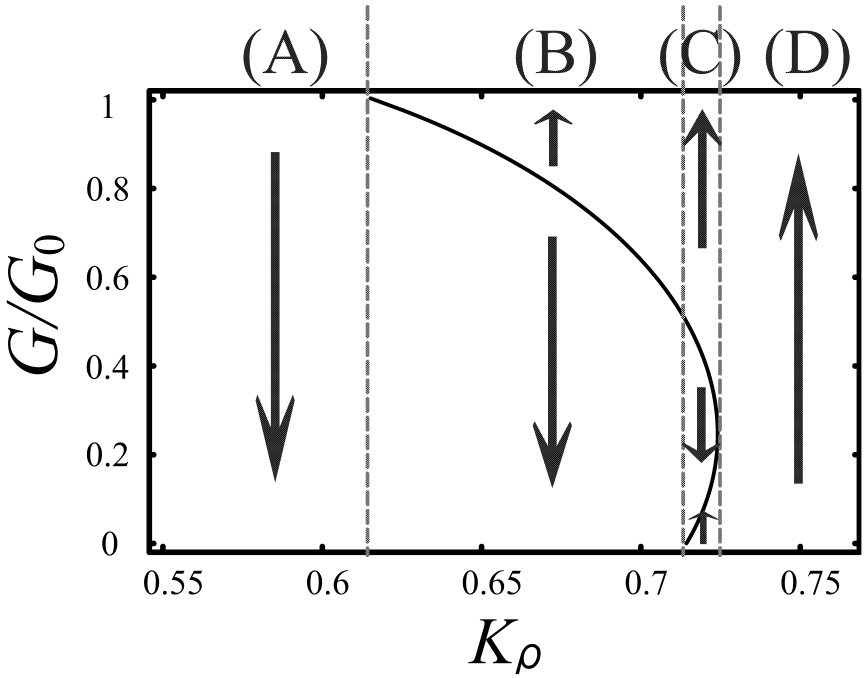

Figure 4.6: Phase diagram of spinful TL liquid with a single potential barrier for $K_s = 1.4$. Vertical axis $G/G_0 = \cos[\theta_{\rm F}]^2$ represents transmission probability through the potential barrier. Directions of the scaling flows towards zero temperature are indicated by arrows.

We have determined the phase boundary of a single potential barrier with arbitrary strength in a spinful TL liquid. We see in the phase diagram the reentrance of the fixed line from weak to strong barrier regime, which indicates the possibility of the stable fixed points at a finite transmission amplitude. It should be clarified in our future studies, whether or not the reentrance is an artifact which comes from the approximation that the phase shifts of all electrons are taken to be the same value at Fermi level.

Chapter 5

Conclusions and Outlook

In conclusions of the thesis, we have studied phase transition and quantum transport in interacting one-dimensional electron systems. In order to study interaction effects, and logarithmically divergent density-density correlations in one dimension, we have applied and developed the perturbative renormalization group (RG) theory by (g-ology) and bosonization method.

In chapter 2, we have studied zero temperature phase diagrams of (5,0) carbon nanotubes, which are known as novel one-dimensional systems and reported to be superconducting at 15 K recently. Based on the electronic band calculation, (5,0) carbon nanotubes have three conduction bands crossing the Fermi level. By assuming the system to be an interacting quasi-one-dimensional electron system with three linear bands, we have derived RG equations for coupling parameters and correlation functions of density waves and superconductivities. The novel feature of (5,0) carbon nanotubes different from conventional one-dimensional material is the new internal degree of freedom of the angular momentum around the nanotube axis. We find several types of superconducting phases in the phase diagrams. Scattering processes, which exchange the angular momentum between incident particles and conserve a total angular momentum, enhance the superconductivity correlations which carry zero total angular momentum. In contrast, scattering processes, like umklapp scatterings, which change the total angular momentum of the incident electrons, enhance the superconductivity correlations with total angular momentum $5\hbar$ in (5,0) carbon nanotubes. We find these superconducting phase for relatively strong attraction between electrons, which indicates that the strong electron-phonon interaction actually exists in (5,0) carbon nanotubes. Recent theoretical works also suggest the possibility of strong electron-phonon couplings in carbon nanotubes with small diameters. In order to examine the possibility and the properties of the superconductivity more precisely, we need to determine how large the interaction parameters are. We leave it to the future

investigations.

In chapter 3, we have studied the effects of magnetic fields on transport in Tomonaga-Luttinger liquid. One of the well-known interaction effects in Tomonaga-Luttinger (TL) liquid, is spin-charge separation. Spin-charge separation originates from the difference of the strength of interactions between charge density waves and between spin density waves. Once a magnetic field is turned onto TL liquid, the spin-charge separation breaks down since a magnetic field couples the spin-charge degrees of freedom. We studied the conductance of the spin polarized TL liquid with double impurity potential. The calculations are done in two limiting cases where the impurity potentials can be assumed to be very weak or strong.

In TL liquid with double impurities, the effect of resonant tunneling of TL liquid can be seen in the conductance oscillations as functions of gate voltage and gate magnetic field, which are applied to the region between double impurities. In spin-charge separated TL liquid without magnetic field, we have shown the conductance peaks form a rectangular lattice shape in the space of gate-voltage and gate-magnetic field, from which we see that the gate voltage changes only charge numbers and magnetic field changes only numbers of the spins accumulated between double impurities. In spin-charge mixed TL liquid under magnetic field, the lattice shapes, formed by conductance peaks, changes and rotates in the space of gate-voltage and magnetic field. This directly means that the magnetic field cause a rotation of spin-charge space.

Another interesting feature in spin polarized TL liquid is, spin dependent scaling laws of the impurity potential. It is well known that a localized potential in TL liquid, perfectly reflects density waves for a system with repulsive interactions, and perfectly transmit them without reflection for a system with attractive interactions at zero temperature. Thus, a single impurity in TL liquid can change the system either to be conducting or insulating at zero temperature, depending on the interaction parameters. For TL liquid under magnetic field, there arises a novel spin-filtering phase in the interaction parameter space, in addition to conducting and insulating phases. In the spin-filter phase at zero temperature, a single impurity perfectly selects one spin component to transmit, and thus a single impurity potential works as a perfect spin-filter. We obtained such spin-filtering phase and the effect of such novel scaling properties are found in the conductance oscillations due to resonant tunnelings. These predictions will possibly be checked by future experiments of the double barrier systems in quantum wires or carbon nanotubes.

In chapter 4, we have developed the boundary bosonization techniques to the problem of arbitrary potential strength. In conventional methods, a localized potential can be treated perturbatively, while interparticle interactions are treated in the non-perturbative ways within bosonization framework. In our framework, interactions and barrier potential are treated on the same footings. The scaling dimensions of operators perfectly recover

the known results in weak barrier and strong barrier limits. From the scaling laws of local density of states around the impurity potential, we have derived the RG equation for the zero-bias conductance. By solving the RG equation, we obtain the temperature dependence of the zero bias conductance, from which we determined the zero temperature phase diagrams for arbitrary strength of a potential barrier. For a spinless model, our phase diagrams confirms the prediction: as temperature lowers, a single potential barrier scales towards a strong barrier for repulsive interaction and towards weak barrier for attractive interactions: the direction of the scaling flow is independent of the initial barrier strength, which was firstly proposed by Kane and Fisher [42]. For a spinful model with spin dependent interactions, we connect the different fixed points (the phase boundary) within the two limits. We found a reentrance of the phase boundary in this case, indicating that the stable fixed points at finite transmission amplitudes, although the ambiguity remains in the physical origin of such reentrance structure. With regard to this point, we will leave it as one of the future problems.

Boundary bosonization method developed here will possibly be applied not only to a single impurity problem, but also to boundary problems on various junctions, metallic contacts to TL liquid, superconductor-TL liquid hybrid junctions. We also leave such applications to various systems to the future investigations.

Appendix A

Luttinger Parameters for Spin-Charge Mixed System

Luttinger parameters in Eq.(3.12) are given,

$$\tilde{v}_\rho^2 = \frac{v_\rho^2+v_s^2+2\Delta^2}{2} + \frac{v_\rho^2-v_s^2}{2}\sqrt{1+\frac{4\Delta^2(v_\rho K_\rho + v_s/K_s)(v_s K_s + v_\rho/K_\rho)}{(v_\rho^2-v_s^2)^2}}, \quad \text{(A.1)}$$

$$\tilde{v}_s^2 = \frac{v_\rho^2+v_s^2+2\Delta^2}{2} - \frac{v_\rho^2-v_s^2}{2}\sqrt{1+\frac{4\Delta^2(v_\rho K_\rho + v_s/K_s)(v_s K_s + v_\rho/K_\rho)}{(v_\rho^2-v_s^2)^2}}, \quad \text{(A.2)}$$

$$\tilde{K}_\rho = \sqrt{\frac{v_\rho K_\rho \cos\alpha^2 + v_s K_s(\frac{\sin\alpha}{y})^2 + \Delta\frac{\sin 2\alpha}{y}}{\frac{v_\rho}{K_\rho}\cos\alpha^2 + \frac{v_s}{K_s}(y\sin\alpha)^2 + \Delta y\sin 2\alpha}}, \quad \text{(A.3)}$$

$$\tilde{K}_s = \sqrt{\frac{v_s K_s \cos\alpha^2 + v_\rho K_\rho(y\sin\alpha)^2 - \Delta y\sin 2\alpha}{\frac{v_s}{K_s}\cos\alpha^2 + \frac{v_\rho}{K_\rho}(\frac{\sin\alpha}{y})^2 - \Delta\frac{\sin 2\alpha}{y}}}, \quad \text{(A.4)}$$

where y and α are given in Eq.(3.10) and Eq.(3.11).

Appendix B

Linear Transformation for Spin-Charge Mixed TL Liquid

Here we represent the linear transformation in Eq.(3.8) and Eq.(3.9) in terms of ladder operators of TL bosons $\alpha_i(k)$, $\alpha_i^\dagger(-k)$, $\tilde{\alpha}_i(k)$ and $\tilde{\alpha}_i^\dagger(-k)$, which diagonalize TL Hamiltonian as $H_{\rm TL} = \sum_{k,i} \tilde{v}_i|k| \left(\tilde{\alpha}_i^\dagger(k)\tilde{\alpha}_i(k) + 1/2\right)$. The phase variables ϕ_i and Π_i are expanded in terms of the ladder operators as

$$\phi_i = \sum_k \sqrt{\frac{\pi K_i}{2|k|L}} \left(\alpha_i(k) + \alpha_i^\dagger(-k)\right) e^{ikx}, \tag{B.1}$$

$$\Pi_i = \frac{1}{i}\sum_k \sqrt{\frac{|k|}{2\pi K_i L}} \left(\alpha_i(k) - \alpha_i^\dagger(-k)\right) e^{ikx}. \tag{B.2}$$

The representations for $\tilde{\phi}_i$ and $\tilde{\Pi}_i$ are obtained similarly by putting $K_i, \alpha_i \to \tilde{K}_i, \tilde{\alpha}_i$ into the above equations. Focusing on a k-component here, we omit the index k for simplicity. From the above expressions, the transformation in Eq.(3.8) and Eq.(3.9) is expressed as

$\mathcal{A} = \mathcal{W}\tilde{\mathcal{A}}$ with $\mathcal{A} = (\alpha_\rho, \alpha_s, \alpha_\rho^\dagger, \alpha_s^\dagger)^T$, $\tilde{\mathcal{A}} = (\tilde{\alpha}_\rho, \tilde{\alpha}_s, \tilde{\alpha}_\rho^\dagger, \tilde{\alpha}_s^\dagger)^T$, and a 4×4 matrix $\mathcal{W}$;

$$\mathcal{W} = \frac{1}{2}\begin{pmatrix} P_\phi + P_\Pi & P_\phi - P_\Pi \\ P_\phi - P_\Pi & P_\phi + P_\Pi \end{pmatrix}, \tag{B.3}$$

$$P_\phi = \begin{pmatrix} \cos\alpha\sqrt{\tilde{K}_\rho/K_\rho} & -\frac{1}{y}\sin\alpha\sqrt{\tilde{K}_s/K_\rho} \\ y\sin\alpha\sqrt{\tilde{K}_\rho/K_s} & \cos\alpha\sqrt{\tilde{K}_s/K_s} \end{pmatrix}, \tag{B.4}$$

$$P_\Pi = \begin{pmatrix} \cos\alpha\sqrt{K_\rho/\tilde{K}_\rho} & -y\sin\alpha\sqrt{K_\rho/\tilde{K}_s} \\ \frac{1}{y}\sin\alpha\sqrt{K_s/\tilde{K}_\rho} & \cos\alpha\sqrt{K_s/\tilde{K}_s} \end{pmatrix}. \tag{B.5}$$

It can be surely checked that the transformation matrix $\mathcal{W}$ satisfies a normalization condition for a Bogoliubov transformation $\mathcal{W}\mathcal{C}\mathcal{W}^\dagger = \mathcal{C}$ with $\mathcal{C} = \mathrm{diag}(1, 1, -1, -1)$.

Appendix C

Effects of Reservoirs on Spin-Charge Mixed TL Liquid

Here we calculate the zero bias conductance of a clean TL wire under magnetic field, connected to Fermi liquid reservoirs. As previous works [84, 85, 86] have shown, the scaling factor of conductance should disappear by the effect of reservoirs. We check whether their statements can also be applied to a polarized TL liquid, and whether our result in Eq.(3.29), which implies that applying bias voltage generates spin current by spin-charge mixing effect, is an artifact of the assumption to be an infinite system. We consider a polarized TL wire is connected to reservoirs of noninteracting Fermi liquid at $x = \pm d$.

From Hamiltonian (3.7), the imaginary time action becomes,

$$S = \frac{1}{2\pi}\int_0^\beta d\tau \int_{-\infty}^{\infty} dx\ \vec{\phi}^T \hat{M} \vec{\phi}\ , \tag{C.1}$$

$$\vec{\phi} = \begin{pmatrix} \phi_\rho & \phi_s \end{pmatrix}^T, \tag{C.2}$$

$$\hat{M} = \begin{pmatrix} v_\rho K_\rho & \Delta \\ \Delta & v_s K_s \end{pmatrix}^{-1} \partial_\tau^2 + \partial_x \begin{pmatrix} \frac{v_\rho}{K_\rho} & \Delta \\ \Delta & \frac{v_s}{K_s} \end{pmatrix} \partial_x. \tag{C.3}$$

Δ, v_i and K_i are x-dependent parameters and abruptly change at the boundaries,

$$v_i(x) = \begin{cases} v_i & -d < x < d \\ v_{\rm F} & \text{otherwise,} \end{cases} \tag{C.4}$$

$$K_i(x) = \begin{cases} K_i & -d < x < d \\ 1 & \text{otherwise,} \end{cases} \tag{C.5}$$

$$\Delta(x) = \begin{cases} \Delta & -d < x < d \\ 0 & \text{otherwise.} \end{cases} \tag{C.6}$$

Conductance can be calculated from the Green's function of bosonic field,

$$\begin{aligned} \hat{G}(\tau, x, y) &= \sum_{\omega_n} \hat{G}_{\omega_n}(x, y) e^{i\omega_n \tau} \\ &= \begin{pmatrix} \langle T_\tau \phi_\rho(\tau, x)\phi_\rho(0, y)\rangle & \langle T_\tau \phi_\rho(\tau, x)\phi_s(0, y)\rangle \\ \langle T_\tau \phi_s(\tau, x)\phi_\rho(0, y)\rangle & \langle T_\tau \phi_s(\tau, x)\phi_s(0, y)\rangle \end{pmatrix}, \end{aligned} \tag{C.7}$$

which satisfies the equation,

$$\hat{M}_{\omega_n} \hat{G}_{\omega_n}(x, y) = \hat{1} \cdot \delta(x - y). \tag{C.8}$$

Here $\hat{M}_{\omega_n}$ is Fourier component of $\hat{M}$ obtained by $\partial_\tau \to i\omega_n$. DC charge current ($I_\rho$) and spin current ($I_s$) induced by a time independent electronic field $E(y)$ in TL wire $-d < y < d$, are determined from Kubo formula for $i = \rho, s$

$$I_i(x) = \int_{-d}^{d} dy \lim_{\omega_n \to 0} \left(-\omega_n \frac{e^2}{\pi} \left[\hat{G}_{\omega_n}(x, y) \right]_{i,\rho} \right) E(y). \tag{C.9}$$

We must solve (C.8) under the boundary conditions at $x = \pm d, y$; (i) The Green's function should be continuous and (ii) the integration should satisfy

$$\int_{-d-0}^{-d+0} dx \hat{M}_{\omega_n} \hat{G}_{\omega_n}(x, y) = \int_{d-0}^{d+0} dx \hat{M}_{\omega_n} \hat{G}_{\omega_n}(x, y) = \hat{0}, \tag{C.10}$$

$$\int_{y-0}^{y+0} dx \hat{M}_{\omega_n} \hat{G}_{\omega_n}(x, y) = \hat{1}. \tag{C.11}$$

One can find the solution to become

$$\hat{G}_{\omega_n}(x, y) = \begin{pmatrix} -\frac{1}{\omega_n} & 0 \\ 0 & -\frac{1}{\omega_n} \end{pmatrix} + \mathcal{O}(\omega_n^0). \tag{C.12}$$

Thus the conductance is given by $G_\rho^{(0)} = \frac{e^2}{\pi}$ and $G_s^{(0)} = 0$ instead of Eq.(3.28) and Eq.(3.29). The result shows the conductance quantization to $\frac{e^2}{2\pi}$ par spin channel also holds for spin-charge mixed systems under the magnetic field, as far as concerned the DC limit $|\omega_n| \ll v_{\rm F}/2d$. Moreover we can ensure this conclusion is unchanged when a magnetic field is also applied to reservoirs besides the one-dimensional region.

Bibliography

[1] P. Drude, Ann. d. Phys. **1**, 556 (1900); *ibid* **3**, 369 (1900); *ibid* **7**, 687 (1902).

[2] C. Kittel,「固体物理学入門 第7版 (Introduction to Solid State Physics, 7th edition)」(丸善, 1998).

[3] Y. Imry, "*Introduction to mesoscopic physics*", (Oxford University Press, Oxford, New York, 1997).

[4] 田沼 静一, 家 泰弘 編,「実験物理科学シリーズ第 4 巻：メゾスコピック伝導」(共立出版, 1997).

[5] R. A. Webb, S. Washburn, C. P. Umbach, and R. B. Laibowitz, Phys. Rev. Lett. **54**, 2697 (1985).

[6] R. A. Webb, Jpn. J. Appl. Phys. **26**, 1926 (1987).

[7] R. Landauer, IBM J. Res. Dev. **1**, 223 (1957).

[8] M. Buttiker, Phys. Rev. Lett. **57**, 1762 (1986).

[9] B. J. van Wees, H. van Houten, C. W. J. Beenakker, J. Williamson, L. P. Kouwenhoven, D. van der Marel, and C. T. Faxon, Phys. Rev. Lett. **60**, 848 (1988).

[10] S. Tarucha, T. Honda, and T. Saku, Solid State Commun. **94**, 413, (1995).

[11] A. Yacoby, H. L. Stormer, K. W. Baldwin, L. N. Pfeiffer, and K. W. West, Solid State Commun. **101**, 77, (1997).

[12] S. Iijima, Nature (London) **354**, 56 (1991).

[13] R. Saito, G. Dresselhaus, and M. S. Dresselhaus, *"Physical Properties of Carbon Nanotubes"* (Imperial College Press, London, 1998).

[14] H. W. Postma, T. Teepen, Z. Yao, M. Grifoni, and C. Dekker, Science **293**, 76 (2001).

[15] S. Frank, P. Poncharal, Z. L. Wang, Walt A. de Heer, Science **280**, 1744 (1998).

[16] J. Kong, E. Yenilmez, T. W. Tombler, W. Kim, and H. Dai, Phys. Rev. Lett. **87**, 106801 (2001).

[17] A. Javey, J. Guo, Q. Wang, M. Lundstrom, and H. Dai, Nature (London) **424**, 654 (2003).

[18] J. Sólyom, Adv. Phys. **28**, 201 (1979).

[19] 斯波 弘行,「電子相関の物理」(岩波書店, 2001).

[20] A. Gogolin, A. Nersesyan, and A. Tsvelik, *"Bosonization and Strongly Correlated Systems"* (Cambridge University Press, Cambridge, England, 1998).

[21] T. Giamarchi, *"Quantum Physics in One Dimension"* (Clarendon Press, Oxford, 2004).

[22] D. L. Maslov, "Fundamental aspects of electron correlations and quantum transport in 1D systems" in *Nanophysics: Coherence and Transport, Proceedings of LXXXI Les Houches Summer School*, H. Bouchiat, Y. Gefen, S. Gueron, G. Montambaux, and J. Dalibard, eds, (Elsevier, North Holland, 2005), pp. 1-108; cond-mat/ 0506035.

[23] L. D. Landau, Sov. Phys. JETP **3**, 920 (1956); *ibid.* **5**, 101 (1957).

[24] A. A. Abrikosov, L. P. Gorkov, I. E. Dzyaloshinski, *"Methods of quantum field theory in statistical physics"* (Dover Publications, New York, 1963).

[25] L. D. Landau, Sov. Phys. JETP **8**, 70 (1959): See also Chapter 4 of [24].

[26] G. M. Eliashberg, Sov. Phys. JETP **11**, 696 (1960); *ibid.* **16**, 780 (1963); S. Doniach and S. Engelsberg, Phys. Rev. Lett. **17**, 750 (1966); W. F. Brinkman and S. Engelsberg, Phys. Rev. **169**, 417 (1968).

[27] D. Coffey and K. S. Bedell, Phys. Rev. Lett. **71**, 1043 (1993); D. Belitz, T. R. Kirkpatrick, and T. Vojta, Phys. Rev. B **55**, 9452 (1997); S. Das Sarma, V. M Galitski, and Y. Zhang, Phys. Rev. B **69**, 125334 (2004); *ibid.* **70**, 035111 (2004).

[28] D. S. Greywall, Phys. Rev. B **27**, 2747 (1983).

[29] D. S. Greywall, Phys. Rev. B **41**, 1842 (1990); M. Ogura and H. Hamaizawa, J. Phys. Soc. Jpn. **66**, 3706 (1997); A. Casey, H. Patel, J. Nyeki, B. P. Cowan, and J. Saunders, Phys. Rev. Lett. **90**, 115301 (2003).

[30] A. V. Chubukov, D. L. Maslov, and A. J. Millis, Phys. Rev. B **73**, 045128 (2006); A. V. Chubukov, D. L. Maslov, S. Gangadharaiah, and L. I. Glazman, Phys. Rev. B **71**, 205112 (2005); *ibid.* Phys. Rev. Lett. **95**, 026402 (2005).

[31] S. Tomonaga, Prog. Theor. Phys. **5**, 544 (1950).

[32] J. M. Luttinger, J. Math. Phys. **4**, 1154 (1963).

[33] K. Kamide, M. Nishida, and S. Kurihara, Physica E, **18**, 218 (2003).

[34] K. Kamide, T. Kimura, M. Nishida, and S. Kurihara, Phys. Rev. B, **68**, 024506 (2003).

[35] Z. K. Tang, L. Zhang, N. Wang, X. X. Zhang, G. H. Wen, G. D. Li, J. N. Wang, C. T. Chan, and P. Sheng, Science **292**, 2462 (2001); Z. K. Tang, N. Wang, X. X. Zhang, J. N. Wang, C. T. Chan, P. Sheng, New J. Phys. **5**, 146 (2003).

[36] X. Blase, L. X. Benedict, E. L. Shirley, and S. G. Louie, Phys. Rev. Lett. **72**, 1878 (1994).

[37] Z. M. Li, Z. K. Tang, H. J. Liu, N. Wang, C. T. Chan, R. Saito, S. Okada, G. D. Li, J. S. Chen, N. Nagasawa, and S. Tsuda, Phys. Rev. Lett. **87**, 127401 (2001).

[38] H. J. Liu and C. T. Chan, Phys. Rev. B **66**, 115416 (2002).

[39] T. Miyake and S. Saito, Phys. Rev. B **68**, 155424 (2003).

[40] I. Cabria, J. W. Mintmire, and C. T. White, Phys. Rev. B **67**, 121406(R) (2003).

[41] R. Barnett, E. Demler, and E. Kaxiras, Phys. Rev. B **71**, 035429 (2005).

[42] C. L. Kane, M. P. A. Fisher, Phys. Rev. Lett. **68**, 1220 (1992); Phys. Rev. B **46**, 15233 (1992).

[43] C. L. Kane, M. P. A. Fisher, Phys. Rev. B **46**, 7268 (1992).

[44] A. Furusaki and N. Nagaosa, Phys. Rev. B **47**, 4631 (1993); *ibid.*, Phys. Rev. Lett. **72**, 892 (1994); *ibid.*, Phys. Rev. B **54**, 5239 (1996).

[45] A. Furusaki and N. Nagaosa, Phys. Rev. B **46**, 7268 (1992).

[46] K. Penc and J. Solyom, Phys. Rev. B **47**, 6273-6292 (1993).

[47] T. Kimura, K. Kuroki, and H. Aoki, Phys. Rev. B **53**, 9572 (1996).

[48] D. Schmeltzer, Phys. Rev. B **65**, 193303 (2002); D. Schmeltzer, A. R. Bishop, A. Saxena, and D. L. Smith, Phys. Rev. Lett. **90**, 116802 (2003); H. Y. Chang and D. Schmeltzer, Phys. Lett. A **345**, 45 (2005).

[49] S. Lal, S. Rao, and D. Sen, Phys. Rev. B **65**, 195304 (2002).

[50] K. Kamide, T. Tsukada, and S. Kurihara, Physica B **359-361**, 645 (2005).

[51] K. Kamide, T. Tsukada, and S. Kurihara, Phys. Rev. B **73**, 235326 (2006).

[52] T. Hikihara, A. Furusaki and K. A. Matveev, Phys. Rev. B **72**, 035301 (2005).

[53] K. Kamide, Y. Tsukada, and S. Kurihara, proceedings of "*24th International Conference on Low Temperature Physics*", 1387 (2005).

[54] S.J. Tans, M.H. Devoret, H. Dai, A. Thess, R.E. Smalley, L.J. Geerligs, and C. Dekker, Nature (London) **386**, 474 (1997); T.W. Odom, J. Huong, P. Kim, and C.M. Lieber, *ibid.* **391**, 62 (1998); J.W.G. Wildöer, L.C.Venema, A.G. Rinzler, R.E. Smalley, and C. Dekker, *ibid.* **391**, 59 (1998).

[55] R. Egger and Alexander O. Gogolin, Phys. Rev. Lett. **79**, 5082 (1997); H. Yoshioka and A. A. Odintsov, Phys. Rev. Lett. **82**, 374 (1999)

[56] J. González, Phys. Rev. B. **67**, 14528 (2003)

[57] Yu.A. Krotov, D.-H. Lee, and Steven G. Louie, Phys. Rev. Lett. **78**, 4245 (1997)

[58] A. Sédéki, L.G. Caron, and C.Bourbonnais, Phys. Rev. B **65**, 140515(R) (2002)

[59] M. Kociak, A. Yu. Kasumov, S. Guéron, B. Reulet, I.I. Khodos, Yu. B. Gorbatov, V.T. Volkov, L. Vaccarini, and H. Bouchiat, Phys. Rev. Lett. **86**, 2416 (2001)

[60] J. González, Phys. Rev. Lett. **87**, 136401 (2001)

[61] A. Yu. Kasumov, R. Deblock, M. Kociak, B. Reulet, H. Bouchiat, I.I. Khodos, Yu. B. Gorbatov, V.T. Volkov, C.Journet and M. Burghard, Science **284**, 1508 (1999)

[62] A. De Martino and R. Egger, Phys. Rev. B **67**, 235418 (2003).

[63] N. Furukawa and T. M. Rice, J. Phys.: Condens. Matter **10**, L381 (1998).

[64] In our previous paper [33], we have refered to this shaded region as gapless phase which can be misleading since a small non-zero gap also exist in this region.

[65] T. Kimura, K. Kuroki and H. Aoki, J. Phys. Soc. Jpn. **67** 1377 (1998).

[66] J. González and E. Perfetto, Phys. Rev. B **72**, 205406 (2005).

[67] M. Bockrath *et. al.*, Nature (London) **397**, 598 (1999); Z. Yao *et. al.*, *ibd.* **402**, 273 (1999).

[68] A. Bachtold *et. al.*, Phys. Rev. Lett. **87**, 166801 (2001).

[69] F. P. Milliken, C. P. Umbach, and R. A. Webb, Solid State Commun. **97**, 309 (1996).

[70] A. M. Chang, L. N. Pfeiffer, and K. W. West, Phys. Rev. Lett. **77**, 2538 (1996).

[71] R. Egger and A. O. Gogolin, Phys. Rev. Lett. **79**, 5082 (1997); C. L. Kane, L. Balents, and M. P. A. Fisher, *ibd.* **79**, 5086 (1997).

[72] X.-G. Wen, Phys. Rev. B **41**, 12838 (1990).

[73] H. Ishii, H. Kataura, H. Shiozawa, H. Yoshioka, H. Otsubo, Y. Takayama, T. Miyahara, S. Suzuki, Y. Achiba, M. Nakatake, T. Narumira, M. Higashiguchi, K. Shimada, H. Namatame and M. Taniguchi, Nature **426**, 540 (2003).

[74] O. M. Auslaender, H. Steinberg, A. Yacoby, Y. Tserkovnyak, B. I. Halperin, K. W. Baldwin, L. N. Pfeiffer, and K. W. West, Science **308**, 88 (2005).

[75] J. Lee, S. Eggert, H. Kim, S. J. Kahng, H. Shinohara, and Y. Kuk, Phys. Rev. Lett. **93**, 166403 (2004).

[76] W. Liang, M. Bockrath, D. Bozovic, J. H. Hafner, M. Tinkham, H. Park, Nature (London) **411**, 665 (2001); W. Liang, M. Bockrath, and H. Park, Phys. Rev. Lett. **88**, 126801 (2002)

[77] M. R. Buitelaar, A. Bachtold, T. Nussbaumer, M. Iqbal, and C. Schonenberger, Phys. Rev. Lett. **88**, 156801 (2002).

[78] A. Furusaki, Phys. Rev. B **57**, 7141 (1998).

[79] Qimiao Si, Phys. Rev. Lett. **81**, 3191 (1998).

[80] L. Balents and R. Egger, Phys. Rev. Lett. **85**, 3464 (2000); L. Balents and R. Egger, Phys. Rev. B 64, 035310 (2001).

[81] C. S. Peca, L. Balents, and K. J. Wiese, Phys. Rev. B **68**, 205423 (2003).

[82] S. Rabello and Q. Si, Europhys. Lett. **60**, 882 (2002).

[83] H. Ajiki and T. Ando, J. Phys. Soc. Jpn. **62**, 1255 (1993); J. Phys. Soc. Jpn. **65**, 505 (1996).

[84] D. L. Maslov and M. Stone, Phys. Rev. B **52**, R5539 (1995).

[85] A. Kawabata, J. Phys. Soc. Jpn. **65**, 30 (1995).

[86] V. V. Ponomarenko, Phys. Rev. B **52**, R8666 (1995).

[87] M. Thorwart, M. Grifoni, G. Cuniberti, H. W. Ch. Postma, and C. Dekker Phys. Rev. Lett. **89**, 196402 (2002); M. Thorwart, R. Egger, and M. Grifoni Phys. Rev. B **72**, 035330 (2005).

[88] M. Fabrizio and A. O. Gogolin, Phys. Rev. B **51**, 17827 (1995).

[89] A. E. Mattsson, S. Eggert, and H. Johannesson, Phys. Rev. B **56**, 15615 (1997).

[90] F. Anfuso and S. Eggert, Phys. Rev. B **68**, 241301(R) (2003).

[91] A. V. Moroz, K. V. Samokhin, and C. H. W. Barnes, Phys. Rev. Lett. **84**, 4164 (2000); A. V. Moroz and C. H. W. Barnes, Phys. Rev. B **60**, 14272 (1999).

[92] V. Gritsev, G. I. Japaridze, M. Pletyukhov, and D. Baeriswyl, Phys. Rev. Lett. **94**, 137207 (2005).

[93] M. Ouyang, J. L. Huang, and C. M. Lieber, Phys. Rev. Lett. **88** 66804 (2002).

[94] S. J. Tans, M. H. Devoret, H. Dai, A. Thess, R. E. Smalley, L. J. Geerligs, and C. Dekker, Nature **386**, 474 (1997); D. H. Cobden, M. Bockrath, P. L. McEuen, A. G. Rinzler and R. E. Smalley, Phys. Rev. Lett. **81**, 681 (1998).

[95] Q. Ramadan, C. Yu, V. Samper, and D. P. Poenar, Appl. Phys. Lett. **88**, 032501 (2006).

[96] M. Köhl, H. Moritz, T. Stöferle, K. Günter, and T. Esslinger, Phys. Rev. Lett. **94**, 080403 (2005); K. Günter, T. Stöferle, H. Moritz, M. Köhl, and T. Esslinger, Phys. Rev. Lett. **95**, 230401 (2005).

[97] K. A. Matveev, D. Yue, and L. I. Glazman, Phys. Rev. Lett. **71**, 3351-3354 (1993).

[98] D. Yue, L. I. Glazman, and K. A. Matveev, Phys. Rev. B **49**, 1966-1975 (1994).

[99] U. Weiss, R. Egger, and M. Sassetti, Phys. Rev. B **52**, 16707 (1995).

[100] M. Tsvelik, J. Phys. A **28**, 625L (1995).

[101] P. Fendley, A. W. W. Ludwig, and H. Saleur, Phys. Rev. Lett. **74**, 3005 (1995); *ibid.* Phys. Rev. B **52**, 8934 (1995).

List of publications

Thesis publications

Kenji Kamide, Yuji Tsukada, and Susumu Kurihara, "Spin-charge mixing effects on resonant tunneling in a polarized Luttinger liquid", Physical Review B, **73**, 235326 (2006).

Kenji Kamide, Yuji Tsukada, and Susumu Kurihara, "Scaling of a Single Impurity Potential of Arbitrary Strength in a Tomonaga-Luttinger Liquid", AIP Conference Proceedings series: 24th International Conference on Low Temperarure Physics, 1387 (2005).

Kenji Kamide, Yuji Tsukada, and Susumu Kurihara, "Zeeman effect on resonant tunneling in spin-polarized Tomonaga-Luttinger liquid", Physica B, **359-361**, 645 (2005).

Kenji Kamide, Takashi Kimura, Munehiro Nishida, and Susumu Kurihara, "Singlet Superconductivity phase in Carbon Nanotubes", Physical Review B, **68**, 024506 (2003).

Kenji Kamide, Munehiro Nishida, and Susumu Kurihara, "Superconducting and Density-Wave Correlation Functions in Carbon Nanotubes", Physica E, **18**, 218 (2003).

Oral presentations

上出健仁, 栗原進, "Renormalization of a single impurity potential of arbitrary strength in a Tomonaga-Luttinger liquid", 第 4 回 21 世紀 COE 自己組織系物理シンポジウム, 早稲田大学, 2006 年 9 月.

Kenji Kamide, Yuji Tsukada, and Susumu Kurihara, "Renormalization of a single impurity potential of arbitrary strength in a Tomonaga-Luttinger liquid", American Physical Society March Meeting, Baltimore, Maryland, USA, March 2006.

上出健仁, 塚田悠司, 栗原進, “Scaling of an impurity potential in Tomonaga-Luttinger liquid for arbitrary transmission”, 日本物理学会 2005 年度秋季大会, 同志社大学, 2005 年 9 月.

Kenji Kamide, Yuji Tsukada, and Susumu Kurihara, “Scaling of a Single Impurity Potential of Arbitrary Strength in a Tomonaga-Luttinger Liquid”, 24th International Conference on Low Temperature Physics, Orland, USA, August 2005.

上出健仁, 塚田悠司, 栗原進, “スピン偏極した朝永・ラッティンジャー流体の共鳴トンネル現象におけるスピン - 電荷混成効果”, 日本物理学会 2004 年度秋季大会, 青森大学, 2004 年 9 月.

Kenji Kamide, Yuji Tsukada, and Susumu Kurihara, “Zeeman effect on resonant tunneling in spin-polarized Tomonaga-Luttinger liquid”, International Conference on Strongly Correlated Electron Systems (SCES04), Karsrue, Germany, July 2004.

上出健仁, 塚田悠司, 栗原進, “Zeeman Effect on Resonant Tunneling in Tomonaga-Luttinger Liquid”, 第 1 回 21 世紀 COE 自己組織系物理シンポジウム, 早稲田大学, 2004 年 2 月.

上出健仁, 栗原進, “カーボンナノチューブによる超伝導相”, 東京大学物性研究所短期研究会 “量子凝縮系研究の新展開”, 東京大学物性研究所, 柏, 2004 年 1 月.

Kenji Kamide, Takashi Kimura, and Susumu Kurihara, “Interaction effects in 4-component Tomonaga-Luttinger liquids in (5,0) carbon nanotubes”, Spin and Charge Transport in Nanostructures (SCTN), Braga, Portugal, September 2003.

上出健仁, 西田宗弘, 栗原進, “(5,0) カーボンナノチューブの低温における秩序相”, 日本物理学会 2002 年度秋季大会, 中部大学, 2002 年 9 月.

Kenji Kamide, Munehiro Nishida, and Susumu Kurihara, “Superconducting and Density-Wave Correlation Functions in Carbon Nanotubes”, 23rd International Conference on Low Temperature Physics (LT23), Hiroshima, Japan, August 2002.

Related presentations

塚田悠司, 上出健仁, 栗原進, “ラッティンジャー液体におけるスピン依存した輸送特性の繰り込み群解析”, 日本物理学会 2004 年度秋季大会, 青森大学, 2004 年 9 月.